POST-PALEOCENE DEFORMATION IN KALECİK REGION, EAST OF ANKARA, TURKEY

A THESIS SUBMITTED TO
THE GRADUATE SCHOOL OF NATURAL AND APPLIED SCIENCES
OF
MIDDLE EAST TECHNICAL UNIVERSITY

BY

PINAR KASIMOĞLU

IN PARTIAL FULFILLMENT OF THE REQUIREMENTS
FOR
THE DEGREE OF MASTER OF SCIENCE
IN
GEOLOGICAL ENGINEERING

MAY 2010

Approval of the thesis:

POST-PALEOCENE DEFORMATION IN KALECİK REGION, EAST OF ANKARA, TURKEY

submitted by **PINAR KASIMOĞLU** in partial fulfillment of the requirements for the degree of **Master of Science in Geological Engineering Department, Middle East Technical University** by,

Prof. Dr. Canan Özgen ____________________
Dean, Graduate School of **Natural and Applied Sciences**

Prof. Dr. Zeki Çamur ____________________
Head of Department, **Geological Engineering**

Assoc. Prof. Dr. Bora Rojay ____________________
Supervisor, **Geological Engineering Dept., METU**

Examining Committee Members:

Prof. Dr. Kadir Dirik ____________________
Geological Engineering Dept., Hacettepe University

Assoc. Prof. Dr. F. Bora Rojay ____________________
Geological Engineering Dept., METU

Prof. Dr. G. M. Vedat Toprak ____________________
Geological Engineering Dept., METU

Prof. Dr. Erdin Bozkurt ____________________
Geological Engineering Dept., METU

Assoc. Prof. Dr. M. Lütfi Süzen ____________________
Geological Engineering Dept., METU

Date: 05. 05. 2010

I hereby declare that all information in this document has been obtained and presented in accordance with academic rules and ethical conduct. I also declare that, as required by these rules and conduct, I have fully cited and referenced all material and results that are not original to this work.

Name, Last name: Pınar Kasımoğlu

Signature :

ABSTRACT

POST-PALEOCENE DEFORMATION IN KALECİK REGION,
EAST OF ANKARA, TURKEY

Kasımoğlu, Pınar
M.Sc., Department of Geological Engineering
Supervisor: Assoc. Prof. Dr. Bora Rojay

May 2010, 147 pages

In order to understand the tectonic evolution of the Kalecik region (Ankara, Turkey), a structural field study was performed in a selected area located in the east of Kalecik, where mostly imbricated thrust sheets of the Cretaceous Ophiolitic melange crop out. In the study area, the Cretaceous Ophiolitic melange, Cretaceous radiolaria-bearing sequences and the Paleocene units are all intruded by sub-vertical dykes. The attitudes of planar structures (dykes, beds and faults) and the kinematic data measured on faults were analyzed by using "ROCKWORKS 2002" and "Angelier Direct Inversion Method (version 5.42)" softwares, respectively.

A major trend of NE-SW (045°N) direction and relatively a post-Paleocene – pre-Miocene age was determined for the dykes indicating an extension in the NW-SE direction during post-Paleocene. The dykes cut bedded units displaying a dominant set trending in WNW-ESE (297°N) direction and mostly dipping towards NE with moderate dip amounts. But at the same time, the Upper Cretaceous units were observed as intensely folded, faulted and thrusted due to the compressional regime that acted in Central Anatolia during Late Cretaceous. The angular difference between the major trend of dykes and the dominant trend of stratification was found as approximately 108°., which may also indicate that the dykes and beds were evolved during different deformation periods.

The results of the kinematic analyses of different age faults revealed that the post-Paleocene – pre-Miocene Kalecik basaltic dykes are deformed under a continuous NW-SE-oriented post-Paleocene compressional to strike-slip tectonic regime which was followed by a NNW-SSE oriented post-Miocene extensional-transtensional regime.

Key words: Dyke, Fault plane-slip analysis, Palaeostress, Cretaceous Ophiolitic Melange, Kalecik.

ÖZ

KALECİK BÖLGESİNİN PALEOSEN SONRASI DEFORMASYONU,
DOĞU ANKARA, TÜRKİYE

Kasımoğlu, Pınar
Yüksek Lisans, Jeoloji Mühendisliği Bölümü
Tez Yöneticisi: Doç. Dr. Bora Rojay

Mayıs 2010, 147 sayfa

Kalecik bölgesinin (Ankara, Türkiye) tektonik evrimini anlayabilmek için, Kalecik İlçesi'nin doğusunda, çoğunlukla üst üste bindirmiş Kretase Ofiyolitli Melanj dilimlerinin yüzeylendiği bir alan seçilmiş ve bu alanın yapısal jeolojisi çalışılmıştır. Çalışma alanında; Kretase Ofiyolitik Melanjı, Kretase radyolaryalı istifleri ve Paleosen birimlerinin tümü dike yakın eğimli dayklar tarafından kesilmiştir. Düzlemsel yapıların (dayklar, tabakalar ve faylar) pozisyonları ve faylar üzerinden ölçülen kinematik veriler, sırasıyla "ROCKWORKS 2002" ve "Angelier Direct Inversion Method (sürüm 5.42)" yazılımları kullanılarak analiz edilmiştir.

Başlıca KD-GB (045°K) yönelimli ve göreceli olarak Paleosen sonrası – Miyosen öncesi yaşlı olduğu belirlenen daykların, Paleosen sonrası dönemde KB-GD yönelimli bir genişlemeyi işaret ettiği tespit edilmiştir. Dayklar, BKB-DGD (297°K) baskın yönelimli ve ortalama eğim miktarlarıyla KD yönüne dogru dalan tabakaları kesmektedirler. Fakat aynı zamanda Üst Kretase yaşlı birimlerin, Geç Kretase boyunca Orta Anadolu'da etkin olan sıkışma rejimi sebebiyle, yoğun bir biçimde

kıvrımlandığı, faylandığı ve birbirleri üzerine bindirdiği gözlenmiştir. Başlıca dayk yönelimi ve baskın tabakalanma doğrultusu arasındaki açısal farkın yaklaşık 108° olması da, dayklar ile tabakaların farklı deformasyon döneminde evrim geçirdiklerinin göstergesi olabilir.

Değişik yaşlı faylar üzerinde yapılan kinematik analizler, Paleosen sonrası – Miyosen öncesi yaşlı Kalecik bazaltik dayklarının; Paleosen sonrası KB – GD yönlü sürekli bir yanal atımlı tektonik sıkışma rejimi ve ardından Miyosen sonrasında süregelen KKB – GGD uzanımlı bir genişleme-transtensiyonel rejim altında deforme olduğunu ortaya çıkarmıştır.

Anahtar kelimeler: Dayk, Fay düzlemi-kayma analizi, Paleostres, Kretase Ofiyolitik Melanji, Kalecik.

…. To My Family

ACKNOWLEDGEMENTS

First of all, I wish to express my gratitude to my supervisor Assoc. Prof. Dr. Bora Rojay, for his guidance, kindness, continual support, sharing his knowledge, and most important of all, for his patience throughout all the stages of this thesis.

I would like to thank my thesis examining committee members; Prof. Dr. Kadir Dirik, Prof. Dr. G. M. Vedat Toprak, Prof. Dr. Erdin Bozkurt and Assoc. Prof. Dr. M. Lütfi Süzen for their corrections and valuable criticisms on this thesis.

I would also like to thank METU Geological Engineering Department's technician Orhan Karaman for his driving, protection and help during my fieldwork. I would also like to express my sincere thanks to my colleague Toygar Tanyıldız, for spending his three days in the field with me and for his enjoyable and teachful company.

I would like to thank research assistant Şule Deveci Gürboğa, for her technical support with the Angelier software and on the kinematic analyses of the faults. I must not forget to thank my colleague Emre Seyrek, for his help during the literature survey.

I am especially indebted to my friends and colleagues; Aksel Tuğba Dinç, Esin Şişman and Hilal Sevindik, for their valuable friendship and besides, for their technical support with the MapInfo software. I would like to extend my thanks to Aksel Tuğba Dinç for her support and understanding. I would also like to thank my oldest friends; İdil Çetintaş for her help with the text, Hakan Önder Olcay and Murat Kandaz, for sharing their experiences with me, and to all three for their support and friendship for so long.

The completion of this study would not be possible without the help of my dearest friend and colleague, Hasan Yetginer. I am mostly indebted to him for his constructive advices, criticisms, continual support, patience, tolerance and standing by me throughout all the stages of this thesis and besides, for helping me in formatting, editing and correcting the text.

Among all, I would like to express my deepest gratitude to my mum, my dad, my grandma and my uncle for their extreme patience, unlimited support throughout all the stages of this thesis and in times when I was discouraged and depressed, their continual motivation and encouragement, and most important of all, for their belief in me unconditionally and for their endless love.

Finally, I would like to thank METU Geological Engineering Department for providing me this opportunity and the field materials (compass, hammer and loop) and also research assistant Özgür Aktürk, for providing me the GPS that I used during my field studies. Besides, all the staff members of METU Geological Engineering Department, for their any kind of help during my studies, are gratefully acknowledged.

The fieldwork of this study was supported by and carried out together with the TUBITAK project “The orientation of principle stress direction during Post-Cretaceous and Post-Eocene periods in northern Central Anatolia” with project no: CAYDAG-106Y122.

TABLE OF CONTENTS

LIST OF TABLES

TABLES

LIST OF FIGURES

FIGURES

CHAPTER 1

INTRODUCTION

1.1. Purpose and Scope of Study

Turkey forms one of the most actively deforming regions in the world as a consequence of north–south convergence between Africa–Arabia and Eurasia, resulting in the westward lateral extrusion of the Anatolian block. Formation of the sedimentary basins (e.g. Çankırı Basin) took place after the closure of the northern branch of Neotethys Ocean along the İzmir–Ankara–Erzincan Suture (IAES) belt, resulting from north–south convergence between the Pontides in the north and the Tauride–Anatolide Platform in the south since Late Cretaceous times. The Cretaceous Ophiolitic melange which is a well-preserved remnant of the subduction complex accreted at the active margin of Mesozoic North Neo-Tethys, crops out as a significant tectonic belt along the İzmir-Ankara-Erzincan Suture (IAES) belt (Figure 1.1).

Kalecik region (Ankara) lies on the IAES belt and on the western margin of the Çankırı basin, both of which are one of the best sites in north Central Anatolia in terms of post-collisional tectonic studies with the consequent structures that include thrust belts, folds, faults, and tectonically active basin formations.

In the study area, which is located in the east of Kalecik, mostly imbricated thrust sheets of the Cretaceous Ophiolitic melange and younger units crop out. In addition, there are exposed dykes which intruded into the Cretaceous Ophiolitic melange and the Paleocene units consisting of volcanics intercalated with sedimentary packages. Although the geological studies in Ankara region have begun in 1930's, the dykes in Kalecik, which are the main subject of this thesis, were mentioned for the first time by Buket (1969). On several following publications, nevertheless, only the general geology, tectonism and petrographic analyses of dike intrusions of the region were mentioned.

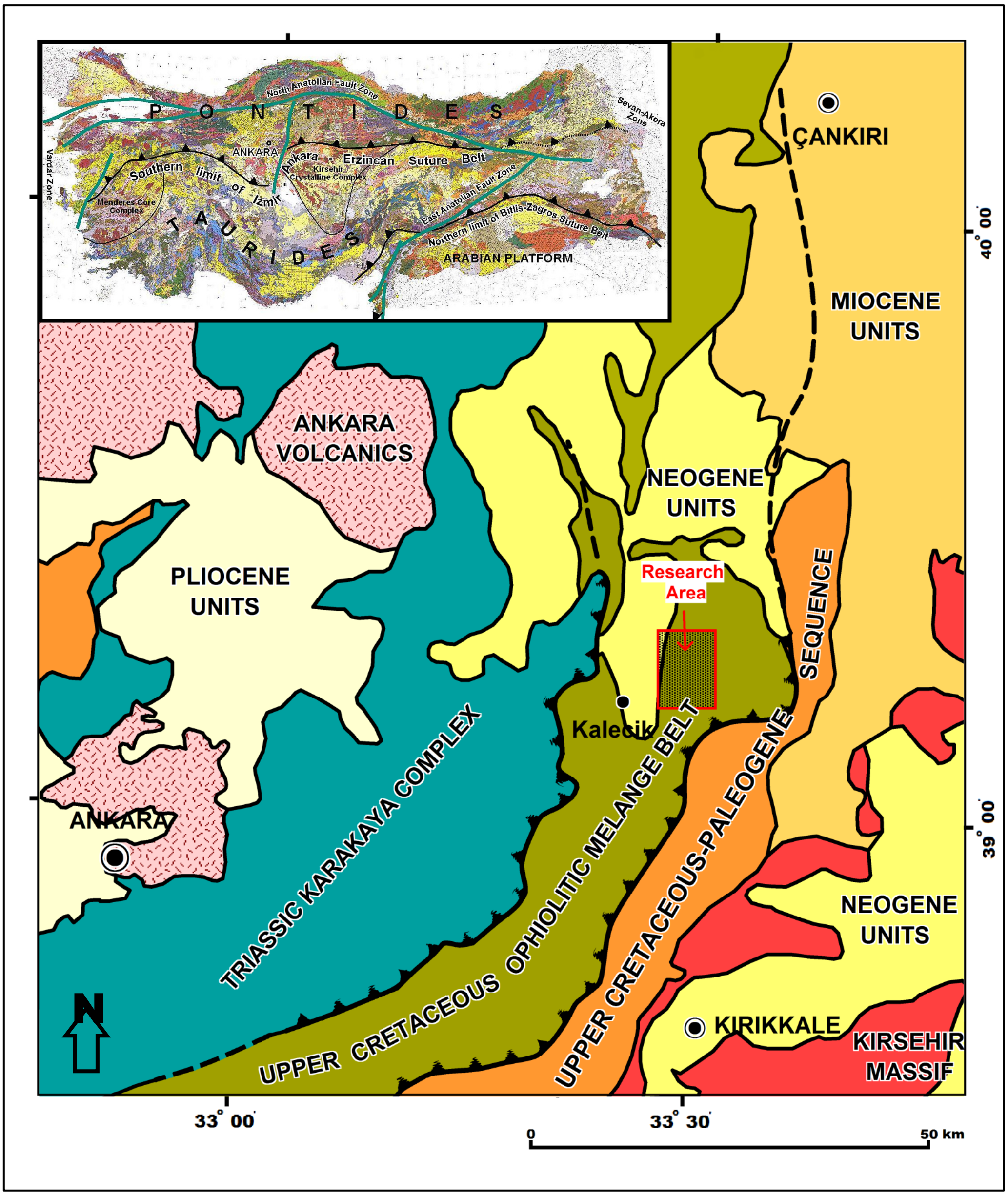

Figure 1.1: Location map of the study area. Inset map shows the structural outline of Turkey. (Simplified geological map of area between Ankara-Çankırı-Kırıkkale provinces from the 1: 500 000 scaled geology map of Turkey by the Institute of Mineral Research and Exploration, 1961).

No study was carried out about the geochemistry of the dyke intrusions apart from the magmatic rocks in general. The precision of the studies performed on the tectonism and age of the dykes are not sufficient either. Some dilemmas about the ages of the units also exist, especially for the Middle-post Eocene period in the studies. Therefore, difficulties occur in relative dating of these dykes even relatively with respect to the dyke-cut units. Thus, in general, the emplacement mechanism, geochemistry, tectonic setting, stresses operating on the dykes and the age relationships of the dykes with other rock units are highly questionable.

Dykes are fractures dilated and filled by magma. Therefore, the extension associated with dyke intrusion can be evaluated using the geometric parameters of dykes. The work in this thesis concerns mainly the geometry of deformational planar structures, especially the dykes, their cross-cutting relationships with related structures and lithologies. This thesis aims to determine the orientation of dykes, their cross-cutting relationships and relative ages with respest to other planar structures (beds and faults), and the distribution of the principle stresses operating in the study area at the time of intrusion or after, in order to reveal the deformational phases/regimes that affected the region. It is anticipated that the results of this study, in correlation with other post-Paleocene dykes in Central Anatolia, may give us an additional view about the tectonic evolution of the terrain.

For this purpose, to understand the post-Paleocene tectonics of the terrain, planar data (dykes, beds and faults) were collected from the study area for structural analysis and evaluated considering the relative ages with respect to each other in geologic time.

1.2. Geographic Location

The study was carried out in an area between the northeast of Ankara, south of Çankırı, and north of Kırıkkale provinces (Figure 1.1). The study area is located more specifically around Aktepe village in the northeast of

Kalecik town, which is about 90 kilometers from Ankara province where extensive dykes are exposed (Figure 1.2). It covers an area approximately about 65 km²s which is included with in the Çankırı H30-c2, H30-c3, H31-d1, H31-d4 quadrangles of 1/25 000 scaled topographic maps of Turkey and lies within the UTM earth coordinates of E 538500-E 544500 and N 4437900-N 4446650.

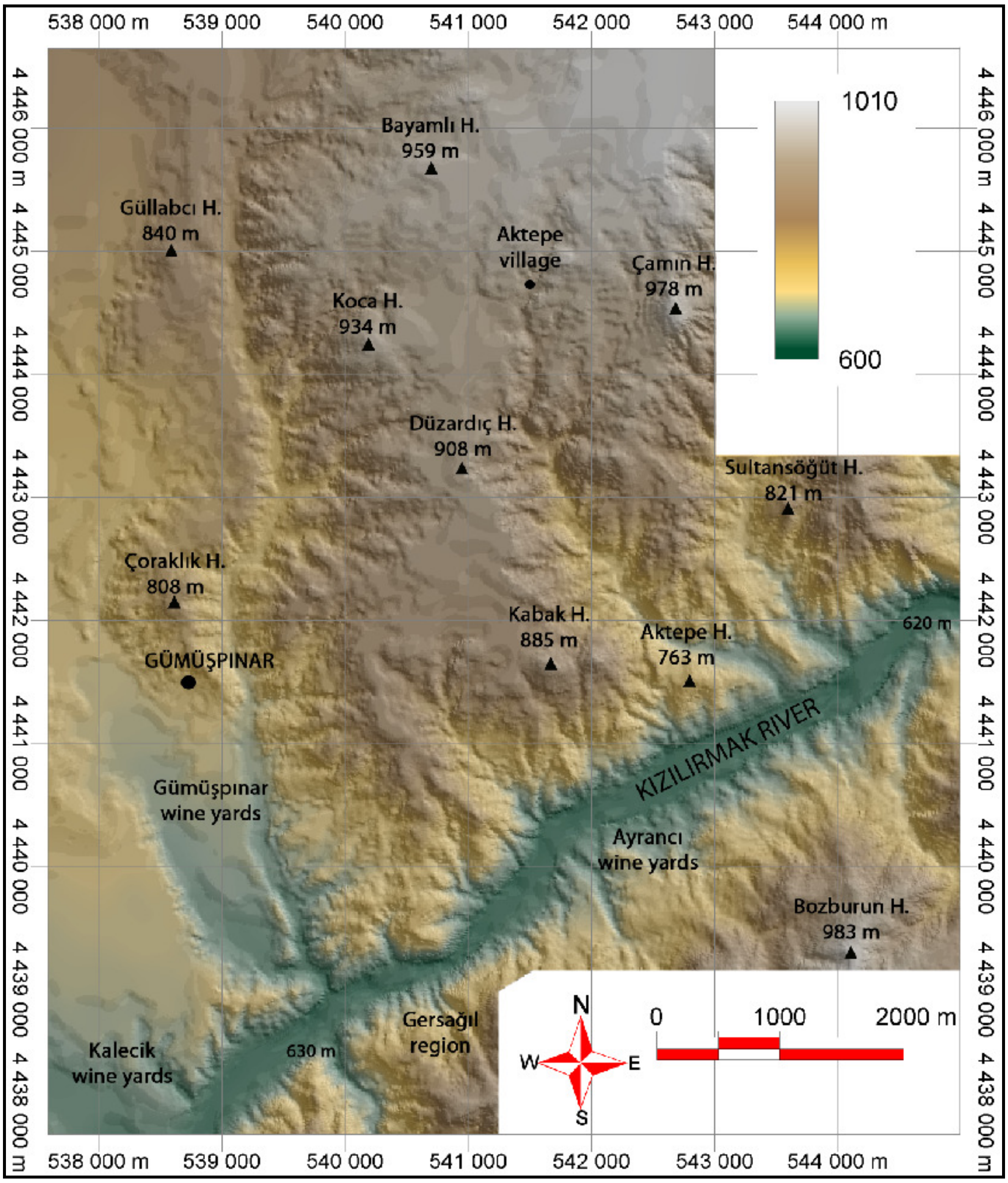

Figure 1.2: Digital Elevation Model (DEM) of the study area prepared by TNTmips.

The Kızılırmak River crosses the study area in SW-NE direction. Both sides of the river consist of short hill ranges with narrow crests trending towards the river. These ranges are rugged and dissected by valleys. The Kızılırmak River flows with meanders in a wide valley floor with unpaired cut and fill terraces (Figure 1.2).

The highest peak in the study area is Bozburun Hill with an altitude of 983 meters. Other important peaks from highest to lowest are: Çamın Hill (978 m), Bayamlı Hill (959 m), Düzardıç Hill (908 m), Kabak Hill (885.2 m), Sultansöğüt Hill (821 m), Ağıl Hill (786 m), and Aktepe Hill (763 m), respectively (Figure 1.2).

1.3. Methods of Study

Under the scope of this thesis, a series of steps were taken professionally throughout the completion (Figure 1.3).

Firstly, in order to have an idea about the regional geology and tectonic evolution of the study area, and to make use of the experiences of the former researchers, a literature survey was performed and related geological literature was compiled about the Kalecik region in the northeast of Ankara province with its close vicinity.

By the use of aerial photographs of the region, the former geological maps are revised and upgraded. Besides, especially the location of the key areas, size and contact relationships of dykes were determined in the region.

In the light of the valuable information from the previous studies and the information which was revealed from the aerial photographs, geological field work was performed in order to verify and revise the gathered information. During the fieldwork, the dip and strike data of the dykes and neighbouring bedded units and the dip and strike data of the faults with slip senses, together with the data locations were taken for structural analysis. Contact, cross-cutting relationships were recorded and relative ages of the structures were determined. Great care was taken in the selection of the critical localities and measurements during the fieldwork in order to avoid imprecise results.

After the data collection and verification process by the field studies, the locations, sizes, geometry and patterns of the dykes, beds and faults in the region were defined. The gathered structural data was processed and analyzed structurally and statistically by using Rockworks 2002 and Angelier softwares.

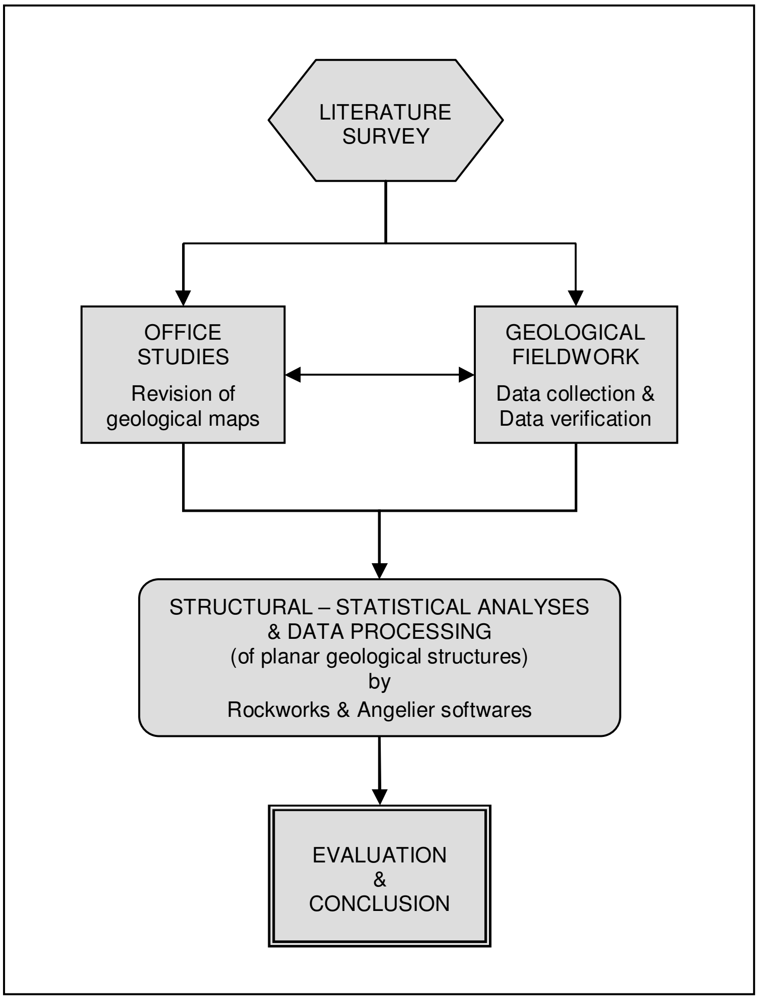

Figure 1.3: Flowchart of the methodology.

Finally, by the evaluation of the results of the analyses on the various structural elements of the region, the dykes, beds and faults were interpreted and the principle stress orientations were determined for the region to achieve a conclusion about the deformational history and to enlighten the tectonic evolution of the terrain.

CHAPTER 2

REGIONAL GEOLOGY

2.1. Previous Studies

Many authors have reported the impressive chaotic nature of a particular belt, containing ophiolitic rock units, around Ankara since the 1930's.

The first detailed geological map at a scale of 1/135 000 of Ankara region was prepared by Chaput (1931). Chaput (1936), concentrated mainly on limestone blocks within an undefined chaotic rock unit, giving an age, ranging from Permian to Cretaceous. He proposed a formation mechanism for this blocky occurrence as large scale faulting without a definition of the mélange. Salomon Calvi (1940) defined for the first time that the basement rock unit around Ankara was represented by 'Dikmen Greywacke Series'.

The Cretaceous ophiolitic melange is initially recognized and named as 'Mesozoique a facies tectonique brouille', for the ophiolite-bearing chaotic rock units around Ankara region by Blumenthal (1941a, b; 1948). That is later named as 'Ankara Mélange' where the Triassic complex and Cretaceous ophiolitic melange were not differentiated and erroneously interpreted as a fragment of Taurides by Bailey and McCallien (1950, 1953). They stated that intensely sheared and boudinaged serpentinized layers called Elmadağ Blocky Series, lying over Dikmen Greywacke Series of Salomon Calvi (1940), show mélange appearance. They suggested a tectonic origin and proposed an age interval of Triassic to Jurassic for this rock assemblage.

The Ankara mélange then renamed and interpreted by various researchers (Erol, 1956; 1961; Boccaletti et al., 1966; Norman, 1972;

1973; Gannser, 1974; Çapan and Buket, 1975; Batman, 1978; 1981; Tekeli, 1981; Akyürek, 1981; Çapan, 1981; Erk, 1981; Ünalan, 1981; Akyürek et al., 1984; Koçyiğit and Lünel, 1987; Koçyiğit et al., 1988; Koçyiğit, 1991; Rojay, 1995; Rojay et al., 2001; 2004).

Bilgütay (1960) agreed with Chaput (1936) about the tectonic mechanism, causing formation of the mélange. She defined the Triassic rock units, for the first time, by fossil evidence around Hasanoğlan region and also stated that Jurassic basal conglomerates unconformably overlie these units. Ketin (1962, 1963) defined the ophiolitic part of the Ankara Mélange as 'Mesozoic Ophiolitic Series'.

Boccaletti et al. (1966) differentiated two different type of rock assemblages within the mélange; (i) thick greywacke series comprising low to highly metamorphosed Paleozoic carbonates with rare ophiolitic blocks, and (ii) ophiolitic blocks emplaced in a chaotic mixture by gravity sliding and slumping, limestones, and flysch type sediments.

Buket (1969) and Çapan and Buket (1975) mapped rock units of the Ankara Mélange around Kalecik region at a scale of 1/25 000. They defined that Aktepe-Gökdere Formation, part of the Ankara Mélange, is ophiolitic melange in nature. The paraautochton matrix material, which is composed of alternated clastics, volcanoclastics, volcanics and carbonates, is named as the 'Ağıltepe Member' of a Barremian-Senonian age, whereas so-called 'Aktepe Member' is composed dominantly of ophiolitic blocks of serpentinites, radiolarites, spilitic basalts, diabases and pelagic limestones. Buket (1969) also described non-deformed, parallel mafic dikes cutting the mélange and a flysch deposit intercalated with mafic volcanic rocks, lying over the mélange.

For the ophiolitic part of the Ankara Mélange, rather than tectonic faulting, Norman (1972) suggested an olistostrome type of flow origin, in an agreement with the opinion of Boccaletti et al. (1966).

In spite of its chaotic nature, Norman (1973) recognized a regular alignment of blocks and lenses within the mélange. Three parallel belts have been described from west to east defined by the abundance of the major constituents as follows: (i) metamorphic mélange belt (the Greywacke Mélange of Norman, 1975), (ii) limestone-blocky mélange belt and (iii) ophiolitic melange belt suggested an olistostromal flow origin.

The metamorphic block melange was described as a chaotic mixture of variably metamorphosed sedimentary, basic-ultrabasic, and pyroclastic rocks in a phyllitic-graywacke matrix and has mostly an olistostromal melange character by Norman (1984). The metamorphic block melange as a whole corresponds to the Upper Karakaya Nappe of Koçyiğit (1991) and the Karakaya Unit of Tüysüz and Dellaloğlu (1992).

Many authors agree on a Triassic age for the metamorphic and limestone belts and a Cretaceous emplacement age for the ophiolitic belt such as Norman (1973), Batman (1978), Çapan (1981), Akyürek (1981), Ünalan (1981). Ünalan (1981) studied the southwestern region of Ankara and suggested that Ankara Mélange is unconformably overlain by the Upper Senonian flysch sequence.

The ages of the limestone blocks of the limestone-blocky melange was described as ranging from Permian through Albian, whereas the depositional ages of the melange matrix range from Liassic through Cenomanian by Norman (1984). The limestone block melange is equivalent of the Lower Karakaya Nappe of Koçyiğit (1991) and of the Sakarya Unit of Tüysüz and Dellaloğlu (1992).

Akyürek (1981) reclassified the Ankara Mélange of Bailey and McCallien (1950) as 'Metamorphics', 'Blocky Series' and 'Eldivan Ophiolite Complex'. The first two units were reported as the Triassic basement of the Ankara region. Akyürek redefined the Eldivan Ophiolitic Melange unit to comprise ultramafics, gabbros, diabase dykes, pillow lavas and pelagic sediments and renamed it as Liassic-Barremian age Eldivan Ophiolite

Complex. The emplacement age has been suggested as Albian-Aptian (Akyürek et al., 1984). The Triassic units, representing the basement of the region, are named as the 'Ankara Group'. The Cenomanian-Campanian 'Kılıçlar Group' unconformably overlay the Eldivan Ophiolitic Complex, and diabase dykes are reported separately in each of these three groups by cross-cutting relationships with their ophiolitic or volcanic host units only.

Koçyiğit and others (1988) described the zone of a chaotic tectono-sedimentary mixture, so called 'Anatolian Nappe' exposed in the İAES belt. The ophiolitic melanges are dated to be older than Campanian in Central Anatolia. Koçyiğit (1991) redivided the rock units exposed around Ankara region, from oldest to youngest, as Upper Triassic slightly metamorphosed tectono-sedimentary mélange ('Karakaya Complex'), Upper Hettangian to Lower Campanian thick transgressive sedimentary sequence ('Ankara Group'), Lower Campanian tectonic mélange with imbricate structure ('Anatolian Complex'), Middle Campanian to Middle Eocene deep marine flysch deposits ('Memlik Group') and terrestrial cover units. The previously named 'Anatolian Nappe' (Koçyiğit and Lünel, 1987), is later renamed as the 'North Anatolian Ophiolitic Melange (NAOM)' by Rojay (1995).

Tüysüz and others (1995) subdivided the Late Cretaceous 'Kalecik Unit' (Tüysüz and Dellaloğlu, 1992) into the 'Upper nappe' comprising mainly of an ophiolitic melange belt, including thick, ordered ophiolite slices, and the 'Lower nappe' which is dominated by volcanic rocks of ocean island and island arc type.

Relative dating of the ophiolitic melanges in Central Anatolia was attempted by bracketing them between dated accretionary basins situated structurally above the accreted ophiolitic slices (Blumenthal, 1948; Norman, 1973; Batman, 1978; Akyürek, 1981; Çapan, 1981; Ünalan, 1981; Koçyiğit et al., 1988; Koçyiğit, 1991; Rojay, 1995; Rojay and Süzen, 1997) or by dating accreted ophiolitic slices situated structurally below (Boccaletti et al., 1966; Batman, 1978) or by the cross-cutting relationships between the ophiolitic slices and dated submarine volcanics (Rojay et al., 2001; 2004).

Rocks of magmatic origin within the ophiolitic melange represent different modes of magmatism, thus providing an opportunity to examine the nature of these magmatic activities during the construction of oceanic lithosphere and ocean floor. From geochemical studies on ophiolites and related volcanics, different tectonic settings and ages were defined (Çapan and Floyd, 1985; Tankut, 1984; 1990; Tankut and Gorton, 1990; Floyd, 1993; Rojay, 1995; Rojay et al., 2001; 2004).

The pillow basalts are reported as cropping out as isolated, detached blocks, or as blocks closely associated with radiolarites, or as lavas alternating with radiolarites and rarely with fossiliferous carbonates in NAOM from Çorum province in the NE, to the Haymana region in the SW (e.g. Akyürek et al., 1984; Boccaletti et al., 1966; Çapan and Floyd, 1985; Floyd, 1993; Rojay et al., 2001; 2004). In some of the studies, the pillow basalts within the Triassic dismembered complex and the Cretaceous ophiolitic melange were analyzed as a member of the same tectonic unit. Therefore, undated pillow basalts and their ophiolitic base, and geochemical studies on these, can not alone define the real picture of the evolution of Central Anatolian ophiolitic melange terrain (Çapan and Floyd, 1985; Floyd, 1993; Tüysüz et al., 1995; Tankut, 1984; 1990; Tankut and Gorton, 1990; Rojay et al., 2004). As a result of the geochemical analyses on the pillow basalts, the presence of Cretaceous seamounts was proven in the region between Dereköy (S of Ankara) and Çankırı (NE of Ankara) during the Mesozoic period (Çapan and Floyd, 1985; Floyd, 1993; Tüysüz et al., 1995; Rojay et al., 2001; 2004). The chemical features suggests that pillow basalts are reflecting an oceanic-island basalt setting (OIB) and may represent the products of an intra-plate hot spot on oceanic crust and enriched MORB setting (Rojay et al., 2004). Similar results are obtained from several researches carried out along the IAES (Çapan and Floyd, 1985; Floyd, 1993; Tankut et al., 1998; Rojay et al., 2001) indicating the presence of OIB-type basalts within the Cretaceous ophiolitic melange in Ankara region (Rojay et al., 2001; 2004).

The Edige and Kalecik massifs in the ophiolitic melange which contain the lower crustal and upper mantle units of the Neo-Tethyan oceanic lithosphere were studied by Tankut and Gorton (1990). They pointed out that the dykes were probably derived from a source between tholeiitic ridge basalts and island arc tholeiites. They interpreted the Edige Unit as a fragment of Tethyan oceanic lithosphere.

Geochemical studies of the ultramafic and basic rocks of the Cretaceous ophiolitic melange revealed a MORB origin for the ophiolitic body, which has subsequently emplaced in a suprasubduction zone setting. Related mafic and basic dyke rocks represent mid-ocean ridge basalts, and also display island arc signatures formed by back arc spreading, in a basin close to the subduction zone where the source magmas of the basic rocks were modified by subduction related contamination (Tankut and Gorton, 1990; Tankut, 1985a, b; 1990).

Basic dykes of ages varying from Cretaceous to Tertiary periods were reported in several previous studies from different localities in Central Anatolia, especially around the Ankara region, such as in Orhaniye (NW of Ankara) (Tokay et al., 1988), in Karapürçek (Ankara) (Chaput 1931; Kleinsorge 1940; Tankut 1985a), in Edige (E of Ankara) (Tankut and Sayın, 1989; Yıldırım, 1974) and in Kalecik (NE of Ankara) (Buket 1969; Çapan 1972; Akyürek et al., 1984; Rojay et al., 2007) regions. The reported characteristics of the dykes in Central Anatolia by various researchers were summarized in the table below (*Table 2.1*). Within this distribution framework, Kalecik dykes shall be the subject of this study.

Table 2.1: Characteristics of dykes reported at various locations by different researchers in Central Anatolia.

DYKES	Trend	Length (m)	Width (m)	Lithology	Minerals	Texture	Age	References
Orhaniye (Ankara)	------	500-630	1-3	Syenite (?)	------	------	post-Early Paleocene-pre-Early Eocene	Tokay et al., 1988
Karapürçek (Ankara)	Set1: N20E Set2: N15W	------	10-12	Dacite-Rhyolite	Qtz, rutile, opal, crystallized alunite, hornblende, alunitized feldspar	------	post-Miocene	Chaput, 1931; Kleinsorge, 1940; Tankut, 1985a
Edige (Ankara)	NE-SW	1-100	20-30	Basic (few dioritic and felsic)	Clino-pyroxene (augite, diopsite), hornblende, plagioclase, opaque	Doleritic	Late Cretaceous	Tankut and Sayın, 1989; Yıldırım, 1974
Kalecik (Ankara)	NE-SW	0.3-8	0.5-3	Analcite basalt Augite-analcite Diabase Lamphropyre Diorite	Augite, analsite, feldspar, boitite, apatite, opaque	------	post-Campanian	Buket, 1969; Buket and Çapan, 1972; Akyürek et al., 1984
							post-Paleocene – pre-Miocene	Rojay et al., 2007
Karakaya (Çorum)	Set1: N75E	------	6-20	Tholeiitic +/- (olivine) basalt	Olivine, plagioclase (labradorite), pyroxene, augite	Subofitic flow structure	pre-Miocene*	Demirer et al., 1992; Özçelik and Savun, 1993 Rojay et al., 2007
	Set2: N05W	------	6-20	Hybritic basalt	Plagioclase, clino-pyroxene, biotite	Intersertal	post-Eocene – pre-Miocene	
Laçin (Çorum)	N60E N70W	------	------	Hbd-Bio Andesite	------	Microlitic matrix, porphyritic	------	Özçelik, 1994

*commented from the related references and maps

The dykes around the Kalecik area were variously defined by several researchers as;

- slightly metamorphosed dioritic intrusions intruded in the members of the Late Cretaceous 'Aktepe-Gökdere Ophiolitic Formation' and Campanian 'Bulduktepe volcanic and intrusive rocks' (Buket, 1969; Çapan and Buket, 1972). Buket (1969) reported that intrusive diorites are dense and compact, generally greenish, fine to medium-grained rocks with almost equigranular texture. The intrusions are slightly metamorphosed. He also reported the petrographic characteristics and constituents of the dykes (Table 2.1).

- diabase intrusions cutting the formations of Triassic 'Ankara Group', gabbro and diabases seen as dykes within the Albian-Apsian aged products of Lower Cretaceous 'Eldivan Ophiolitic Complex' and a dyke-sill system within the volcanite member of Cenomanian-Campanian 'Kılıçlar Group' in close relation with spilite and diabase pillow structures (Akyürek et al., 1984),

- doleritic to microgabbroic dyke swarms intruded in the Edige and Kalecik ophiolitic massifs at all structural levels of which petrographic characteristics were reported (Table 2.1) (Tankut, 1985a, b; 1990; Tankut and Gorton, 1990),

- lamprophyre dykes within the Cenomanian-Turonian sequence (Tüysüz and Dellaloğlu, 1992; Tüysüz et al., 1995). According to Tüysüz and others (1995), the dykes have a porphyritic texture with pilotaxitic groundmass. Alkali magmatics represented by pyroxene and sometimes leucite phenocrysts bearing basalts, basanites and lamprophyres.

- dolerite, plagiogranite and microgabbroic intrusions crosscutting the several lithologies of the ophiolitic assemblage at all structural levels (Dilek and Thy, 2006).

- Basaltic dykes cross-cutting the Cretaceous ophiolitic melange and Paleogene units (Rojay et al., 2007).

Furthermore, to define the tectonic evolution of the terrain, paleomagnetic analyses and kinematic studies were carried out by several researchers in the region (e.g. Piper et al., 1997; Gürsoy et al., 1999; Kaymakçı, 2000; Kaymakçı et al., 2003a, b; Kissel et al., 2003) indicating a counter-clockwise rotation.

Kaymakçı and others (2003a, b) have provided the first palaeomagnetic results relevant to the evolution of the Çankırı Basin and unravel the paleostress history of the southern part of the Çankırı Basin, including the Kırşehir Block, and to constrain the timing of each deformation phase. Palaeomagnetic data in combination with palaeostress data and anisotropy of magnetic susceptibility orientations were utilized for the Ω-shaped Çankırı Basin (Kaymakçı, 2000; Kaymakçı et al., 2000). The results reveal clockwise rotations in the northeast and counter-clockwise rotations in the west and southeastern corner of the basin. It is proposed that the Ω-shape of the Çankırı Basin was the result of the indentation of the Kırşehir Block into the Sakarya Continent during the northwards migration accompanying the closure of Neotethys (Kaymakçı, 2000). It appears that the indentation started prior to Eocene and ended before Middle Miocene times.

2.2. Tectonic Setting of North Central Anatolia, Turkey

Turkey is one of the important segments of the Tethyside orogenic collage and has a complex structure formed by the amalgamation of continental blocks (micro-continents) along several ophiolitic suture zones as a result of the closure of different branches of the Neo-Tethyan Ocean during Late Cretaceous to Miocene time which were once part of Laurasia and Gondwana (Şengör and Yılmaz, 1981; Robertson and Dixon, 1984; Şengör et al., 1984).

Turkey is broadly divided into three tectonic belts from north to south; the Pontides, Anatolides and the Taurides (Ketin, 1966). The Pontides are the eastern continuation of the Rhodope–Pontide fragments including the Sakarya Continent (Şengör and Yılmaz, 1981; Şengör et al., 1984). The Anatolides are the metamorphic massifs that include the Menderes Massif and the Kırşehir Block (Şengör and Yılmaz, 1981) and the southern fragments are termed as the Taurides (Ketin, 1966) (Figure 1.1).

The Sakarya Continent and the Kırşehir Block each had a different geological evolution from Late Paleozoic to Mesozoic times (Şengör and Yılmaz, 1981; Şengör et al., 1984). The Sakarya Continent was separated from the rest of the Pontides by the Intra-Pontide Ocean during Early Mesozoic times (Robertson and Dixon, 1984), while the Kırşehir Block was separated from the Taurides by the Intra-Tauride ocean. Further, it has been proposed that the two microcontinents, namely the Sakarya Continent and Kırşehir Block, were separated from each other by the main branch of the Tethys Ocean throughout the Mesozoic and both drifted from equatorial latitudes in Late Cretaceous times to their present positions. Rifting and drift of continental fragments detached from the Gondwanian margin created new basins in several time periods (during Late Permian, Triassic, and Early Cretaceous).

At the end of the Cretaceous, Eurasia and Africa initiated a north–south convergent movement. Along the Anatolian transect, the oceanic basins progressively declined first by subduction and subsequently by obduction onto the neighbouring continents. The northern Neotethys closed definitely between the Campanian and the Late Paleocene (Okay and Tüysüz, 1999). The Pontic belt represents the southern margin of the Eurasian plate which collided with the Anatolian microcontinent when the North Neotethyan Ocean sutured in Late Cretaceous–Paleocene times (Okay and Tüysüz, 1999). The Anatolian block separated from the Pontides by the İzmir–Ankara–Erzincan suture (IAES) belt is composed mainly of ophiolitic nappes and ophiolitic melanges of Late Cretaceous age (Şengör and Yılmaz, 1981) (Figure 1.1). All the tectonic units derived during this period were unconformably overlain by Late Paleocene, Early Eocene and the Lutetian shallow marine deposits. Although the timing of collision and amalgamation of these two micro-continents along the İzmir–Ankara–Erzincan Suture (IAES) belt is debated, it is generally constrained within the Late Cretaceous to Early Tertiary interval (Şengör and Yılmaz, 1981).

A well-preserved remnant of an accretionary forearc basin, the Çankırı basin, formed during the convergent destruction of the Neo-Tethys in Turkey. It is located in a very unique area in Turkey within the IAES belt and between the Sakarya continent in the north and the Kırşehir block in the south, where different continental and ophiolitic units met from Upper Cretaceous up to Late Miocene. Therefore, it enables us to study the subduction and collisionary processes as well as the post-collisional history of the region through stratigraphical and structural analyses. Understanding of the tectonic development of the Çankırı basin provides valuable up-to-date information to unravel the tectonic development of the Anatolian block, which may help to understand the Alpine orogenic system (Kaymakçı, 2000; Kaymakçı et al., 2001).

The study area is located on the western margin of Çankırı basin, in the Kalecik, Ankara region. In the Ankara region, two tectonic belts of dissimilar age, structure and origin are superimposed in a complex structural pattern, which consists of Late Triassic Karakaya and Early Tertiary İzmir-Ankara-Erzincan Suture belts (Şengör and Yılmaz, 1981). Therefore, Ankara region (Central Anatolia) is one of the key regions in Turkey where all of the evolutionary events of the Tethys are documented as imbricated piles (Figure 1.1). In order to get a better understanding of the region and its evolution, a brief tectono-stratigraphic outline of the basement rocks and sedimentary fill of the forearc sequences of the study area is given first.

CHAPTER 3

TECTONO-STRATIGRAPHY

The region consists of allochthonous and relatively autochthonous units. The allochthonous units are the members of the Cretaceous accretionary prism, which are composed of the Triassic Karakaya Complex and the Cretaceous ophiolitic melange (North Anatolian Ophiolitic Melange: NAOM). The autochthonous Post-Cretaceous units exposed in the region are the Paleogene Granitoid (Kırşehir Massif), Late Cretaceous-Paleogene units, pre-Miocene Dykes, Miocene units, Pliocene clastics and Quaternary clastics, respectively (Figure 3.1, 3.2, 3.3, 3.4 and 3.5).

3.1. Allocthonous Units

3.1.1. Triassic Karakaya Complex

Around the Çankırı Basin, Triassic is represented by the slightly metamorphosed Karakaya Complex, which is found as one of the tectonic slices of the imbricated tectonic belt over the Paleozoic aged metamorphics forming the stratigraphic basement of this imbricated structure. It is the equivalent of the Karakaya Formation (Bingöl et al., 1973), Mixed Series (Çalgın et al., 1973), Ankara Group (Akyürek et al., 1984), Karakaya Complex (Koçyiğit, 1987; Yılmazer, 1994), Karakaya tectonic unit (Tüysüz and Dellaloğlu, 1992).

Triassic Karakaya Complex is exposed in the west of Kalecik as a tectonic nappe which is thrusted over the Cretaceous ophiolitic melange and unconformably overlained by Miocene and Pliocene clastics (Figures 3.1 and 3.4).

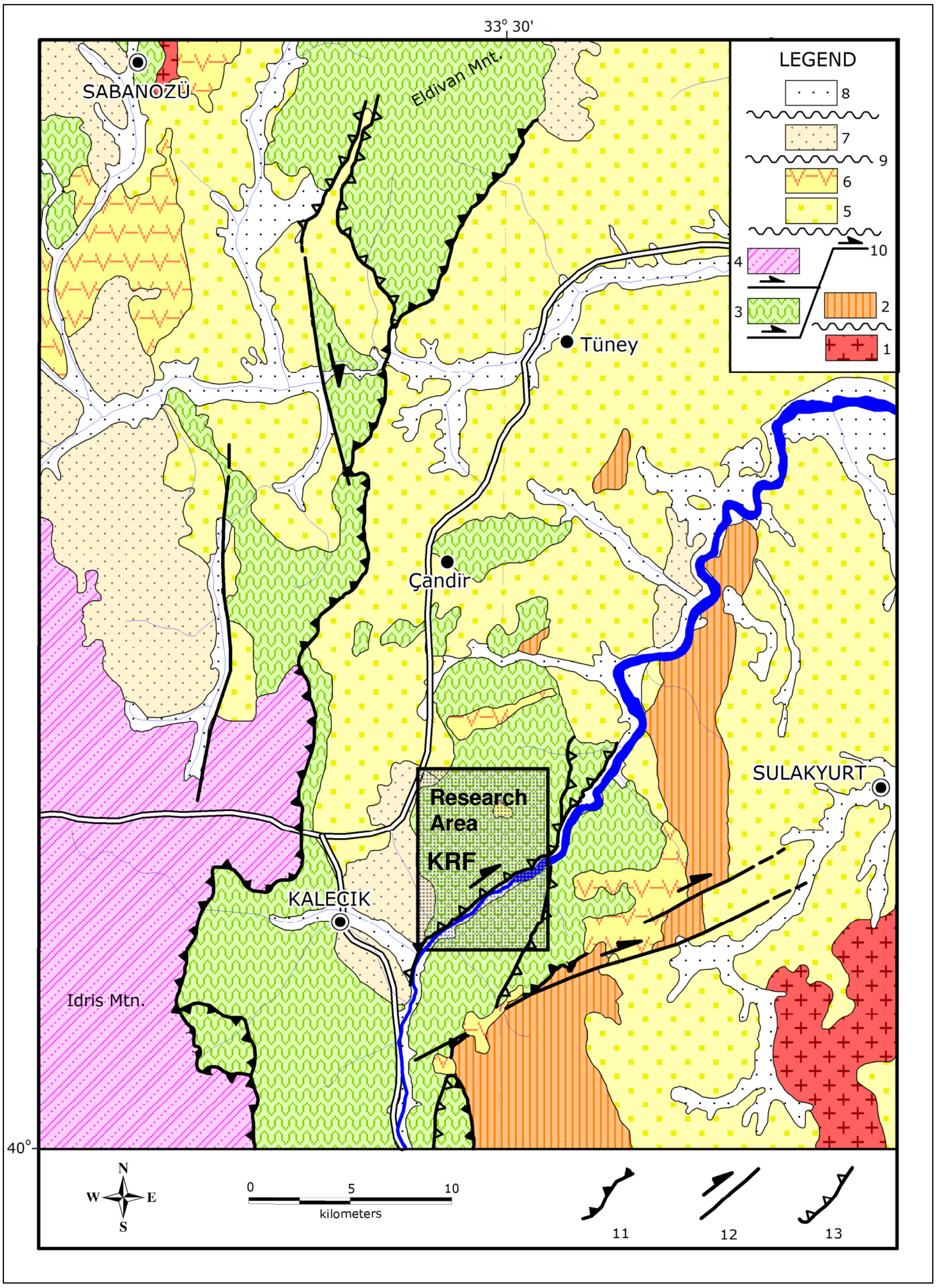

Figure 3.1: Geological map of the region around Kalecik (simplified and modified from the 1:500,000 scaled geological map of Turkey, Mineral Research and Exploration, 2002. The dashed rectangle shows the location of the study area. 1. Kırşehir Massif (Paleogene Granitoid), 2. Paleocene-Eocene units, 3. Cretaceous Ophiolitic Melange, 4. Triassic Karakaya Complex, 5. Miocene clastics, 6. Miocene volcanics, 7. Pliocene clastics, 8. Quaternary units, 9. Unconformity, 10. Overthrust, 11. Thrust fault, 12. Strike-slip fault, 13. Reverse fault. KRF: Kızılırmak River Fault.

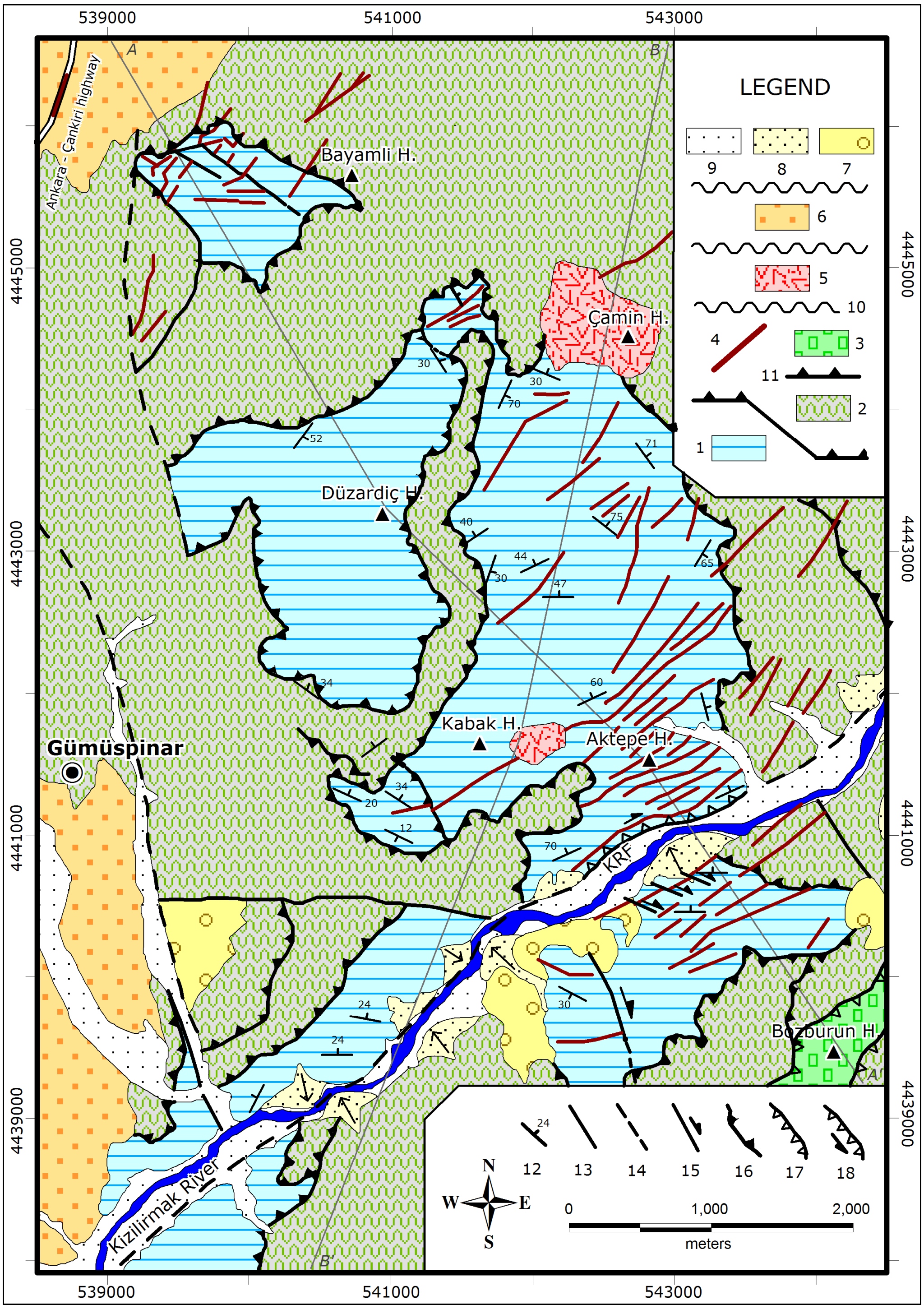

Figure 3.2: Geological map of the study area. 1. Upper Cretaceous radiolaria bearing limestone/radiolarite, 2. Cretaceous ophiolitic melange, 3. Upper Cretaceous pelagic clayey limestone, 4. Basic dykes, 5. Miocene volcanics, 6. Pliocene clastics, 7. Quaternary terraces, 8. Aluvial fan deposits, 9. Alluvium, 10. Unconformity, 11. Overthrust, 12. Dip/Strike, 13. Fault, 14. Probable fault, 15. Strike-slip fault, 16. Thrust fault, 17. Reverse fault, 18. Strike-slip fault with reverse component, KRF: Kızılırmak River Fault.

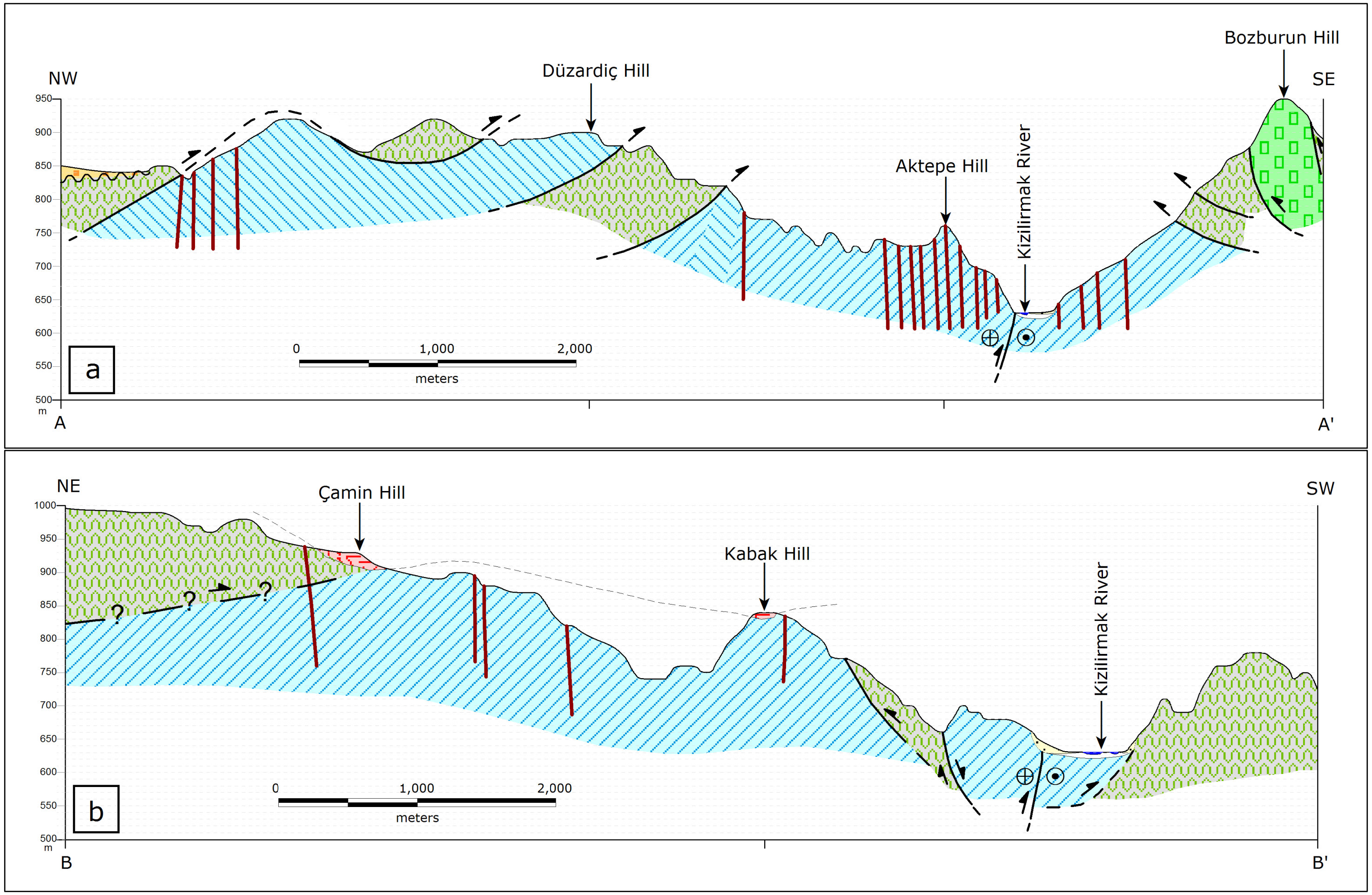

Figure 3.3: Sketch geological cross sections along profiles on Figure 3.2. a) Sketch cross section along profileA-A', b) Sketch cross section along profile B-B' (for explanation see Figure 3.3).

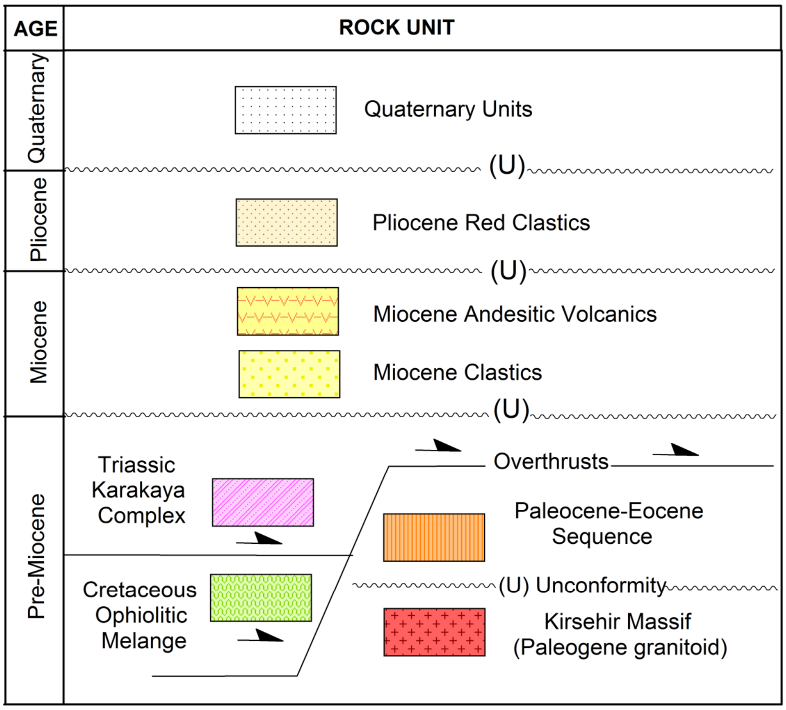

Figure 3.4: Tectono-stratigraphic columnar section of the Kalecik region.

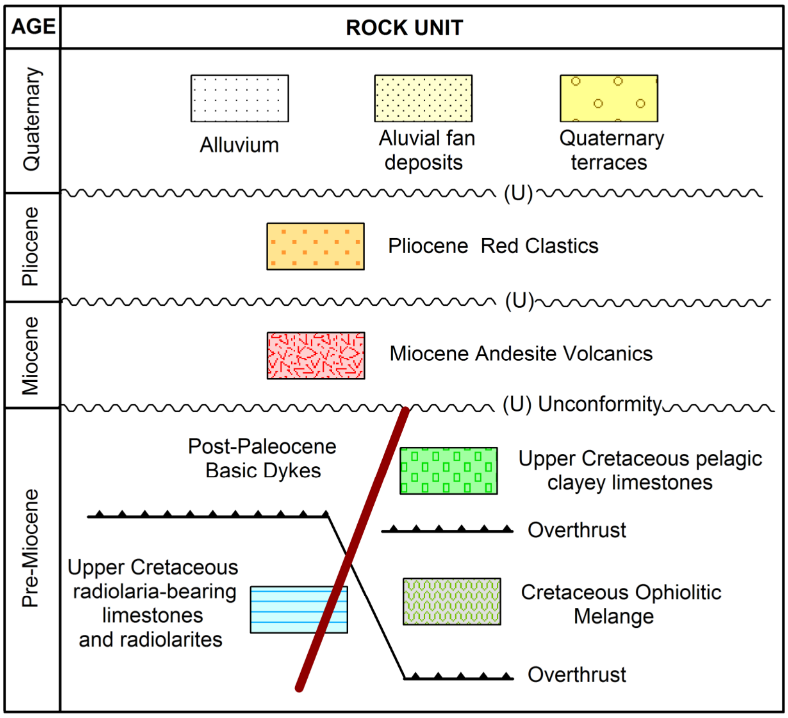

Figure 3.5: Tectono-stratigraphic columnar section of the study area.

It unconformably overlies the Paleozoic aged metamorphic basement and developed on a Permian aged shallow neritic carbonate platform succession (Koçyiğit, 1987). It is overlained unconformably by the Jurassic-Cretaceous sequences (clastics and carbonates) of Liassic-Aptian age (Akyürek et al., 1984; Koçyiğit, 1987).

The Karakaya complex is characterized by blocks of intensely deformed and dismembered pre-Mesozoic low grade metamorphics, Carboniferous to Permian shallow marine neritic platform carbonates, and blocks of the later deposited Triassic flysch type sequences and the metamorphosed derivatives of these (phyllite and schist, meta-volcanites, meta-ultramafites) that are all partially set in a matrix of graywackes (Bingol et al., 1973; Çalgın et al., 1973; Akyürek et al., 1984; Koçyiğit, 1987; Yılmazer, 1994; Okay and Göncüoğlu, 2004).

The age of the complex which was deposited in a tectonically active deep sea environment with a syncronous volcanism, is accepted as Triassic according to the fossils fauna of the limestone bands in the unit (Akyürek et al., 1979; 1980; 1984; Tüysüz and Dellaloğlu, 1992).

The region stayed under the influence of the evolution of Paleotethys which improved during Permo-Carboniferous and continued its evolution during Triassic (Akyürek et al., 1984). The region, being a carbonate platform in Permian, in post Permian-Triassic time by fracturing left its place to a short-lasting, narrow but long and deep sea. This sea, of which the remnants can be observed all around the North Anatolia, is known as Karakaya Sea (Okay and Göncüoğlu, 2004). These rocks are the oldest products of the rapidly deepening Karakaya basin, which opened and closed as a marginal basin of Paleo-Tethys during the Triassic. The Karakaya Sea, which is an important part of Cimmerides Orogeny, was closed at the end of Triassic (Akyürek et al., 1984). As a result, the sedimentary units, volcanites and blocks gained a complex structure and the metamorphosed remnants, formed the basement of the Sakarya continent (Akyürek et al., 1984). The Kırşehir massif and the Karakaya units acted as the amalgamated basement during the Neo-Tethyan evolution of the region.

3.1.2. Cretaceous Ophiolitic Melange Belt

a. General definition

Cretaceous is represented by an ophiolitic melange, a volcanic-volcanoclastic-sedimentary alternation of deposits containing ophiolitic blocks and slices with a flysch type succession. The Cretaceous ophiolitic melange, which is erroneously counted together with the Triassic Karakaya Complex as a single unit and named as the “Ankara Melange” by Bailey and McCallien (1953), crops out as a significant tectonic belt in Central Anatolia along the İzmir-Ankara-Erzincan Suture (IAES) zone. As a general definition, the Cretaceous Ophiolitic melange is a chaotic tectono-sedimentary mixture of various blocks of different age, origin and facies embedded in an intensely sheared, brecciated and partially mylonitized matrix associated with Cretaceous clastic basins (Koçyiğit and Lünel, 1987; Koçyiğit et al., 1988; Koçyiğit, 1991; Rojay, 1995; Rojay and Süzen, 1997; Rojay et al., 2001; 2004). In other words, it is a well-preserved pre-Campanian remnant of the subduction complex accreted at the active margin of Mesozoic North Neo-Tethys (Koçyiğit et al., 1988). It is mainly composed of blocks derived from the oceanic crust, epi-ophiolitic pelagic units, the active continental margin units, subduction related volcanics and flysch type sequences belonging to related fore-arc basins.

b. Distribution and stratigraphic position

The Cretaceous ophiolitic melange units were exposed in a N-S trending tectonic belt in the Kalecik region (Figure 3.1). They are seen as tectonic slices which were thrusted over the Paleocene-Eocene units and thrusted by the Triassic Karakaya complex in the Kalecik region (Figure 3.4).

Around the Kalecik region, the Cretaceous melange units can also be observed as thrusted onto the Miocene clastics.

However, at places where the original stratigraphical contacts are preserved, it tectonically overlies the Jurassic-Cretaceous sequences and is unconformably overlained by the Upper Cretaceous-Paleogene sequences (Akyürek et al., 1984; Koçyiğit et al., 1988; Koçyiğit, 1991). In fact, there are no direct exposures of the Jurassic-Cretaceous sequences in the Kalecik region. However, various sized Jurassic aged limestone blocks of Liassic-Aptian age were recorded within the Cretaceous ophiolitic melange in the Kalecik region. These units are generally located as a tectonic slice between the Karakaya Complex above and Cretaceous ophiolitic melange below due to the Upper Cretaceous thrusts and most of the Jurassic-Cretaceous sequences cropped out as blocks in Cretaceous ophiolitic melanges and as olistoliths in Upper Cretaceous basins (Rojay and Süzen, 1997).

The study area is located on this ophiolitic melange belt in which the blocks of different lithologies belonging to this belt crop out as tectonic slices on each other (Figures 3.2, 3.3 and 3.5). Thrusting of ophiolitic melange over Paleocene and younger formations, is obscured by tuffaceous cover of Miocene age and further tectonic movements in the study area and around the Kalecik region (Figure 3.6).

c. Components

In the observable lowermost parts of the Cretaceous ophiolitic melange, of which the stratigraphic base cannot be seen, either thick and regular ophiolite slice or tectonic mélange is found. It contains wide variety of sizes and kinds of blocks which can be grouped as:

i) Ophiolitic and related basaltic blocks

They include intensely sheared, highly fractured and altered rock fragments of almost all the magmatic members of an ophiolite suit, such as dark green-gray peridotites, gabbros, gray-dark purple diabases, serpentinites, serpentinized ultramafics, related mafic volcanics (spilites, pillow basalts) and dyke rocks (Figure 3.7).

The pillow basalts are found as isolated, detached blocks or as blocks closely associated and alternating with red-green colored, intensely folded-fractured, thin-bedded radiolarites (Rojay et al., 2004). They are mostly basalts and basaltic andesites with radial cooling joints. The vesicles in pillows are generally filled with calcite, zeolite and quartz and the interstices between the pillows were filled by Globotruncana-bearing red pelagic limestones, pelagic mudstones or tuffs (Tüysüz et al., 1995). They were either produced by island-arc or hot-spot magmatism (Tüysüz et al., 1995; Gökten and Floyd, 2007).

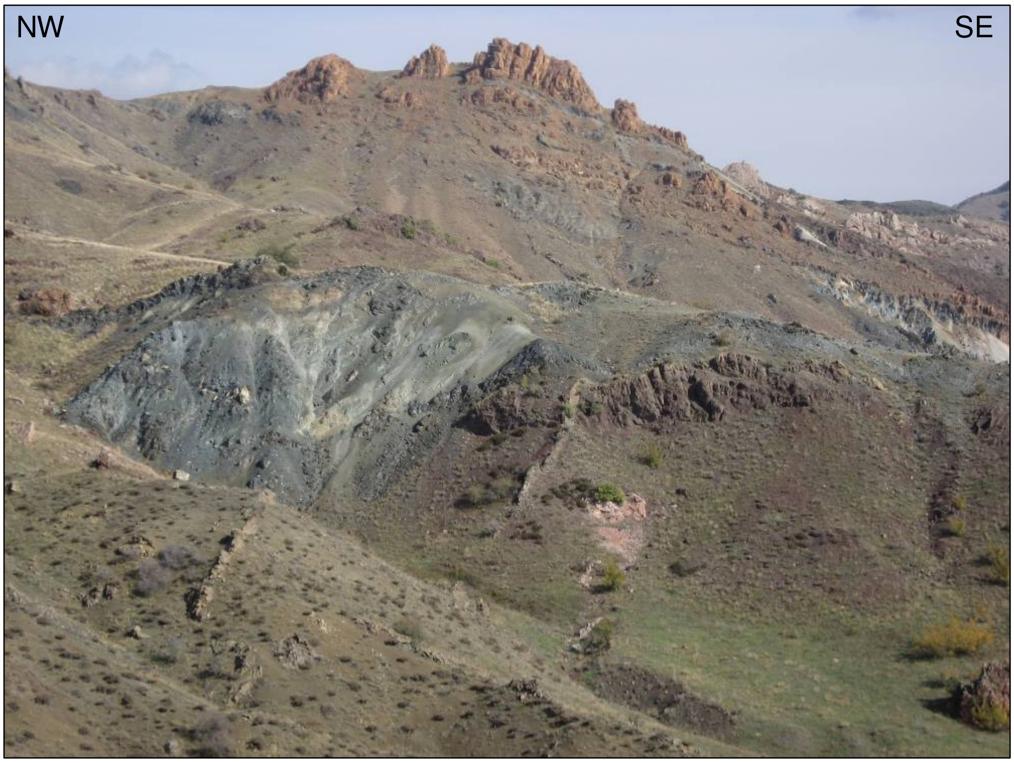

Figure 3.6: General view of the Cretaceous Ophiolitic Melange, east of Kalecik.

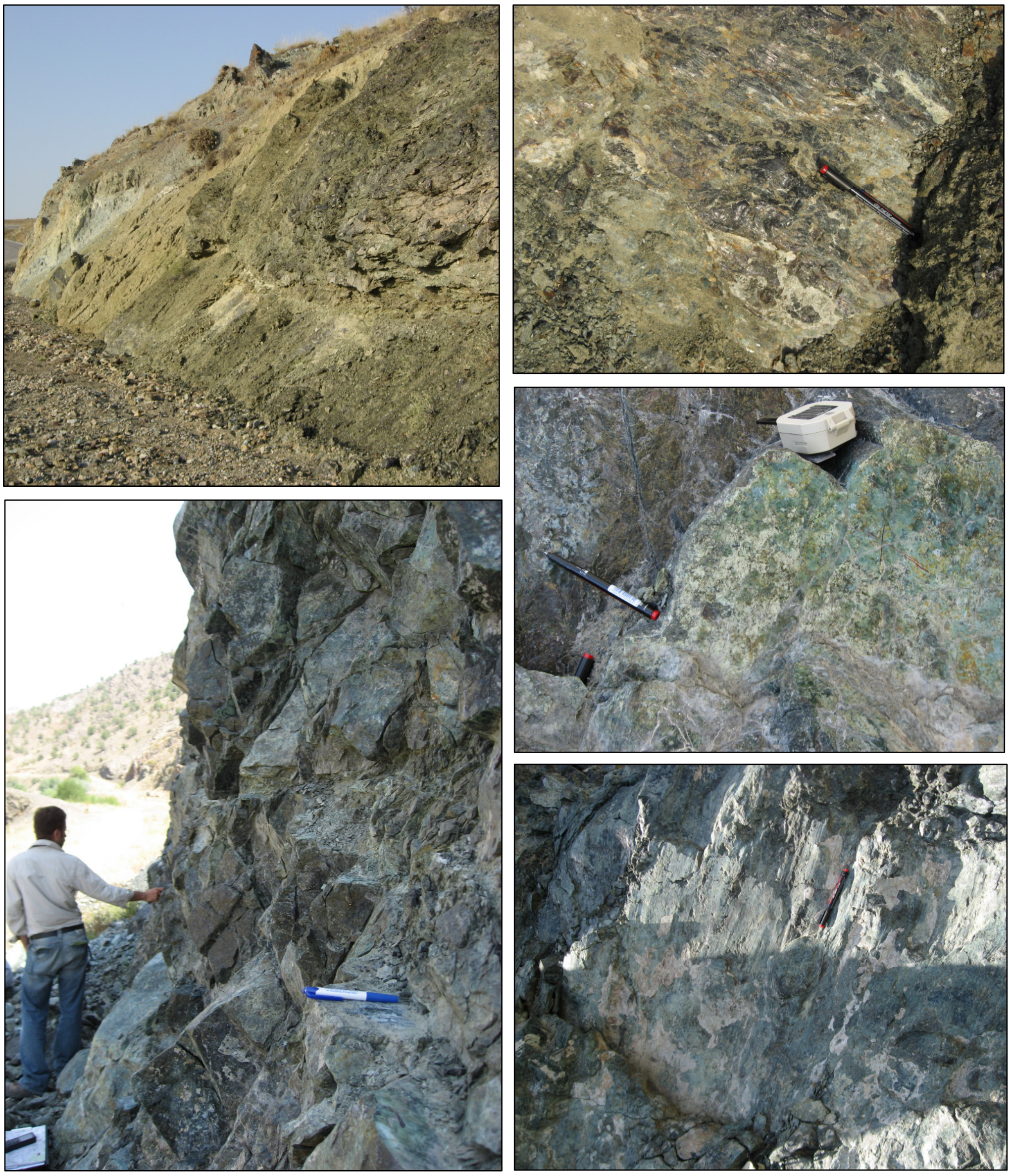

Figure 3.7: Serpentines with faulted, polished, shiny surfaces, east of Kalecik.

The mélange is also reported to contain few isolated ordered ophiolite slices, which are considered to be preserved oceanic lithosphere (Akyürek et al., 1979; 1980; 1984; Norman, 1984; Tankut, 1985b; 1990; Tankut and Sayın, 1989; Tankut and Gorton, 1990). The lowest level of these ophiolite slices which can be seen is composed of dunite, harzburgite, peridotite and pyroxenite. Above these, gabbro and diabase are seen as the second part of ordered ophiolitic series. Transitions are seen from gabbros to banded amphibolites and they pass into serpentinites.

ii) Jurassic-Cretaceous limestone blocks

The Upper Jurassic-Lower Cretaceous carbonate blocks of neritic limestones, gray-beige-cream colored, folded and fractured, thin-medium bedded, cherty and argillaceous carbonates interbedded with some olistostromal levels are very common (Figure 3.8).

iii) Epi-ophiolitic sedimentary (radiolarite) blocks

These are pelagic blocks of intensely folded and fractured radiolaria bearing red-green colored Mesozoic siliceous limestones, white-cream colored Cretaceous pelagic limestones and cream-beige colored, thin bedded Malm-Cretaceous pelagic carbonates (Figure 3.9 andFigure 3.10).

d. Matrix

Within this mélange belt, there are 'tectonic melange' parts in which the blocks came together by tectonic contacts or with an intensely sheared, mylonitized and brecciated matrix composed of red to dark green ophiolitic breccias so called arenaceous ophiolitic matrix (Figure 3.11).

d. Related basins

The base of the ophiolitic melange is always tectonic whereas the top is often marked by the transgression of sedimentary sequences of Cenomanian-Turonian or by unconformably overlying sedimentary sequences of Santonian-Maastrichtian (Koçyiğit et al., 1988; Rojay and Süzen, 1997).

In the lowermost part of the mélange, oceanic materials such as ophiolitic and epi-ophiolitic rocks are the dominant lithologies.

Figure 3.8: Radiolaria bearing limestone blocks within intensely sheared ophiolitic matrix, east of Kalecik.

Figure 3.9: Intensely deformed radiolarite blocks, east of Kalecik.

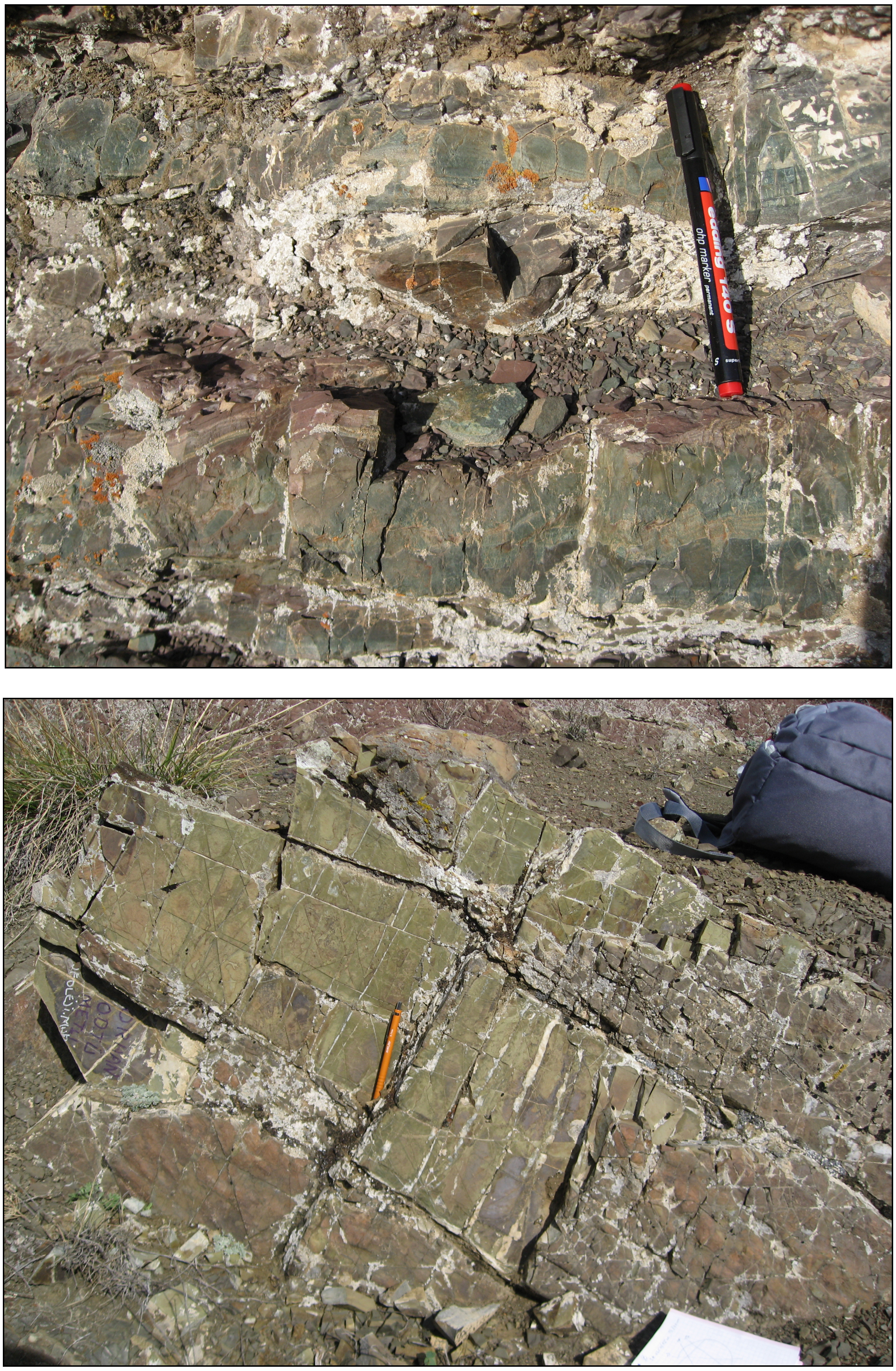

Figure 3.10: Close-up view of red-green thin-medium bedded radiolarites, east of Kalecik.

Figure 3.11: Intensely sheared sedimentary ophiolitic matrix, east of Kalecik.

The most common lithologic assemblage of Cretaceous, which is transitional with these olistostromal parts of the ophiolitic melange, containing the melange and serves as a matrix for it and mostly sliced together with it, is mainly composed of Cenomanian-Turonian aged pelagic micritic carbonates, lava, tuff, agglomerate and thin clastic alternation. Within this succession, there are a lot of syn-depositional ophiolite and ophiolitic melange blocks.

The Cenomanien-Turonian sequences that were accumulated on the dynamic accretionary ophiolitic melange prism along active subduction zone, consist of alternating red-white-greenish colored, thin bedded pelagic micritic limestone, thin tuff intercalations and clastics with Malm-Lower Cretaceous limestone olistoliths/blocks. These tuff intercalations turn into agglomerate levels towards the top and locally become dominant together with thick levels of lava flows representing a Late Cretaceous magmatic belt.

The magmatic rocks within this sequence are andesitic and basaltic lavas with mostly in pillow structures and their pyroclastics (*Figure 3.12*). Besides there are a great amount of intrusive magmatites intruded into the unit. These are andesitic dykes and sills, little granodioritic stocks or rarely lamprophyre dykes.

In almost all levels of this above succession, there are ophiolitic blocks and slices, which are represented by a matrix composed of a sedimentary and volcanic rock alternation and blocks within this matrix.

e. Age of initiation and emplacement

According to Akyürek et al. (1979, 1984) and Akyürek (1981), these ophiolites were emplaced in Early Cretaceous (Albian-Aptian) at north Central Anatolia and most of the olistoliths and olistostromes are formed as a result of later transportation of it by mass flows and gravity slides during different times into the Cenomanian-Campanian age flysch sequences. Çapan and Buket (1972) suggested that emplacement of ophiolites took place during early stages of Upper Cretaceous in the region by the pouring out of magma into a wet flysch-like sedimentary matrix and mixing up with it, thus yielding a para-autochthonous melange structure. They related the highly chaotic structure of the melange to the west to east transportation due to tectonic forces in which orogenic gravity and thrusting were also involved.

The geochemical properties of the magmatites shows that most of these are derived from an ensimatic island arc, a part of these are derived from oceanic islands (Tüysüz et al., 1995; Rojay et al., 2001; 2004; Gökten and Floyd, 2007). It is the equivalent of Cenomanian-Campanian aged Cengizpinar vulcanite member of Akyürek et al., 1984. It is stated that the dykes spreaded as a product of deep sea volcanism and cut the units up to Maastrichtian (Akyürek et al., 1984).

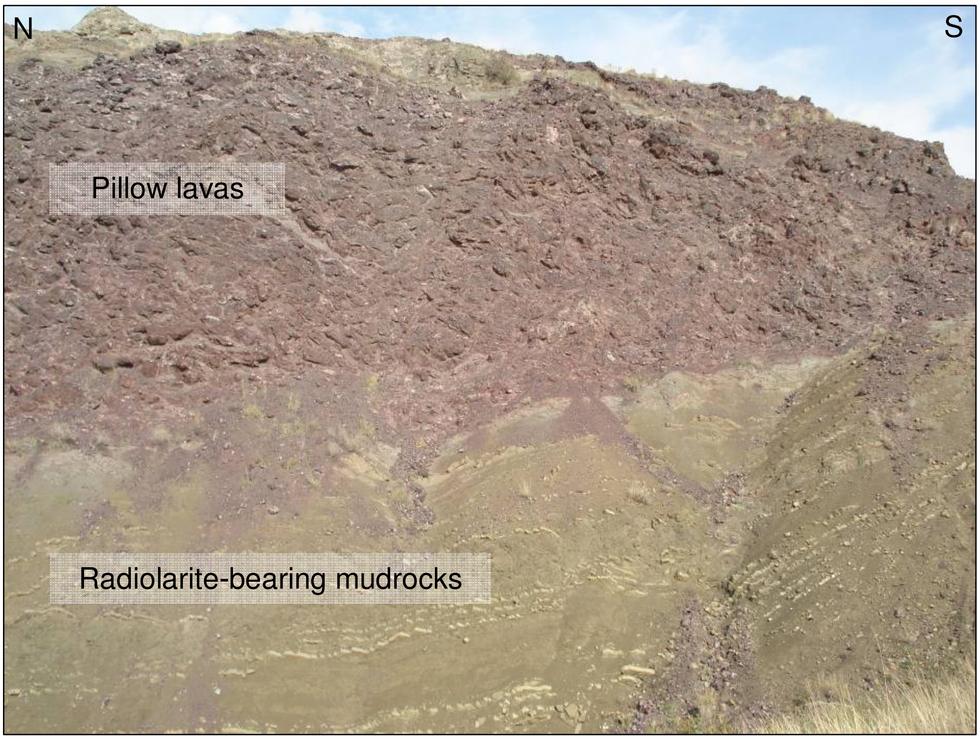

Figure 3.12: Pillow lavas on top of radiolarite bearing mudrock sequence, along the Kızılırmak River east of Kalecik.

The fossils found in the sedimentary matrix of the mélange, indicate a Cenomanian-Maastrichtian age for the mélange (Tüysüz and Dellaloğlu, 1992). On the other hand, the ages from the infillings of the vesicles in pillow basalts reveal an age of evolution broadly between Callovian-Barremian and the possible reefal build-up as Late Barremian-Early Aptian in age (Rojay et al., 2001; 2004; 2007).

f. Correlation

The Cretaceous ophiolitic melange can be regarded as the equivalent of the ophiolitic part of the Ankara mélange (Bailey and Mc.Callien, 1950), the Mesozoic Ophiolitic Series (Ketin, 1962), the Aktepe Ophiolitic Formation (Buket, 1969), the Irmak Formation (Norman, 1972), the Aktepe-Gökdere Formation (Çapan and Buket, 1975), Yapraklı Formation (Birgili et al., 1975), Dereköy Formation (Batman, 1978; 1981), Ophiolitic Melange (Ünalan, 1982), Kırıkkale Melange (Özkaya, 1982), Eldivan Ophiolite Complex, Hisarköy and Karadağ Formations (Akyürek et al., 1984), Anatolian Nappe or Anatolian Complex (Koçyiğit and Lünel, 1987; Koçyiğit et al., 1988; Koçyiğit, 1991), the Upper Nappe of the Kalecik Unit (Tüysüz and Dellaloğlu, 1992) and the North Anatolian Ophiolitic Melange (NAOM) (Rojay, 1995; Rojay et al., 2001; 2004; 2007).

The Cenomanian-Turonian flysch sequences can be thought as the equivalent of the Ağıltepe member (Buket, 1969; Çapan and Buket, 1975), a part of the Gökçeviran Formation (Ünalan, 1982). The volcanics intercalated with these sequences can be thought as the equivalent of Bulduktepe Formation (Buket, 1969; Çapan and Buket, 1975), Ilıcapınar, Bölükdağ and Yahsihan Formations (Norman, 1972), Mart Formation (Akyürek et al., 1979), a part of the Gokceviran Formation (Ünalan, 1982), Yaylaçayı Formation (Yoldaş, 1982), the Cenomanian-Campanian aged Cengizpınar volcanite member (Akyürek et al., 1984) and the lower nappe of the Kalecik unit (Tüysüz et al., 1995).

g. Tectonic setting

The abundance of the ophiolites and mélange blocks within the micritic limestones and volcanics proves that the Cretaceous units were deposited in a dynamic accretionary prism in front of a subducting oceanic slab in deep sea close to an eruptive volcanism. In fact, this situation was explained by the subduction of the Neo-Tethyan Ocean towards the north underneath the Sakarya Continent beginning from

Cenomanian. Southern margin of the Sakarya Continent turned into an active margin at the beginning of the Late Cretaceous by the inception of a north-dipping subduction of the Neo-Tethyan ocean floor (Şengör and Yılmaz, 1981). The environment, in which the mélange developed, was regressively shallowed from place to place during the Late Maastrichtian.

The oceanic crust material were formed in the northern part of the region and emplaced by thrusts as a result of the subduction (Akyürek et al., 1984). The Cretaceous ophiolitic melange emerged with various contemporaneous dynamic arc trench basins and progressively comixed since Cenomanian (Rojay and Süzen, 1997). The great variety of lithologies derived from all these different but related environments, are found together within the mélange as piles imbricated with each other forming a south-vergent imbricate structure. The ophiolitic melange is always extremely complex due to the progressive Cretaceous-Paleogene tectonic recycling, imbrication, lateral/strike-slip deformation and/or rotation of blocks in the accretionary prism due to the compressional regime since the Upper Cretaceous around the region.

3.2. Autocthonous Units

3.2.1. Central Anatolian Crystalline Complex (Kırşehir Massif)

a. General definition

The Central Anatolian Crystalline Complex (CACC) (Göncüoğlu et al., 1992) is located to the south of the Northern Branch of NeoTethys (Şengör and Yılmaz, 1981) within the metamorphosed northern extension of the Tauride-Anatolide platform. The CACC (i.e., Kırşehir Massif (Seymen, 1985)) comprises medium to high grade metamorphic rocks of Paleozoic-Mesozoic age, overthrusted by Upper Cretaceous ophiolites and intruded by Paleogene age granitoids. In the Kırşehir block, the granitoids are large plutons which form a north-west convex arcuate belt and cropped out along the southwestern tip of the Çankırı basin (represented by the Sulakyurt granitoids).

b. Distribution and stratigraphic position

The Kırşehir Massif granitoids are exposed in the south of Sulakyurt in the region, lie within the northernmost part of the Kırşehir block and directly underlies the southern part of the Çankırı basin. The Cretaceous ophiolitic nappes were thrusted from north towards south on these units (Figures 3.1 and 3.4). Both the Cretaceous ophiolites and the metamorphic basement are intruded by Upper Cretaceous-Paleogene age arc granites (Ayan, 1963; Ataman, 1972). The Upper Maastrichtian-Paleocene age granodiorite intrusion (Paleogene Granitoid) displays a distinct crosscutting relationship with the Middle Campanian to Early Paleocene sequences.

c. Lithology

The rocks of Kırşehir massif is defined by Seymen (1985) as granulite, gneiss, schist at the base and alternating with these schists passes to meta-quartzite, calc-schist, marble and chert towards the top. The granitoid is composed of intensely altered micro-phaneritic to phanaritic hornblende granite, granodiorite, diorite, syenite and monzonite (Erler et al., 1991; Akıman et al., 1993). It also includes various felsic dykes ranging from aplite to vitric rhyolite.

d. Age of initiation and emplacement

The undated highly metamorphic rocks of the Kırşehir massif have possibly been formed by the metamorphism of a pre-Mesozoic succession of an Atlantic-type continental margin developed on a Pan-African basement (Tüysüz and Dellaloğlu, 1992), which were later intruded by Paleogene granitoids.

The granitoids were generated during and after the southward obduction of the ophiolites from the northern branch of the Neotethyan Ocean, onto the Taurides during the Late Cretaceous period and before the Late Masstrichtian (Erler et al., 1991; Akıman et al., 1993). They are the consequences of crustal thickening due to arc to arc or arc to continent collision (Göncüoğlu et al., 1992; 1993). Granitoids of the Central Anatolian Crystalline Complex indicate that they were generated mainly by partial melting of the continental crust (Göncüoğlu and Türeli, 1994). They propose that this process occurred due to a two-stage collision related to the closure of İzmir-Ankara branch of Neo-Tethys during Late Upper Cretaceous. The first stage comprises the collision and subsequent obduction of an ensimatic arc with the northeastern edge of Tauride-Anatolide Platform, generating CACC. The second stage is the collision of Sakarya continent with CACC giving way to the formation of Granitoids.

An indirect age is indicated by the presence of its pebbles in the various Early to Middle Eocene units. It intrudes the NAOM and Campanian-Maastrichtian units indicating that it was emplaced during Post-Campanian and pre-Early to Middle Eocene interval (Norman, 1972).

3.2.2. Upper Cretaceous-Paleogene Sequences

a. General definition

In general, deep-marine flyschoidal and shallow-marine to continental sedimentary sequences of Middle Campanian-Middle Eocene age occur in numerous but discontinuous outcrops in the Ankara region (Koçyiğit et al., 1988; Koçyiğit, 1991). The Late Maastrichtian-Paleogene sequences of the post-collisional sedimentary basin that is unconformably overlying the Cretaceous ophiolitic melanges in Kalecik region are interpreted as fore-arc units and the Çankırı basin is interpreted as a Late Maastrichtian-Paleogene fore-arc basin (Tüysüz and Dellaloğlu, 1992; Kaymakçı, 2000).

b. Distribution and stratigraphic position

In the study area, Paleocene-Eocene units are exposed in a NE-SW trend between the Kalecik and Sulakyurt region where they are thrusted by the sheets of the Cretaceous ophiolitic melange and intruded by the Paleogene granitoids of the Kırşehir massif (Figures 3.1, 3.4). However, in its stratigraphic position, the Paleogene units unconformably overlie the ophiolitic melange (e.g. Koçyiğit and Lünel, 1987; Koçyiğit et al., 1988; Gökten et al., 1988; Rojay and Süzen, 1997). Rock units of Paleogene sequences and tectonic contacts are all covered by the Neogene continental clastic carbonates and associated volcanics (Erol, 1961; Akyürek et al., 1984; Koçyiğit, 1991).

c. Lithology and age

The lowermost unit displays a time conformable boundary relationship with the underlying ophiolitic melange dominated by an imbricate thrust zone and is made up of an olistostromal facies of Early-Middle Campanian age (Koçyiğit et al., 1988; Koçyiğit, 1991). Within this imbricate thrust zone, various pelagic facies alternate with the subduction-complex-derived polygenic olistostromes of diverse thickness and composition (Norman, 1972; Koçyiğit et al., 1988; Koçyiğit, 1991).

It is conformably succeeded by a thick turbiditic horizon and continues upward in a deep-marine flysh facies of Middle Campanian-Late Maastrichtian age. Maastrichtian is represented by red-brown thick conglomerate and green colored sandstone alternation. The bottom is faulted. It contains abundant ophiolitic melange derived material. These flysch-type transgressive units are deposited in the upper portions of a submarine fan after the decrease in volcanic activity (Norman, 1972; Çapan and Buket, 1975; Akyürek et al., 1984). It continues with conglomerate-sandstone-shale alternation. There are transported corals of the same age within the sequence.

During Paleocene, the deposition continued with a typical flysh sequence which is composed of conglomerates, green-brown colored calcerous sandstones, green shales, mudstone, gray colored clayey-limestones, and detrital limestones as olistoliths. The units include Paleocene olistoliths in reefal limestone character. In some places, the boundary of the unit is faulted. In previous studies, the age of the formation is determined as Paleocene (Norman, 1972; Çapan and Buket, 1975; Akyürek et al., 1984). These units are composed of turbidites deposited in upper and medium parts of a submarine fan with olistoliths. Olistoliths are broken masses, which are detached from the fringing reefs. The clastics were also derived from these same age shelf deposits. The detrital component of flysch consists mostly of ophiolitic material. Syn-depositional structures suggest an unstable depositional setting at the time of the fore-arc basin development (Koçyiğit et al., 1988; Koçyiğit, 1991).

It gradually grades into a coarse-grained sandstone with lensoidal conglomerate intercalations and gains a coarsening upward sequence character. Red continental clastics with a relative age interval of Latest Maastrichtian-Early Eocene display both vertical and lateral gradational lower-contact relationships with the underlying marine sequence. Eocene is represented by red-green rare conglomerates, which are sometimes observed as lenses, green-brown sandstones, marls and dark colored thin bedded shales. In many places, it shows angular unconformity with the Paleocene units. The dominant lithofacies are red sandstones and polygenic conglomerates. Clasts of the conglomerate are mostly ophiolitic in origin. It is composed of shelf and delta deposits. In the upper parts, there are yellow colored tuffaceous sandstones, tuffs and white-yellow colored sandstones with thin intercalations of coal seams. They include yellowish-blueish limestones with abundant algae and coral fossils. According to these fossils, Ypresian-Lutetian age is determined for this succession (Norman, 1972; Çapan and Buket, 1975; Akyürek et al., 1984).

An Upper Maastrichtian-Paleogene aged granodiorite intrusion (Paleogene Granitoid) displays a distinct crosscutting relationship with the Middle Campanian to Early Paleocene sequences. The crosscutting boundary is unconformably overlained by dark green and fine-grained terrestrial clastic rocks and it has a sharp and conformable top boundary with the overlying shallow-marine reefal limestone of Early to Middle Eocene age.

The last member of the unit, is the red colored conglomerates of Oligocene age unconformably overlying the below carbonate succession and sandstones and siltstones alternating with it. The units are composed of red conglomerate, mudstone, sandstone, marl, gypsum alternation. According to Akyürek and others (1984), it is conformable with the underlying units, however, Çapan and Buket (1975) reported an angular unconformity between the Eocene and Oligocene formations. They are alluvial fan, meandering river and finally evaporitic lake deposits which were deposited in a shallow sea to lagoon environment due to uplift in the basin during the Oligocene.

d. Correlation

Maastrichtian units are the equivalents of the Ilıcapınar and Bölükdağ formations (Norman, 1972), Kenanındere and Sakızlıktepe formations (Çapan and Buket, 1975), Malboğazı and Yapraklı formations (Birgili et al., 1975), Ilıcapınar and Samanlık formations (Akyürek et al., 1984).

Paleocene units can be thought as the equivalents of Dizilitaşlar formation (Norman, 1972; Akyürek et al., 1984), Tatarilyas formation (Çapan and Buket, 1975).

Eocene units can be thought as the equivalents of Keçili, Hacıbali and Bulanıkdere formations (Norman, 1972), Kışlabağtepe and Yanıkkafatepe formations (Çapan and Buket, 1975), and Mahmutlar formation (Akyürek et al., 1984).

Oligocene units can be thought as the equivalents of the base of the 'Gypsum Oligocene series' (Ketin, 1963), Bahşili formation (Norman, 1972), Oligocene aged red conglomerates and sandstones (Çalgın et al., 1973), Kazmaca formation (Çapan and Buket, 1975) and Miskincedere formation (Akyürek et al., 1984).

e. Depositional setting

Due to the continued convergence, the original stratigraphic relations were destroyed by the late Eocene-Oligocene thrusts (Tüysüz et al, 1995). Both the forearc sequences and their basement rocks of the accretionary wedge (the ophiolitic melange), were tectonically stacked up in an imbricate thrust zone, and they were finally thrusted onto Upper Eocene-Lower Oligocene fluvial to lacustrine deposits towards the center of the basin (Koçyiğit,1991; Tüysüz et al, 1995).

3.2.3. Pre-Miocene Dykes

a. General definition, distribution and contacts

Two different dyke sets are exposed in the study area. First group of dykes are observed as highly altered, intensely folded and emplaced within ophiolites and pre-Cretaceous radiolaria bearing clayey carbonates. They die out within the boundaries of the ophiolitic units thus; they have no significant age difference from the units they cut. They constitute the relatively older dykes in the study area, which are mostly dark, greenish colored, mafic intrusions without any significant positive morphologic structure, even showing mostly negative morphology with random strikes. They have differing compositions and can be observed as multiple (repeated injections of the same or similar types of magma) or composite (repeated injections of different types of magma) injections in some places (Figure 3.13). They commonly crop out in the southeast of the study area along a road cut, but some examples can also be seen in the north of Kızılırmak River.

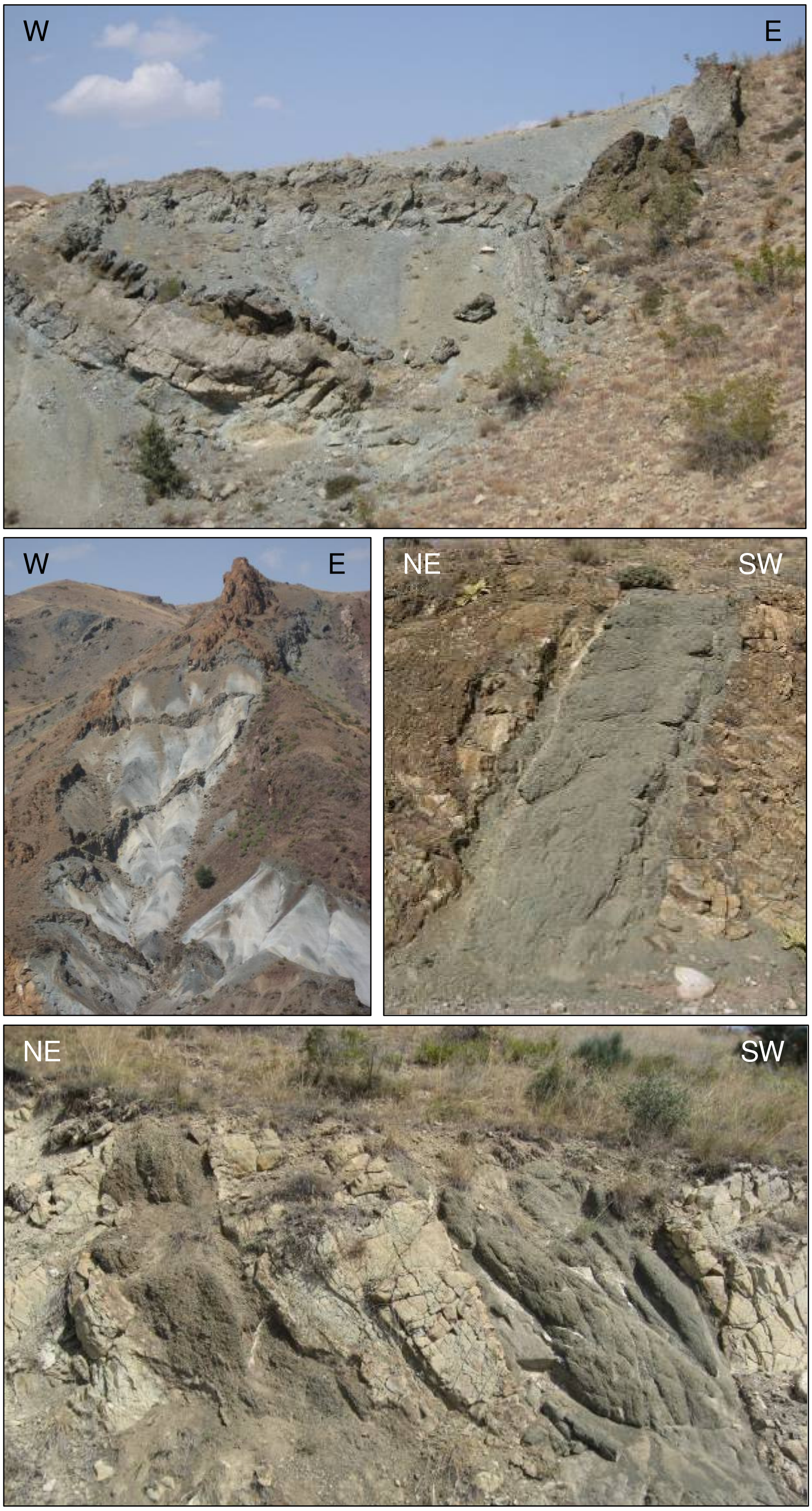

Figure 3.13: Intensely folded and altered mafic dykes of an older system in the study area.

The other group, for which the analyses carried out in this study, is the systematic sets of basic dykes, showing a certain strike tendency (NE-SW) with a positive morphology. They mostly crop out in the east of Gümüşpınar village, more specifically, along the two sides of Kızılırmak river valley, around the Aktepe Hill, in the southwest of Kabak Hill, in the south of Çamın Hill and around the Bayamlı Hill within the study area. They are cutting the Cretaceous mélange units and post-Cretaceous sequences and unconformably overlain by Miocene volcanics, Pliocene clastics and Quaternary terraces (Figure 3.2, 3.3, 3.5, 3.14 and 3.15).

They can easily be distinguished with their fresh, resistant morphologies and long lasting exposures up to 1500 meters across the study area. Buket (1969) also stated that the length of the dykes ranges from a minimum of 30 meters to a maximum of 800 meters.

A general strike in N70E direction and dip about 75-85 degrees towards north were stated by Buket (1969) for the Aktepe-Gökdere region. However, Dilek and Thy (2006) noted dykes having northwest to northeast azimuths with steep dips to the east around the Kalecik region. The orientations of dykes were studied and explained in detail in the next chapter.

The observed thicknesses of dykes in the field varies from 20 centimeters to 3.5 meters but most measured values are within rather narrow limits (between 0.4-1.4 meters) with an arithmetic mean of 1.15 meters (Figure 3.16). According to the observations of Buket (1969) around the Aktepe-Gökdere region, dyke thicknesses were reported as reaching up to 3 meters and in the Kalecik tectonic unit of Tüysüz and others (1992; 1995), cross-cutting intrusives are identified as 1-3 m thick dikes which were similar observations with respect to this study. However, some researchers (Tankut, 1985a, b; 1990; Tankut and Gorton, 1990; Tankut et al., 1998; Dilek and Thy, 2006) reported a more significant variation in thicknesses of dykes as ranging from 0.2 to 20.0 meters, within the Edige and Kalecik ophiolitic massifs around the Kalecik region.

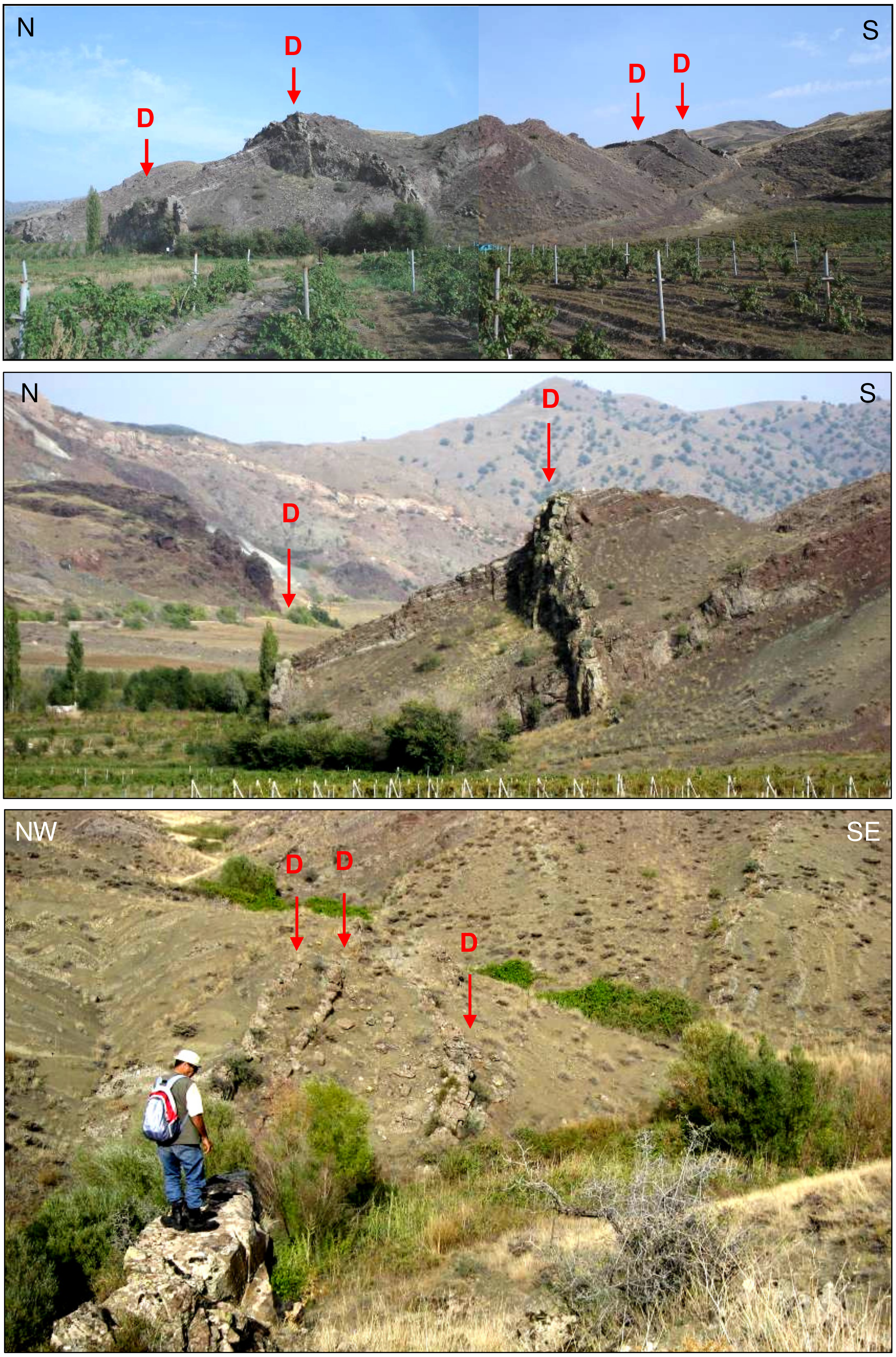

Figure 3.14: General view of the basic dyke (D) exposures extending in the study area.

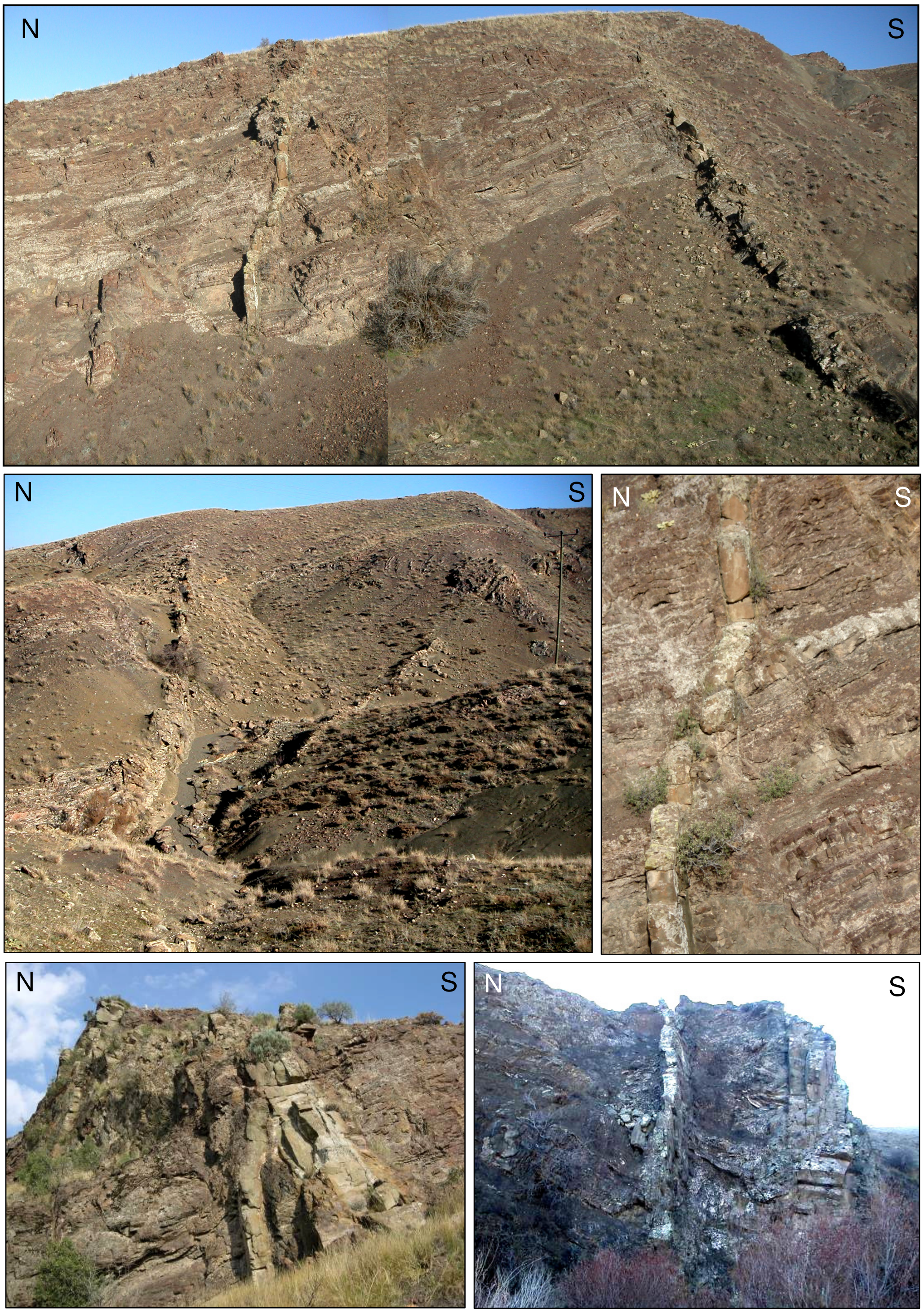

Figure 3.15: The basic dykes cutting the Cretaceous radiolarites, east of Kalecik.

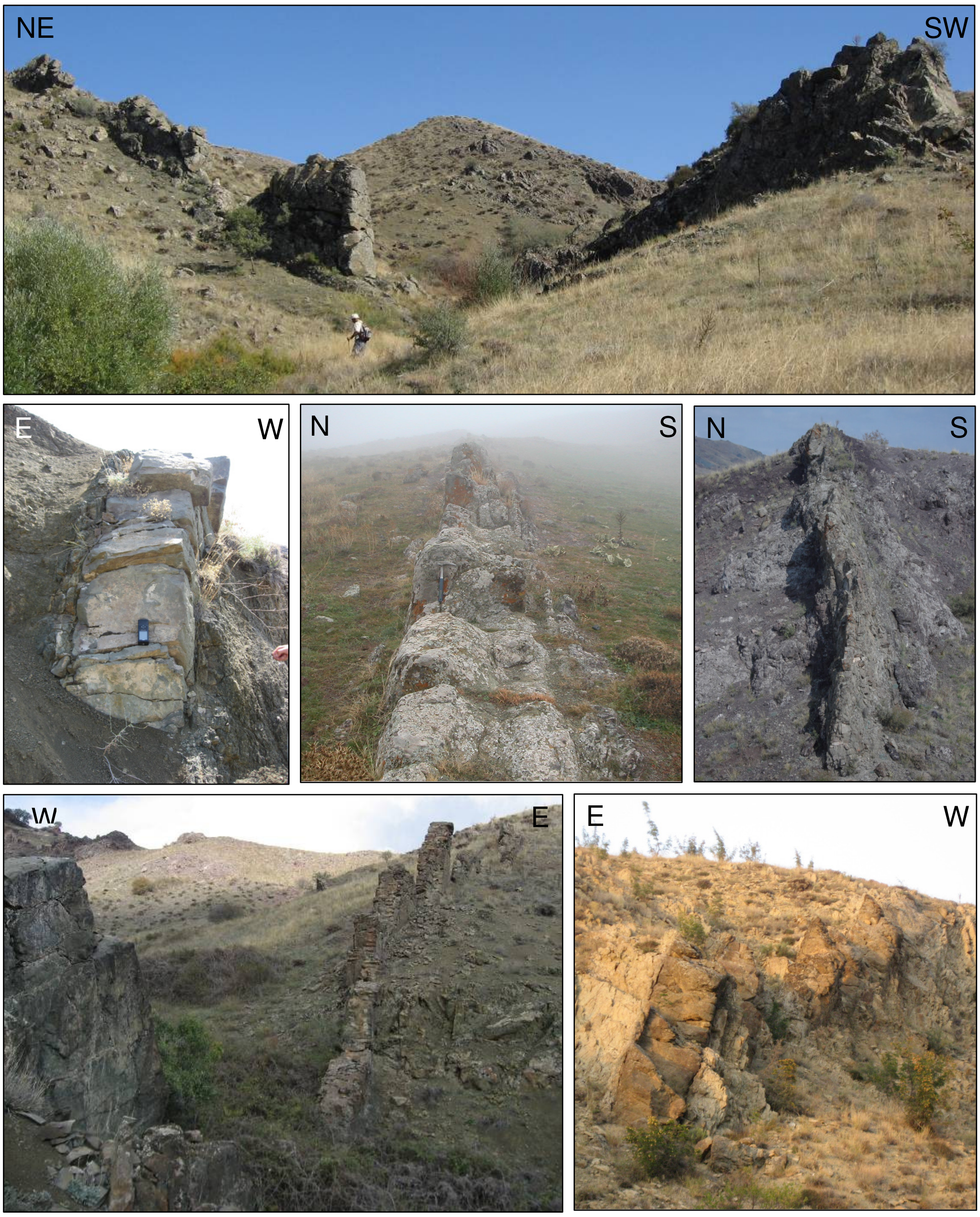

Figure 3.16: Closer view of the Kalecik basic dykes in the study area.

The dyke spacing changes from an order of a few tens of meters to a few hundreds of meters in the study area but at some locations dykes can also be observed with higher intrusion frequency in a parallel close fashion.

Many dykes display exposures of a single continuous linear tabular body, but some are composed of several separate offset segments, resulting in an undulating sinuous shape at some places also with dip direction changes.

In the study area, the systematic dykes occur as single intrusions possessing two sided symmetrical, well developed chilled margins with decreasing grain size from interior (centre) towards the margins of the dykes and baked zones on the wall rocks at the contacts indicating that the majority of the dykes were injected into cold host rock (Figure 3.17). Same observations on the features of dyke margins were previously reported around the Kalecik region (Buket, 1969; Dilek and Thy, 2006).

Figure 3.17: The chilled margins at the contacts of the basic dykes.

b. Petrography

According to the petrographic observations, the dykes are defined as basalts composed mostly of clinopyroxene (augite and augerine augite) minerals, nepheline crystals and biotite phenocyrists in various amounts. There are epidote, actinolite, calcite and chlorite formations as secondary minerals. Opaque and apatite are determined as accessory minerals. They were emplaced in spilitic basalts. Vesicular basalts showing vitrophyric characteristics are composed of nepheline minerals and plagioclase microlites within a glassy matrix and very rare plagioclase phenocyrists are also observed (Rojay et al., 2007).

c. Age

In the Aktepe-Gökdere region, Buket (1969), Çapan and Buket (1972) reported that the members of Aktepe-Gökdere ophiolitic formation of Late Cretaceous and Bulduktepe volcanic and intrusive rocks of Campanian age are intruded by slightly metamorphosed dioritic intrusions. The detailed descriptions about these intrusions in Buket (1969) fits the previously mentioned systematic NE-SW trending dykes that are observed in the field study of this work, which implies that the relative age assigned to these intrusions is Post-Campanian (Table 2.1).

Akyürek and others (1984) also studied the Ankara, Elmadag, Kalecik region and reported three dyke intrusions within three different aged formations. First one is the intrusions cutting the formations of the Ankara Group of Triassic age mentioned here as the Triassic Karakaya Complex. The second group of intrusions was described as the gabbros and diabases seen as dykes within the Albian-Apsian age ophiolitic material of the Eldivan Ophiolitic Complex of Lower Cretaceous. The third group, a dyke and sill system cross-cutting the spilit and diabase pillow structures, was reported within the Cenomanian-Campanian age volcanite member of Kılıçlar Group. This third group with a relative age of again post-Campanian, is more likely to be the dykes concerned in this study (Table 2.1).

According to the studies on the magmatic rocks within the Cenomanian-Turonian age sequence of Tüysüz and others (1995) around the Kalecik region, cross-cutting intrusives as lamprophyre dykes were identified implying a relative age of post-Turonian.

Dilek and Thy (2006) observed dykes at all structural levels cross-cutting the ophiolitic assemblage units which show mutually intrusive relations indicating their synchronous emplacement which is likely to be Early Jurassic or older in age according to them.

According to the field observations in this study, dykes show obvious cross-cutting relationships with the Cretaceous ophiolitic melange units and the Late Cretaceous-Paleogene sequences (Figure 3.18). The dykes were unconformably covered by the Miocene volcani-clastics and in some places directly by the Pliocene clastics and Quaternay river terraces (conglomerates) in the study area (Figure 3.2, 3.3 and 3.5). Therefore the Kalecik dykes might be accepted as the products of a fracture infilling intrusive magmatism which took place sometime in between post-Paleocene and pre-Miocene interval.

d. Origin and Emplacement

Buket 1969 reported that, Bulduktepe volcanic and intrusive rocks are produced from a magma, which either might be the differentiation product of ultrabasic magma or might be provided from a reservoir with guite a different composition compared to ultrabasic magma.

Akyürek and others (1984) related the dyke intrusions as the products of the volcanism resulted in the 'Ortakoy formation'. According to them, they can be thought as if the equivalents of spilites and diabases in the Ortakoy Formation. They reported the gabbros and diabases seen as dykes are in close relation with the preserved spilite and diabase pillow structures. The other dyke and sill system are thought as the products of the Eldivan Ophiolitic Complex (Akyürek et al.,1984).

The dyke intrusions in the ophiolitic massifs are separated into two geochemical groups on the basis of their rock chemistry (Tankut, 1985a,b; 1990; Tankut and Gorton, 1990).

Figure 3.18: Determination of the relative age of the dykes according to cross-cutting relationships in the study area. The dykes crosscutting the Upper Cretaceous Ophiolitic Melange (JK Lst: Upper Jurassic-Lower Cretaceous limestone) can be seen.

One group of dikes, combined with basaltic lava fragments from the melange, has subalkaline characteristics and shows N-MORB chemistry. The second group of dikes displays typical island-arc tholeiite signatures. Combined with their stratigraphic relations with the deep marine sedimentary rocks, these alkaline mafic rocks are interpreted to represent volcanic build-up and/or seamount related volcanism on the Neo-Tethyan ocean floor.

Dilek and Thy (2006) reported dolerite and plagiogranite dykes which show mutually intrusive relations indicating their synchronous emplacement into the pre-existing oceanic lithosphere. The spatial relations of the dolerite and plagiogranite dykes indicate that they were coeval in their intrusive emplacement into the upper mantle and lower crustal rocks in the ophiolitic assemblage, and that they were most likely derived from the same magmas. They relate all the intrusions with a seamount.

Even though some undetailed mapping and petrographic studies on these dykes were carried out, neither geochemical nor structural geologic studies have been performed yet. The former geochemical analyses and their results are all about the ophiolitic mass and the intrusives are related with the synchronous dyke complex of the ophiolites. In these studies, dykes were defined within the ophiolitic masses belonging to the Cretaceous ophiolitic melange and their geochemistries and structural meanings were interpreted together with these ophiolitic formations (Tankut and Sayın 1989; Dilek and Thy 2006).

3.2.4. Miocene Sequences

a. General definition

The Miocene units that were deposited in the study area, are represented by clastics, evaporates, volcanics and volcanic clastics which displays a wide spatial cover all around the Çankırı basin (Kaymakçı, 2000; Karadenizli et al., 2003).

b. Distribution and stratigraphic position

The Miocene volcanic clastics are exposed on top of the Çamın hill and in the west of the Aktepe hill in the study area (Figure 3.2, 3.3 andFigure 3.19). The thrusting of ophiolitic melange onto the Tertiary formations, which probably took place after Paleocene and dykes are unconformably covered by the Neogene units (Norman, 1972).

c. Lithology

Miocene units were observed as volcanics and dominantly their tuffs in the study area. Tuffs are grey-white colored and become yellowish in altered part. They displays thin-medium beds with alternated with agglomerates in some parts and intruded by sills.

It is also reported that; Miocene units display a widely distributed thick evaporitic successions in Çankırı basin composed of conglomerates, sandstones, tuffs, laminated shale, marl with gypsum flakes, thin clayey limestone and intercalations of thin coal (Buket, 1969; Buket and Çapan, 1975; Akyürek et al., 1984; Kaymakçı et al., 2001, Karadenizli et al., 2003). The Miocene volcanics are reported as dacites, andesites, and basalts of which andesites are seen as red, pink, gray colored, in some parts alternated with tuffs and agglomerate or intruded as sills (Akyürek et al., 1984).

d. Correlation and age

The volcanics are dated as Miocene by Ketin (1961). The Miocene clastics and volcanics can be thought as the equivalents of Kabaktepe formation (Buket, 1969; Çapan and Buket, 1975), Hançılı formation (Akyürek et al., 1979; 1980), Karapınar and Kavaklı formations and Tekke volcanites (Akyürek et al., 1984).

Figure 3.19: Çamıntepe hill composed of Neogene volcanics unconformably overlying the Cretaceous Ophiolitic Melange and radiolaria-bearing sequences.

e. Depositional setting

The Miocene clastics are alluvial fan, river and lake deposits in a continental basin, in the effect of an ongoing volcanism. The tuffs and lavas of the volcanism continue their evolution in lakes and rivers. This volcanism was very widespread between Oligocene-Miocene interval around the Ankara region.

Neogene regime is distinguished by the marked change in depositional styles and tectonic settings around the Çankırı basin (Kaymakçı, 2000; Karadenizli et al., 2003). After termination of the marine conditions in the Middle Eocene, the evolution of the region continued under extensional continental settings and resulted in red clastics characterized by conglomerates, sandstones, siltstones and widespread evaporates in the Çankırı basin (Kaymakçı, 2000; Karadenizli et al., 2003).

These units were deposited in a closed basin which took its present shape under the effect of younger faults. Today, the basin is an intermountain basin in nature containing nappe packages developed from Cretaceous to Miocene, surrounded by high mountains with Kızılırmak River flowing through it.

3.2.5. Pliocene Clastics

a. General definition

Pliocene clastics are represented by red colored fluvio-lacustrine sediments.

b. Distribution and stratigraphic position

The Pliocene units can be observed in the south of Gumuspinar and in the northwest of Bayamlı hill (Figure 3.2). It overlies the Cretaceous ophiolitic melange and dykes with an angular unconformity (Figures 3.3 and 3.5).

c. Lithology

Pliocene units are mostly composed of red colored, bedded conglomerates, sandstones, siltstones, mudstones and intercalations of gypsum. It laterally grades into thick, white gypsum alternating with red mudstones towards the Çankırı basin and uncomformably overlain by poorly sorted, non-bedded polygenic gravels and sands of Quaternary age.

d. Age and correlation

Pliocene clastics can be thought as the equivalents of Kağnıtepe formation (Çapan and Buket, 1975), Gölbaşı formation (Akyürek et al., 1984), Süleymanlı, Bozkır and Deyim formations (Kaymakçı, 2000). The Pliocene age is given by Erol (1958) and Kaymakçı (2000).

e. Depositional setting

The Pliocene clastics, mostly fluvial, were deposited in a closed basin where fluvial conditions dominates.

3.2.6. Quaternary Units

It is best observed along the course of the Kızılırmak River as river terraces and composed of poorly cemented detrital materials (sand, pebbles and boulders) derived from the local exposures. Alluvial fan deposits can be observed at the ends of the tributaries of the Kızılırmak River.

CHAPTER 4

STRUCTURAL ANALYSES

4.1. Previous Studies on Structural Analysis of Planar Structures

The relationship between faults and the stress ellipsoid in combination with the Mohr-Coulomb law of failure, was firstly mentioned by E. M. Anderson (1942). Anderson's (1951) dynamic classification of faults is based on the fact that no shearing stress can exist at the Earth's surface and one of the principle stresses (σ_1, σ_2, or σ_3) must be perpendicular to the Earth's surface. Although, it is now known that Anderson's assumptions are not always valid, his theory of faulting has proved to be extremely useful and yet remains the basis for all dynamic analysis. It explains the occurrence of three classes of fault; (i) Normal faults (σ_1 is vertical, σ_2 and σ_3 are horizontal, the dips of the fault planes are ~60°), (ii) Wrench or strike-slip faults (σ_2 is vertical, σ_1 and σ_3 are horizontal, the fault planes are vertical and the movement direction is horizontal), (iii) Reverse faults (σ_3 is vertical, σ_1 and σ_2 are horizontal, the fault planes dip at approximately 30° to the horizontal).

In the case of conjugate faults, the maximum compressive stress direction (σ_1) bisects the acute angle between conjugate shear planes; intermediate compressive stress (σ_2) is parallel to the intersection line of the conjugate shear planes; the minimum compressive stress (σ_3) bisects the obtuse angle between the conjugate shear planes. The acute angle between conjugate shear planes, is bisected by an extension fracture (Twiss and Moores, 1992).

The most widely used geological method of determining stress directions and relative magnitudes is the analysis of fault slip data. Based on the fundamentals of stress-shear relationship described by Wallace (1951) and Bott (1959), a number of inverse methods have been devised for determining regional stresses from populations of fault-slip data (e.g. Arthaud, 1969; Angelier 1979; 1984; 1989; 1990; 1994; Etchecopar et al., 1981; Armijo et al., 1982; Gephart and Forsyth, 1984; Michael, 1984; Reches 1987; Hardcastle, 1989; Gephart, 1990; Lacombe et al., 1992; Pollard et al., 1993; Twiss and Unruh, 1998; Yamaji, 2000).

Where a lineation was generated during slip in a stress field of identical orientation to that responsible for fracture initiation, it is possible to infer the approximate attitudes of axes knowing that a plane containing the lineation and normal to the fault defines the σ_1 σ_3 plane, and that σ_2 was perpendicular to the lineation in the fault plane. σ_1 and σ_3 orientations can be estimated if the displacement sense is known and a realistic Φ value is assumed (Hancock, 1985).

The basic approach is to find a uniform stress tensor, which in some way minimizes the discrepancy between the predicted shear stress direction and the observed slip direction on each fault plane. In most cases, the inversion yields an estimate of the best-fitting principal stress directions and magnitude of the intermediate principal stress relative to the maximum and minimum stresses (e.g. $\Phi=(\sigma_2 - \sigma_3)/(\sigma_1 - \sigma_3)$ of Angelier, 1984). The various methods differ in their descriptions of misfit, normative measures of misfit, and strategies for locating the best model.

Angelier (1984, 1990 and 1994) has been a key worker from the perspectives of methodology and application. To apply Angelier's method (Angelier, 1984) the sense of movement on each fault examined must be known. Angelier assume that each population of fault measurements corresponds to a single tectonic event, governed by a single regional stress tensor. As fault populations generally observed commonly result from several events, a preliminary distinction between successive events must be done in the field, based on stratigraphic and structural observations. However, faulting commonly uses previous discontinuities as older faults, joints, tension gashes or stratifications. Thus, slickensides are the only key to the reconstruction of principal stress axes, within a given framework of fault planes (Angelier, 1979).

Although many studies related with palaeostress reconstruction focus on the major faults, the analysis of small structures can yield a reliable palaeostress history (e.g. Eyal & Reches, 1983) such as minor faults, veins, brittle shear zones, fissures, fractures, and joints. Furthermore, they record more stress episodes than are expressed by map-scale structures (Dunne and Hancock, 1994).

An examination of a Mohr-Coulomb failure envelope suggests that there are three different types of fractures each of which is associated with a specific stress state. *Extension* fractures form under the condition that one of the principal stresses is tensile. *Shear fractures* form when all principal stresses are compressive. A third fracture type also forms when one of the principal stresses is tensile; this third type of fracture has been called either a *transitional tensile fracture* or a *hybrid shear fracture* (Hancock, 1985). Extension fractures form perpendicular to σ_3 and parallel to σ_1, whereas shear fractures and hybrid shear fractures form at an angle to the principal stresses (Marshak and Mitra, 1988).

In discussion of conjugate fractures, orientations of principle stress axes can be inferred from conjugate fractures as in the case of faults because the attitude of the acute bisector between conjugate sets yields the σ_1 axis, the orientation of the obtuse bisector gives σ_3, and the attitude of the intersection direction between sets yields σ_2. The following ranges of 2θ values can be regarded as characterizing three different genetic categories of fractures; (i) Extension fractures: 2θ is between 1°-10°, (ii) Conjugate hybrid fractures: 2θ is between 11°-50°, (iii) Conjugate shear fractures: $2\theta > 50°$ (Dunne and Hancock, 1994).

The term *joint* is most commonly used in reference to relatively continuous and through-going fractures that are reasonably planar and along which there has been imperceptible movement (Davis, 1984). They play an important role in the emplacement of dykes.

Where kinematic indicators are rare or absent it is necessary to analyze systematic joint systems to derive stress trajectories (Hancock, 1985). A joint set comprises a family of parallel joints or merely, the set maintains a constant angular relationship to some other structural trend. Joints should be assigned to sets in the field on the basis of joint style, including joint-system architecture (Hancock, 1985). They are interpreted as products of stress fields of deep-seated origin. However, small faults can locally perturb the stress fields responsible for jointing. Many of the joints in major deformation zones, such as thrust-fold belts, are also related to local stresses (Dunne and Hancock, 1994).

The majority of joints are extension fractures, that is, fractures formed normal to the direction of σ_3 at the time of failure. Such joints are cracks that propagated normal to the direction of opening of the crack. If σ_3 was tensile at the time of fracturing the joints are tension joints (Dunne and Hancock, 1994).

To infer the orientations of principle stress axes from a joint spectrum, it is necessary to determine the attitude of the symmetry axes bisecting the continuum, which yields σ_1, the common coaxial direction gives σ_2, and the perpendicular to the plane containing these two axes which is parallel to σ_3. A joint spectrum is unlikely to comprise fractures intersecting at a common node, but its presence will be reflected on a stereoplot by a girdle of poles that encloses a maximum angle of about 45°. From joints belonging to conjugate sets or defining a joint spectrum, not only can the orientations of all three principal stresses be determined, but an estimate can also be made from 2θ values of the likely differential stress (σ_1 - σ_3) in terms of multiples of tensile strength of the rock (Dunne and Hancock, 1994).

Although the orientations of σ_1 and σ_2 cannot be inferred from a single set of featureless extension joints, they can be determined in two ways from extension joints provided that either: (1) some of the surfaces display the linear axis of a plumose marking, or (2) the joints belong to a network of orthogonal sets that are coeval. Plume axes form locally parallel to the direction of σ_1. Caputo and Caputo (1988) presented the first attempt to estimate a complete stress tensor from orthogonal extension joint sets, and proposed that they are a product of the rapid 90° switching of σ_2 and σ_3 axes of roughly equal magnitude. The direction of σ_1 remains oriented parallel to the intersection direction between sets (Dunne and Hancock, 1994).

The genetic class of a joint must be identified in order to infer palaeostress axes from single or conjugate sets. (Dunne and Hancock, 1994).

The systematic relationships that exist between conjugate faults, tension fractures, and principal stress directions provide a basis for interpreting paleostress directions in rocks (Davis ,1984).

In regions of flat-lying rock, it is common for prominent joint sets to be either parallel or perpendicular to the earth's surface. In regions where rocks have been folded, however, a greater range of joint orientations with respect to bedding commonly occur and it may be useful to define the geometry of the joint in terms of their geometric relation to the folds (Marshak and Mitra, 1988).

Joint sets that are symmetrically arranged within a fold are often (e.g. Hancock, 1985; Price and Cosgrove, 1990; Turner and Hancock, 1990) interpreted as being extension or conjugate joints on the basis of whether they are normal or oblique to symmetry lines or planes, such as hinge lines, axial planes and layering. Not all joint sets symmetrically enclosing fold hinge lines are conjugate; some are unrelated paired sets of extension fractures (e.g. Engelder and Geiser, 1980).

The jointing of folded rocks is subject to many local variations, but a broad geometrical classification into three types is often possible for joints that appear to be genetically related to the folds:

1) Longitudinal joints are normal or nearly normal to the bedding, and are subparallel to the axial surfaces of folds (fold axis). They tend to be through-going, planar, continuous structures (Davis, 1984). They are often ascribed to tension consequent on the bending of the beds. Billings (1972) interpreted longitudinal joints as release joints that open up in folded layers when fold-forming shortening stresses are relieved. In general, it appears that such joints form at a late stage in the folding, and, again they are present equally on straight fold limbs as on the curved sectors of folds. In folds with straight limbs, they may represent complementary shear directions or Griffith fractures, operative after the fold form was achieved. However, some longitudinal joints may reflect shortening perpendicular to their average attitude, a shortening taken up by pressure-induced dissolution along stylolitic surfaces (Davis, 1984).

2) Transverse, or cross joints are usually clean-cut fractures that transverse several beds with little or no deviation in direction. Cross joints ideally are aligned perpendicular to the longitudinal axis of folding, thus may serve as a rough indication of the plunge. Cross joints clearly have some connection with the deformation of rocks along the strike of a folded belt. They reflect stretching of brittle rock during hinge-parallel elongation of folded layers. Hinge-parallel elongation partly compensates for the room problems that can develop in the inner arc of a folded layer as it becomes more and more tightly appressed. Cross joints are unusually planar and are unusually regularly spaced. Often-times they are vein filled, clearly expressing stretching (Davis, 1984).

3) Diagonal joints are two of main types, (i) those that are restricted within each bed, and (ii) those that cut across the whole folded structure, being diagonal master-joints. These latter may be assumed to have some genetic connection with the folding where this appears to be caused by horizontal shearing movements. The restricted type of diagonal jointing is little-understood. It is best seen in interbedded harder and softer beds but appears to be much less prominent below the zone of weathering, suggesting that differential expansion and contraction due to weathering processes, or unloading by erosion, may account for certain examples. This may apply particularly where the beds are polygonally jointed, with two or three sets of oblique joints normal to the bedding, these having different angular relationships in adjoining beds. Master joints that cut across several beds in folds are not necessarily unrelated to the folding processes. Shear joints may be related to tear faults of synchronous origin, and in the final stages of any folding, the continued application of stress may be expected to yield both shear and tension joints, as well as faults. Oblique joints ideally comprise two conjugate sets that are symmetrically disposed to the hinge and axial surface of a given fold. The oblique joint sets are arranged such that the the axial surface of the fold bisects the obtuse angle of intersection of the joint sets. Oblique joints are classically interpreted as conjugate shear joints that form in folded layers as a response to shortening perpendicular to the axial surface of a fold. The acute angle of intersection of the joints is thus bisected by a line that describes the direction of shortening (Davis, 1984).

One way of referring to joints in folded regions is to define joints that are parallel to the strike of fold axial planes as *strike joints* and to define joints that cut across the axial plane as *cross-strike joints.* Hancock (1985) described joint orientation with relation to symmetry axes of a fold using a procedure similar to the definition of Miller indices for crystals.

Dykes can be formed either (i) by forceful injections indicated by highly folded neighbouring strata or (ii) by dilating and filling the previously formed weakness zones such as fractures or joints. The extension associated with dyke intrusion can be evaluated using the geometric parameters of dykes (e.g. Marinoni and Gudmundsson, 2000). Therefore, vertical dykes can also be used as paleo- and neotectonic stress indicators (Dunne and Hancock, 1994). Anderson (1951) also made the distinction that faults are shear fractures; dykes, on the other hand, are intruded along tensile fractures with no lateral or horizontal dislocation, in general. He also noted that a regional tension is unnecessary for dyke formation, in fact, which is impossible beneath a certain limiting depth.

At the first stage, the normal stress acting perpendicular to the weakness plane, tends either to open the weakness plane or to close it. If this normal stress acts alone and is large enough, a tension gash (e.g. a vein or dyke) or a stylolitic seam forms (Angelier, 1994). For purely dilatational fractures, veins form perpendicular to a minimum effective tensional principal stress σ_3 and in the plane of σ_1 and σ_2. Shear veins have little previous history of success as paleostress indicators (Dunne and Hancock, 1994).

Aligned active volcanic vents and linear trains of vents, including elliptical zones of eruptive vents are presumed to overlie approximately vertical fissures that are extension fractures which propagated in the σ_1-σ_2 principal stress plane as a result of 'hydraulic' fracturing by magma. Thus, from such alignments the direction of the greatest horizontal stress can be inferred to have been parallel to the trend of the alignment. Active fissure and active dyke segments in areas of present-day spreading, strike roughly perpendicular to the direction of the least horizontal stress (tensional), although an array of short fissure segments can be oblique to the direction of least horizontal stress as a consequence of the influence of older underlying fractures (Gudmundsson, 1987). Steep normal faults or faulted fissures, are surface expressions of some zones that have been extended by dyking.

Ductile shear zones have only limited value as palaeostress indicators. The distinctive signature of brittle-ductile shear zones is an array of dilatational en echelon veins. En echelon dilatational veins face against the shear directions. Zone parallel faults commonly offset veins in some shear zones, indicating a transition to more brittle behaviour with increasing deformation. The faults are usually located near zone centers and have the same shear sense as the zone. Arrays of en echelon Riedel fractures are secondary shear fractures that can develop alone in brittle-ductile shear zones and commonly form at an angle of about 15° to shear zone boundaries (Dunne and Hancock, 1994). The use of en echelon veins in brittle-ductile shear zones to determine internal palaeostress is fraught with problems simply because agreement is lacking about whether vein development is controlled by stress or strain. One view considers that they form perpendicular to the maximum extension direction (Ramsay, 1980).

Conjugate brittle-ductile shear zones, rather than individual veins, reliably indicate regional stress directions. Unlike conjugate faults, which have an inward-moving acute wedge with a dihedral (2θ) angle of about 60°, the inward-moving wedge between conjugate shear zones can enclose angles ranging from 40° to 130° (Dunne and Hancock, 1994).

It is also possible to use the axial trends of folds (e.g. Yeats, 1986; Billings, 1972; Davis, 1984; Marshak and Mitra, 1988; Ragan, 1985; Ramsay, 1980; Twiss and Moores, 1992) that are amplifying ahead of blind thrusts, and are oriented roughly at right angles to the direction of the greatest horizontal stress. The orientation of the fold axis can be determined by a stereographic plot of poles of the measured planes. If they define a great circle, the pole of this great circle is the fold axis (β-axis) (Ragan, 1984).

Therefore, the dykes, beds-intruded by the dykes, and faults-mainly displacing the dykes are measured as structural elements in the study, in order to reveal the regional angular cross-cutting relationships between these planar structures and their age relationships with respect to each other.

The analyses of the attitudes of planar data (dykes, beds and faults) were performed by "ROCKWORKS 2002" software and displayed by the use of rose diagrams, contour diagrams and histograms. Schmidt net (equal area net) was preferred for rose and contour diagrams to prevent unreliable preferred alignments of the data. Besides, length weighted rose diagrams were used for the lineament analyses of faults. On the other hand, the analyses of the kinematic data measured on faults were performed by using "Angelier Direct Inversion Method (version 5.42)" software by the use of palaeostress tensors. The dominant trends of dyke, bed, fault orientations, their structural and angular relationships and the types of faults were aimed to be determined in order to detect the principal stress directions that had taken effect over the region and thus to understand the mechanism of deformation in geologic time since post-Paleocene.

4.2. Dykes and Beds

The study area mostly consists of thrust sheets of Upper Cretaceous bedded radiolaria-bearing limestone/radiolarite units alternating with mudrocks at some places, and also Cretaceous Ophiolitic melange lithologies, both of which are cut by the basic dykes (Figures 4.1 and 4.2)

During the measurement of dykes an almost NW-SE profile was followed across the study area, in order to catch most of the dykes and make the data reflect mostly individual dykes. But different profiles were also preferred locally, to be able to detect the dykes with srikes out of the general trend, in order to make the overall data reflect a real situation for the study area in terms of dyke trends. Besides, a few folded dykes and some faulted/detached dyke segments which posses abrubt changes in orientations, or some outcrops which cannot be followed in a considerable distance, were also treated as individuals and added to the analyzed data.

The majority of the bedding plane measurements were taken from both sides of the cross-cutting contacts of the dykes in order to reveal both the cross-cutting angular relationships between the dykes and bedded units, and to detect if any offset or change in the attitudes of beds occur with respect to both sides due to intrusion (Figure 4.1). Therefore, it is found suitable to evaluate the interlinked dykes and beds under a common heading.

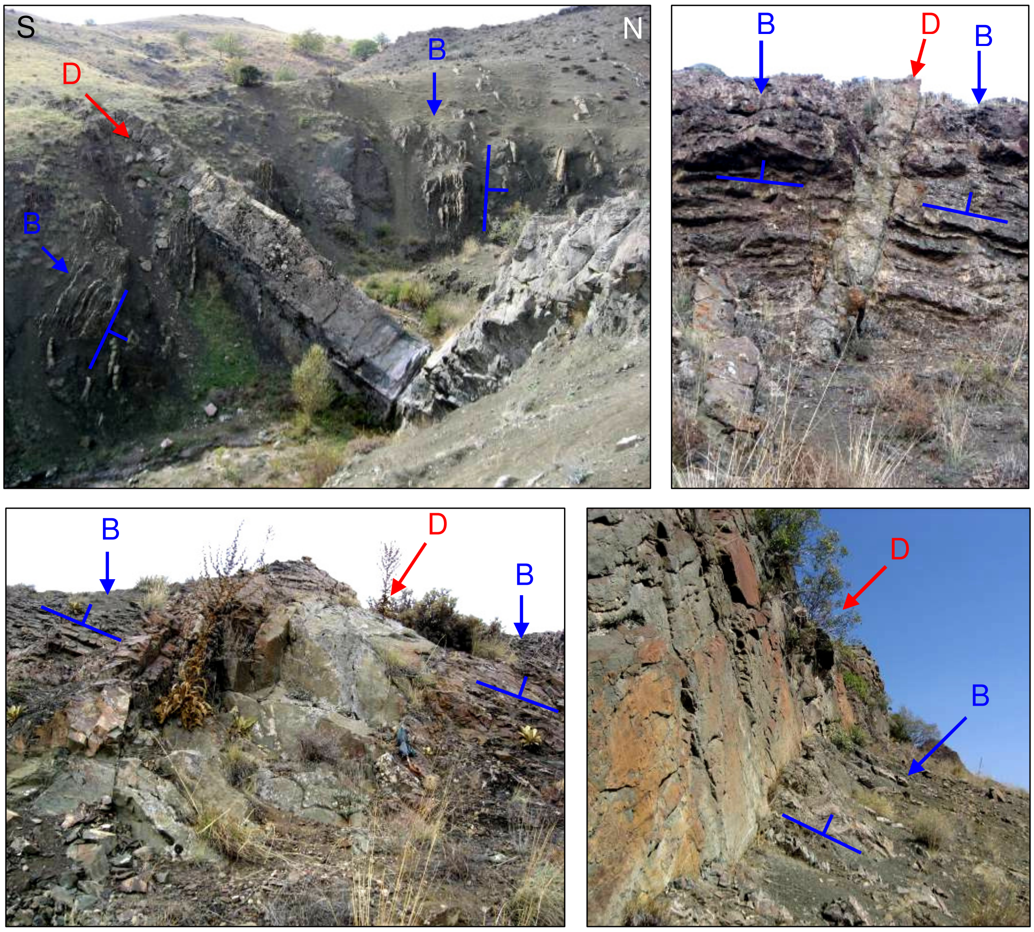

Figure 4.1 Dykes cross-cutting the bedding planes in the study area.

Unfortunately, as the study area is included entirely in the Cretaceous ophiolitic melange belt, it is not clear how much autochthonous the bedded units are. In the study area, there are red to green, thin-bedded units displaying a generally thick succession of Upper Cretaceous radiolaria-bearing limestones/radiolarites and there are red color dominated, intensely folded and faulted radiolarite blocks that are certainly known as allochthonous. Besides, not all the units which are cut by the dykes could be observed as displaying distinct bedding planes and the concerning dykes are not only observed as cutting the bedded units. Nevertheless, all the dykes in the concern of this thesis, with or without a contact bedding plane data, and only the bedding planes belonging to the above mentioned thick succession of bedded radiolarites at the crosscutting contact or in close relevance with the dykes, are measured and the data were evaluated through statistical and structural analyses.

The dykes in the study area are observed as cutting different intensely deformed lithologies of the Cretaceous ophiolitic melange and thrusted Upper Cretaceous-Paleocene bedded units, but overlain by Miocene volcanics. Thus, with in this time interval the lithologic boundaries are nonfunctional in terms of dyke studies. Instead, to understand if the major trends and behaviours of dykes or beds are differ (i.e. rotated) by the effects of other structural elements which do not possess a direct cutting relationship with the dykes (such as “Kızılırmak River” Fault), and to be able to make conclusions about the relative ages of such structures with respect to dykes, the orientation data analyses were carried out in three different domains (Figure 4.2).

Domain I and II are tectonic windows and outliers of the Upper Cretaceous radiolaria-bearing units that were overthrusted by ophiolitic mixture on each side of the Kızılırmak River (or the Kızılırmak River Fault) (Figure 4.2). Domain III is also a tectonic windows of Upper Cretaceous radiolaria-bearing units in the north of the study area.

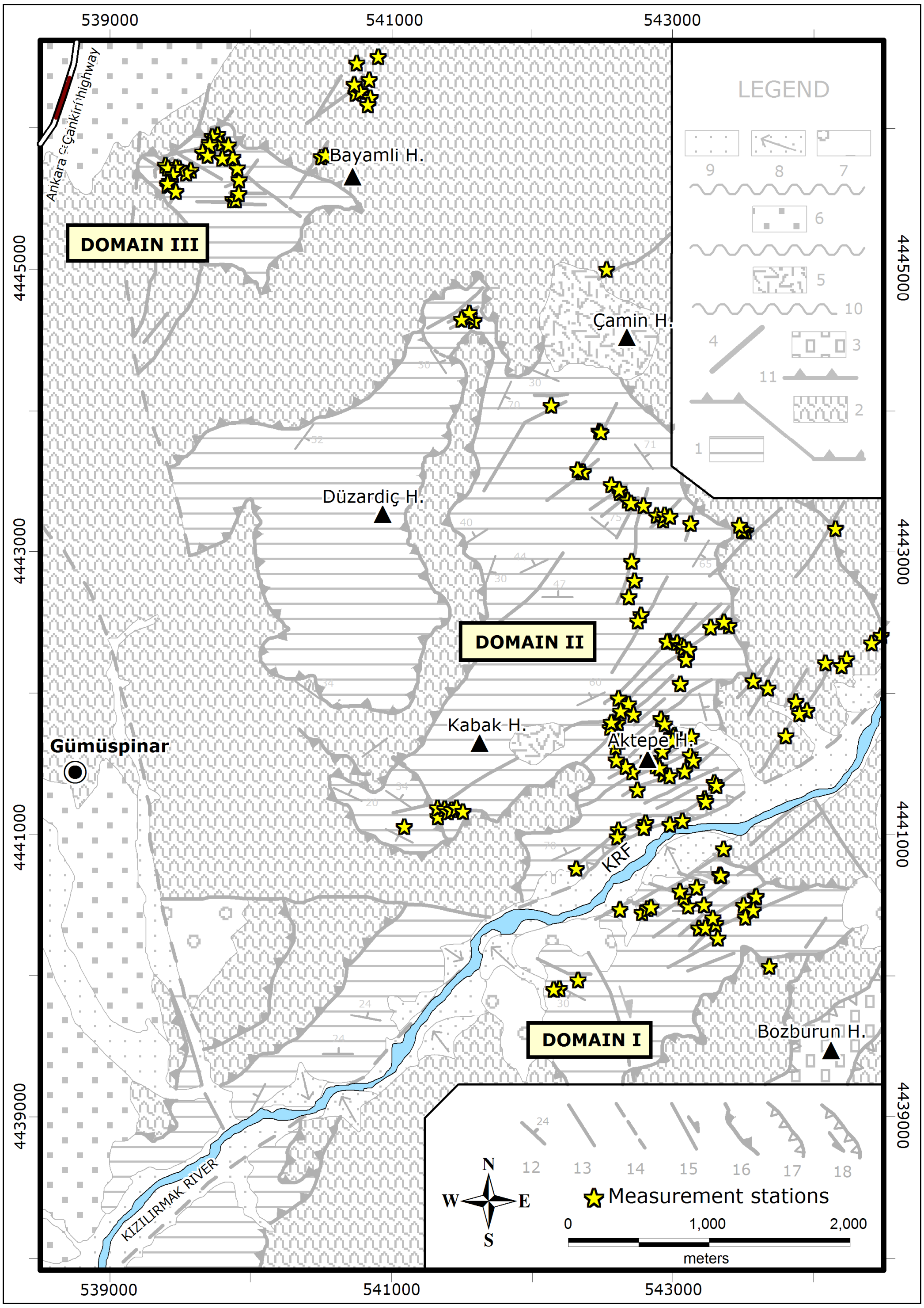

Figure 4.2: The measurement stations shown on the geological map of the research area (for the explanations of the map, please refer to the Figure 3.2)

The area between Domain II and III is widely covered by the thrusted mélange units.

The results of measurements were firstly evaluated separately for each domain by the use of rose diagrams, contour diagrams and histograms, and then the results for 3 domains were compared with each other and the overall situation of dykes and beds was tried to be revealed for the whole study area.

4.2.1. Domain I

Domain I covers the southeast of the study area along the southern side of the Kızılırmak River (i.e. Kızılırmak River Fault) (Figure 4.2). Orientation measurements of 34 dykes and 44 bedding planes from 34 different stations were taken along the southern slope of Kızılırmak valley from the Upper Cretaceous radiolaria-bearing units which were thrust by the Cretaceous ophiolitic melange units (Figure 4.2). The thrust is covered by Quaternary river terrace conglomerates. The measured dykes cut both the radiolarites and the Cretaceous ophiolitic melange.

4.2.1.1. Dykes

a. Strike of the Dykes

The prepared rose diagram of the measured 34 dykes in domain I, indicates a major trend of roughly NE-SW but peaking in two class intervals, namely 060°N-070°N (more than 25%) and 040°N -050°N (Figure 4.3a). Vector mean is ~46°. Most of the data is gathered between 030°N and 070°N and the 95% confidence interval for the true population covers the 035°N-057°N interval.

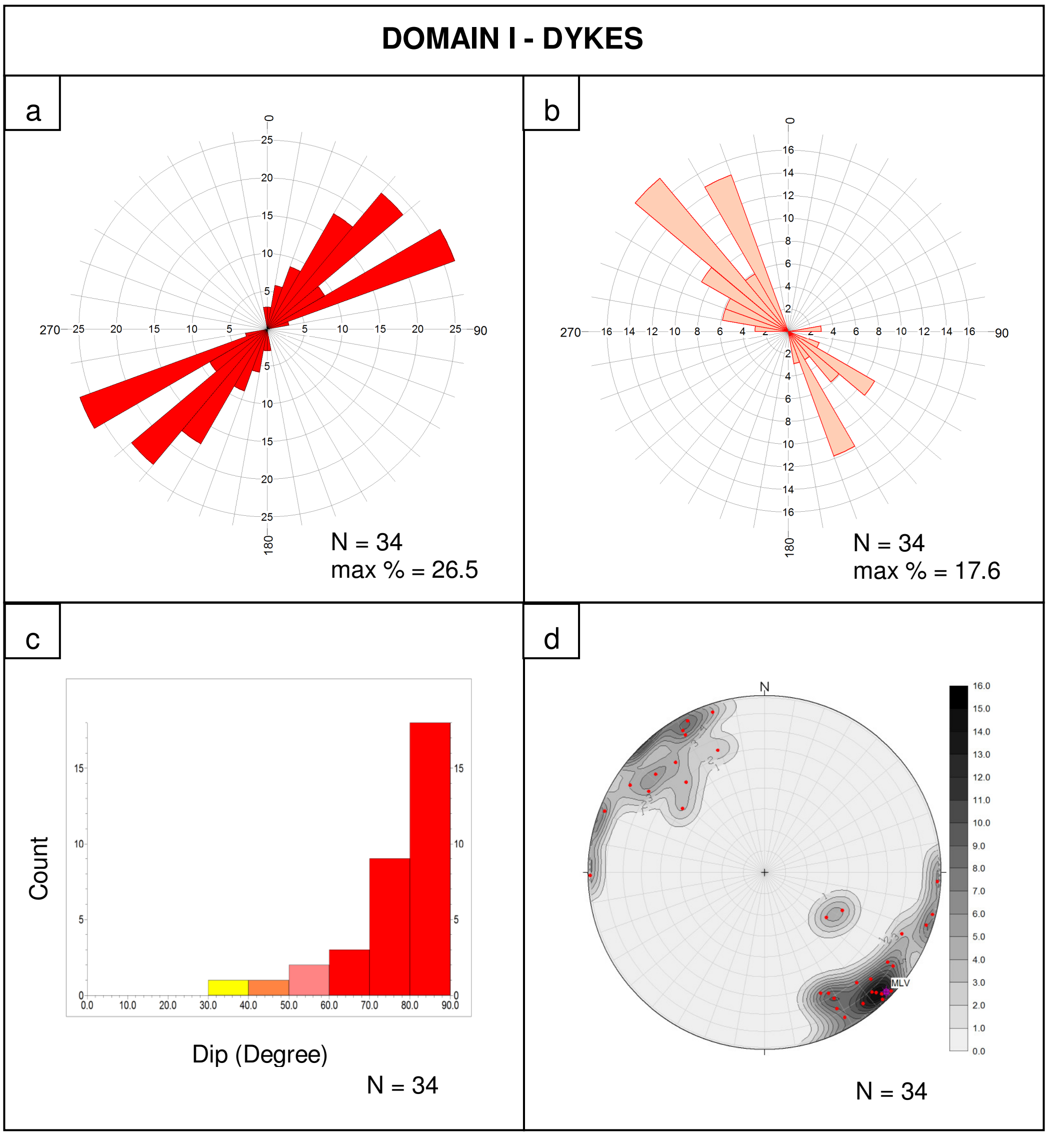

Figure 4.3: Diagrams for the dykes in Domain I. (a) Rose diagram of strikes; (b) Rose diagram of dip directions; (c) Dip amount histogram; (d) Contour diagram.

b. Dip Direction and Dip Amount of the Dykes

The dip towards NW is dominant for the dykes in Domain I, represented by 21 out of 34 measurements which indicates that the preferred dip direction, is towards NW, for all the NE-SW trending dykes. (Figure 4.3b). The most crowded class of 310°N-320°N (17.6% of total) and the secondmost crowded class of 330°N-340°N (~15% of total) are reversely representing the second and first order trends of the dykes, respectively. The SE dipping dykes constitutes only 12 measurements out of 34, with one remaining dyke dipping towards E. The dykes in Domain I are generally steeply dipping with an arithmetic mean of dip amounts as ~76° (Figure 4.3c). The dominant class is 80°-90° for dip amounts with more than half of the population (18 out of 34) and the second crowded class follows closely the dominant class with dip amounts between 70°-80° (9 out of 34).

The contour diagram shows that the poles of the planes are distributed in the NW and SE margins of the diagram which indicates that there is one major trend for the dykes in the opposite NE-SW direction with steeply inclined planes (Figure 4.3d).

4.2.1.2. Beds

a. Strike of the Beds

44 measurements of bedding planes were analyzed for Domain I. The rose diagram displays a major trend as WNW-ESE represented by the interval of 290°N-310°N with the maximum peak of the rose diagram (290°N-300°N class with 20.5% of population) (Figure 4.4a).

b. Dip Direction and Dip Amount of the Beds

The dominant WNW-ESE trending set of bedding planes are dipping mostly towards NE with the peak (020°N-030°N) and the secondmost crowded interval (030°N-040°N) of the dip direction diagram (Figure 4.4b). The other distinguished sets of bedding planes are observed trending in the NNW-SSE (320°N-330°N), ENE-WSW (050°N-080°N), N-S (350°N-010°N) and E-W (270°N-280°N) directions, in decreasing order of size of populations.

As it can be observed from the dip direction rose diagram, majority of beds are dipping towards N, in general. There are a very few beds which are on the southern half of the diagram (belonging to the major WNW-ESE trend, NNW-SSE trend and N-S trend), thus the southern half of the dip direction rose diagram is almost empty.

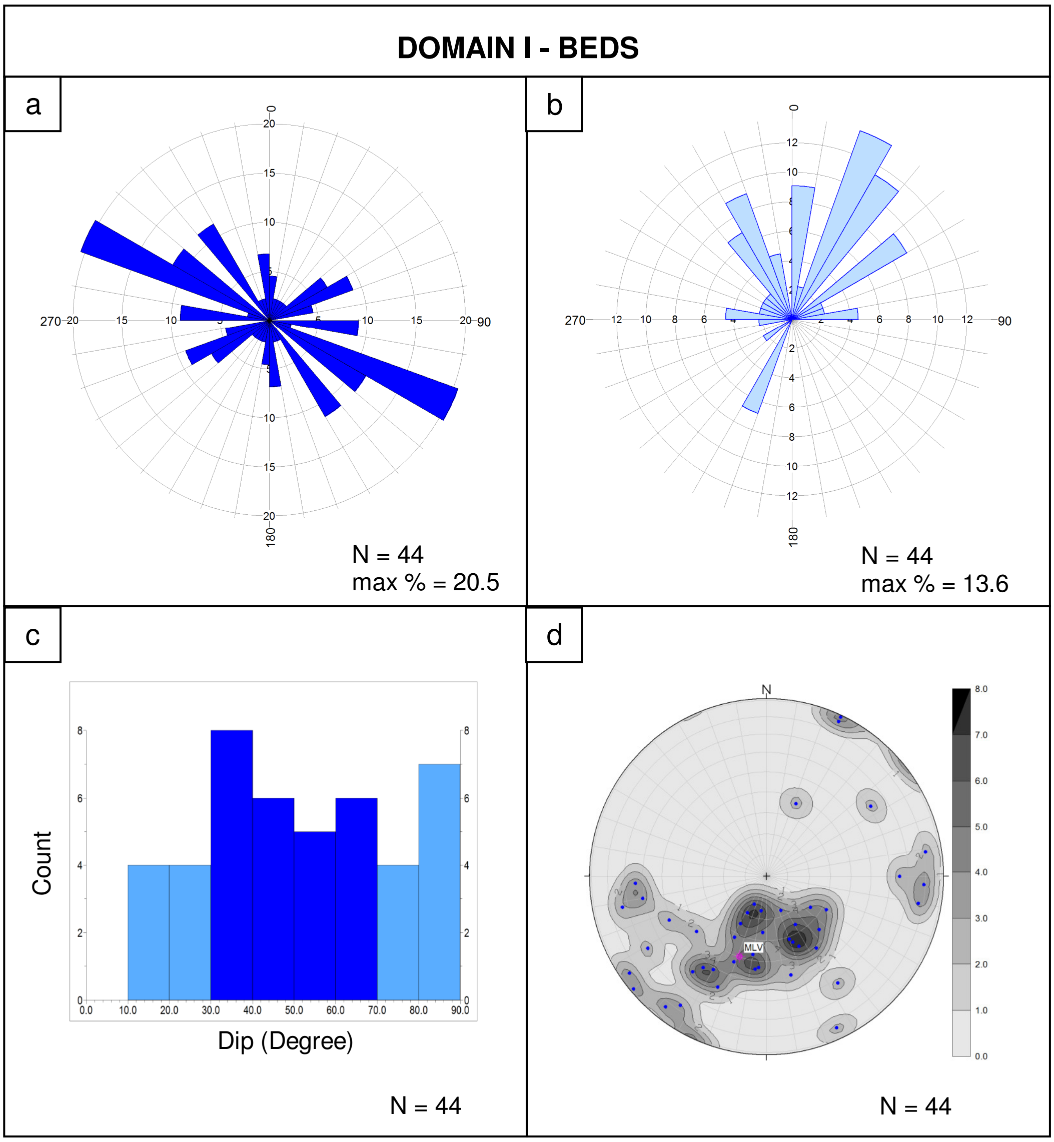

Figure 4.4: Diagrams for the bedding planes in Domain I. (a) Rose diagram of strikes; (b) Rose diagram of dip directions; (c) Dip amount histogram; (d) Contour diagram.

More than half of the measured bedding planes of Domain I have moderate to steeply inclined dips ranging between 30°-70° (25 out of 44) with an arithmetic mean of ~ 51° (Figure 4.4c). The dominant class for dip amounts, is the 30°-40° degree interval (with 8 measurements out of total). The number of beds dipping between 70-90 degrees is considerably high (11 out of 44) with the second highest peak of the histogram as 80-90 degree interval (7 out of 44). Nevertheless, there are also gently dipping beds in lesser amounts between 10°-30° intervals.

According to the contour diagram, there are five dense circles indicating each of the mentined sets. The majority of poles are in the southern half of the contour diagram indicating the dominant dip direction of the beds towards N, and most of the data are gathered between the center and the margin corresponding to the moderate dip amounts. Three of the circles correspond to the same great circle, which indicates that these three populations are the members of a folded unit (Figure 4.4d). The scatter of the data indicates the tectonic complexity of the region.

4.2.2. Domain II

Domain II is covers the largest area along the north of the Kızılırmak River, corresponding to the central part of the study area (Figure 4.2). It involves measurements especially around Aktepe hill, Kabak hill, Ağıl hill and Çamın hill and along the Kızılırmak river valley. The measurements are contained mainly within the Upper Cretaceous radiolarian-bearing units which were thrusted by the Cretaceous ophiolitic melange units along the course of Kızılırmak River. Some measurements were taken from the dykes directly crosscutting the Cretaceous ophiolitic melange. The crosscutting and thrusting relationships were covered by Miocene volcanics and younger units.

Highest amount of measurements were taken from Domain II (115 dyke measurements and 92 bed measurements from 101 stations).

4.2.2.1. Dykes

a. Strike of the Dykes

The strikes of dykes in Domain II display a major NE-SW trend (Figure 4.5a). The vast majority of the whole data falls in between 010°N-080°N indicating a NE-SW trend. Half of the population falls in a narrow interval, between 040°N-060°N with the two major peaks of the diagram. Calculated vector mean is ~052°N. The 95% confidence interval for the true population covers approximately an interval between 045°N-059°N.

b. Dip Direction and Dip Amount of the Dykes

Almost all of the dykes are dipping towards NW thus it is no surprise to observe that all the classes trending NE-SW in the strike rose diagram, each have greater populations in the NW side of the dip direction rose diagram (Figure 4.5b). Besides, the maximum peak (the 310°N-320°N class interval with 20.9% of the total population) and the most crowded class intervals in the NW side of the dip direction rose diagram displays similar growth patterns as the NE-SW trending intervals of the strike rose diagram. In general, it can be concluded that the dykes in Domain II have a NW preferred dip direction.

Most of the population has dip amounts higher than 60° (100 out of 115) (Figure 4.5c). Those of which are almost vertical with the highest peak of 80°-90° class interval containing almost half of the population (46 out of 115). The arithmetic mean of the dip amounts is calculated as ~74°.

The two assemblages of poles in the NW and SE margins of the contour diagram with the most in the SE margin, also indicates sub-vertical to vertical planes with one major trend and a general NW direction of dip (Figure 4.5d).

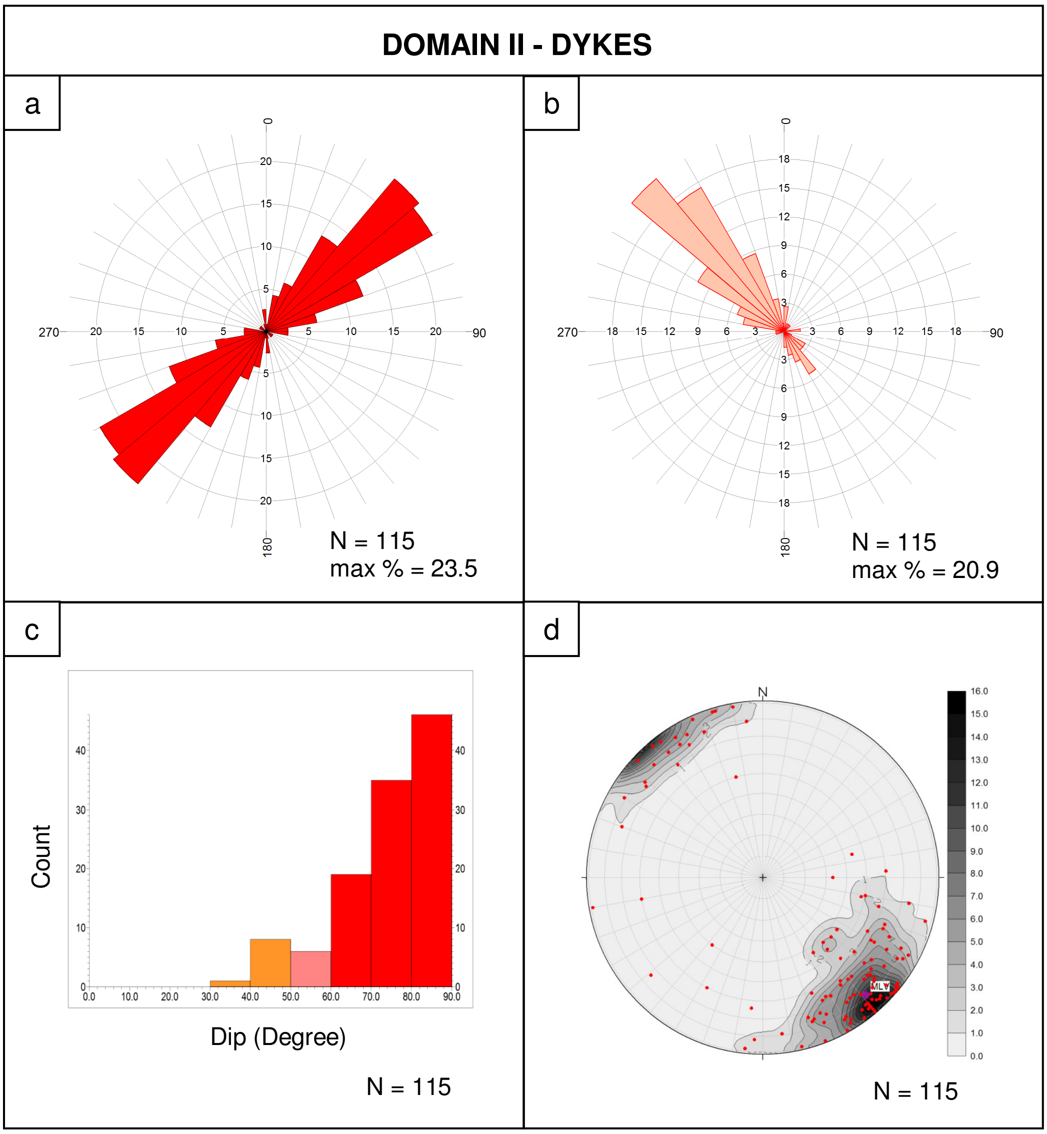

Figure 4.5: Diagrams for the dykes in Domain II. (a) Rose diagram of strikes; (b) Rose diagram of dip directions; (c) Dip amount histogram; (d) Contour diagram.

4.2.2.2. Beds

a. Strike of the Beds

According to the rose diagram prepared by 92 bedding plane measurements, 2 major strike trends can be observed in WNW-ESE and NNW-SSE directions which can roughly be represented by the 290°N-

310°N (with the maximum peak (22.8%) of the diagram as 290°N-300°N) and 320°N-350°N class intervals, respectively (Figure 4.6a). The vector mean is ~296°N. The true population represented by the 95% of confidence interval lies between 284°N-307°N. Two other minor bed trends can be distinguished in E-W and NE-SW directions with the peaking classes of 260°N-270°N and 030°N-040°N, respectively.

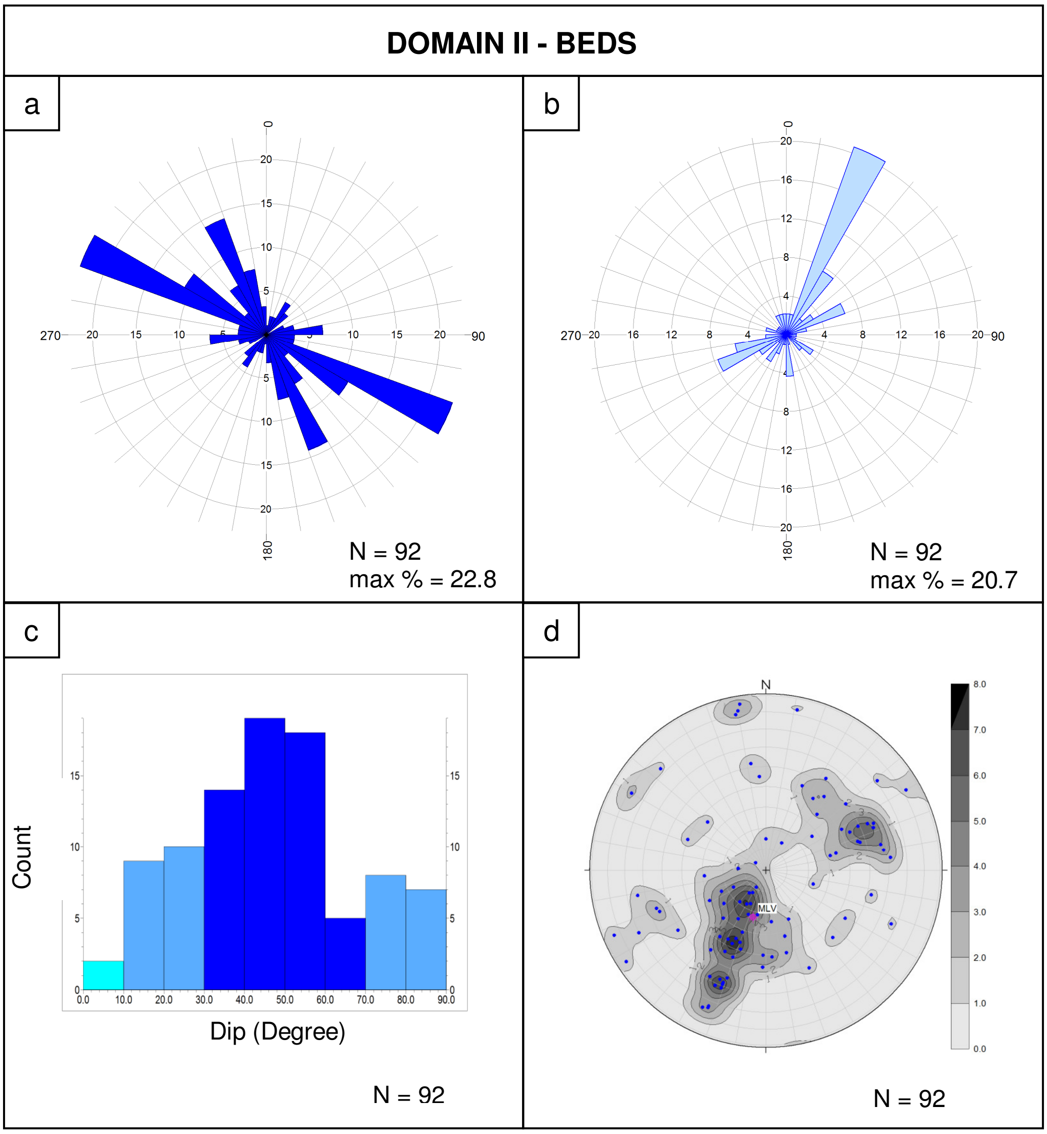

Figure 4.6: Diagrams for the bedding planes in Domain II. (a) Rose diagram of strikes; (b) Rose diagram of dip directions; (c) Dip amount histogram; (d) Contour diagram.

b. Dip Direction and Dip Amount of the Beds

Most of the population lies within the 020°N-040°N interval of the dip direction rose diagram with the highest peak of the diagram (20.7%) as the 020°N-030°N corresponding to the major WNW-ESE trend in the strike rose diagram (Figure 4.6b). Thus the WNW-ESE trending beds which form most of the population in Domain II, preferred to dip towards NE.

The dip amount of bedding planes range in between 06°-86° degrees and the histogram displays a more or less normal distribution with a peaking class of 40°-50° degrees with 19 measurements (Figure 4.6c). The arithmetic mean for dip amounts is ~ 46 degrees.

The poles of the beds display 4 populations, 3 of which correspond roughly to the same great circle (Figure 4.6d). The deviation of the 4th population from the great circle may be the result of faulting.

4.2.3. Domain III

Domain III is a tectonic window of Upper Cretaceous radiolaria-bearing units exposed on top and foots of a hill in the west of Bayamlı hill in the northwest of the study area, surrounded by the over thrusting Cretaceous ophiolitic melange units (Figure 3.2). The dykes outcropping within this domain cut both the Cretaceous ophiolitic melange and folded Upper Cretaceous radiolarian bearing units, which were unconformably overlain by Pliocene clastics.

In Domain III, measurements were taken from 35 different measurement stations and 41 dyke measurements were analyzed. Unfortunately, only 5 bedding plane measurements could be taken in domain III, because bedding planes were not easily observable or measurable due to the high exposure of the concerning formations to erosion, or even some formations cut by the dykes do not posses any bedding planes. Due to the insufficiency of bedding plane data in Domain III, only measured dykes were analyzed under this heading and the bed measurements of Domain III were used in the overall bedding plane analysis of the study area.

4.2.3.1. Dykes

a. Strike of the Dykes

On the prepared rose diagram of strikes for domain III, the general trend is determined as NNE-SSW represented roughly by the 010°N-060°N intervals (Figure 4.7a). The vast majority of this NNE-SSW trending set falls between 020°N-050°N intervals, which at the same time includes the most crowded three classes of the whole diagram. The peak of the strike rose diagram is the class of 030°N-040°N with a 22% maximum percentage of the total measurements. There is also a minor population trending roughly in E-W direction. The calculated vector mean is ~50°N and the true population interval is 036°N-064°N.

b. Dip direction and Dip Amount of the Dykes

The dykes belonging to the major NNE-SSW trend, are almost distributed equally to both of the dip directions, NW and SE, on the rose diagram of dip directions with two highest peaking classes of dip directions, namely the 300°N-310°N (14.6% of total) and 110°N-120°N (12.3% of total) intervals (Figure 4.7b). The E-W trending dykes are also dipping in both N and S directions. In general, the dykes dip almost equally towards N and S directions in Domain III.

Almost all dykes in Domain III (39 out of 41) have dip amounts greater than 60° (Figure 4.7c). The dip amount histogram increases suddenly towards the vertical and almost half of the dykes (20 out of 41) are included in the 80°-90° interval resulting in a high arithmetic mean of dip amount (~77 degrees).

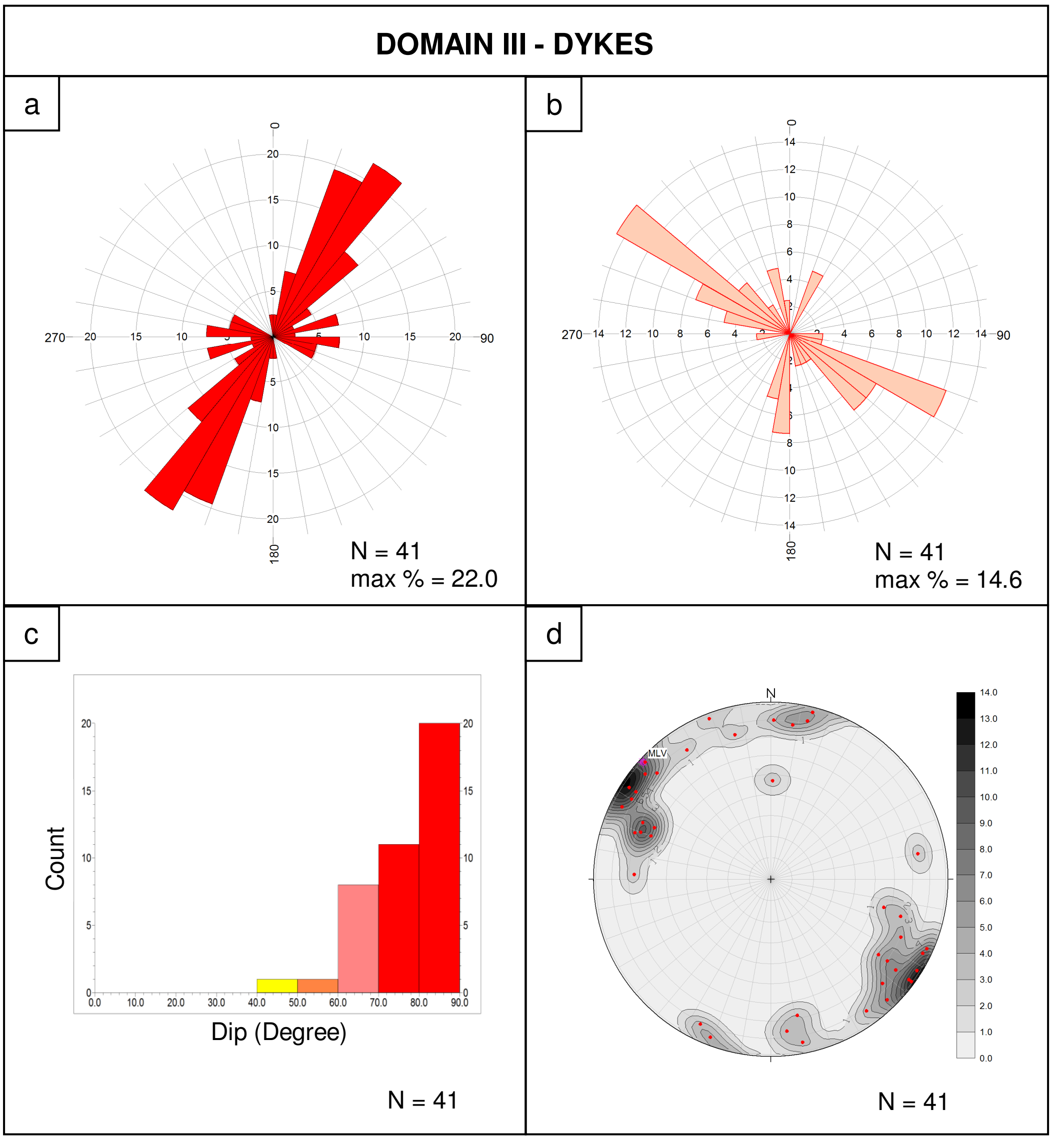

Figure 4.7: Diagrams for the dykes in Domain III. (a) Rose diagram of trends; (b) Rose diagram of dip directions; (c) Dip amount histogram; (d) Contour diagram.

According to the contour diagram, the majority of the dyke poles are mostly in the WNW and ESE margins of the diagram indicating a major trend in NNE-SSW direction (Figure 4.7d). However, the distribution deviates towards the N and S margins with fewer poles indicating the minor trend in the opposite E-W directions. The point maximum is on the NW quadrant but the poles are distributed almost equally to both sides, indicating the dip directions towards both NW and SE. The steep dips of dykes can also be recognized from the gathering of the poles on the margins of the diagram.

4.2.4. All Domains

Results of the analyses performed on the attitudes of dykes and beds on domain basis pointed out that they do not reflect major distinctive differences (Table 4.1). Therefore, analyses were also carried out for the whole study area to visualize the overall patterns for both dyke and bed data.

4.2.4.1. Dykes

a. Strike of All Dykes

A total of 190 dyke measurements were taken from the three domains. The overall data displays one major dyke set trending in NE-SW direction on the rose diagram of dyke trends for the whole study area (Figure 4.8a). In fact, the most populated class is the 040°N-050°N interval with a considerable difference (21.1% of total) from the rest, which corresponds to the NE-SW direction. The populations of other class intervals on each side of this maximum, are decreasing stepwise nearly symmetrical towards both the N and E axes. A slight increase in the populations trending N-S and E-W can also be distinguished from the rose diagram of trends. The vector mean of the whole population of dykes is ~50 degrees. A very narrow range is defined between 45°N-56°N for the true population of dyke trends with a 95% of confidence. The minor scattered measurements from the main trend may be due to the displaced, folded or conjugate dykes.

Table 4-1: Comparison of the three domains based on the analyses of dykes and beds.

Structure	Parameters	DOMAIN I	DOMAIN II	DOMAIN III
DYKES	Population	34	115	41
	Strike range (min-max)	021°N-359°N	020°N-350°N	002°N-296°N
	Peaking interval of strikes (max%)	060°N-070°N (26.5%)	040°N-050°N (23.5%)	030°N-040°N (22.0%)
	Vector mean of strikes	46.18°N	52.36°N	49.57°N
	Confidence interval of strikes (95%)	10.97°	6.92°	13.91°
	Major trend set / preferred dip direction	(1) NE-SW / NW	(1) NE-SW / NW	(1) NNE-SSW / NW, SE
	Other trend sets / preferred dip directions	(2) ENE-WSW / NW		(2) E-W / S, N
	Dip direction range (min-max)	089°N-335°N	003°N-353°N	021°N-354°N
	Peaking interval of dip directions (max%)	310°N-320°N (17.6%)	310°N-320°N (20.9%)	300°N-310°N (14.6%)
	Overall preferred dip direction	NW	NW	NW, SE
	Dip amount range (min-max)	36°-90°	33°-90°	47°-89°
	Peaking interval of dip amounts (max%)	80°-90° (52.9%)	80°-90° (40.0%)	80°-90° (48.8%)
	Arithmetic mean of dip amounts	75.71°	74.13°	76.73°
	Mean lineation azimuth/plunge	134.4°N / 2.9°	138.6°N / 11.5°	312.6°N / 1.1°
	Great circle azimuth/plunge	315.1°N / 75.4°	343.1°N / 26.1°	289.8°N / 2.7°
BEDS	Population	44	92	
	Strike range (min-max)	112°N-357°N	004°N-355°N	
	Peaking interval of strikes (max%)	290°N-300°N (20.5%)	290°N-300°N (22.8%)	
	Vector mean of strikes	282.63°N	295.54°N	
	Confidence interval of strikes (95%)	17.55°	11.25°	
	Major trend set / preferred dip direction	(1) WNW-ESE / NE	(1) WNW-ESE / NE	
	Other trend sets / preferred dip directions	(2) ENE-WSW / NW	(2) NNW-SSE / SW, NE	
		(3) NNW-SSE / NE	(3) E-W / S	
		(4) N-S / E, W	(4) NE-SW / SE	
		(5) E-W / N		
	Dip direction range (min-max)	004°N-346°N	002°N-356°N	
	Peaking interval of dip directions (max%)	020°N-030°N (13.6%)	020°N-030°N (20.7%)	
	Overall preferred dip direction	NE	NE	
	Dip amount range (min-max)	14°-90°	06°-86°	
	Peaking interval of dip amounts (max%)	30°-40° (18.2%)	40°-50° (20.7%)	
	Arithmetic mean of dip amounts	51.34°	45.54°	
	Mean lineation azimuth / plunge	198.9°N / 50.4°	195.6°N / 67.4°	
	Great circle azimuth / plunge	065.5°N / 59.0°	043.9°N / 78.8°	

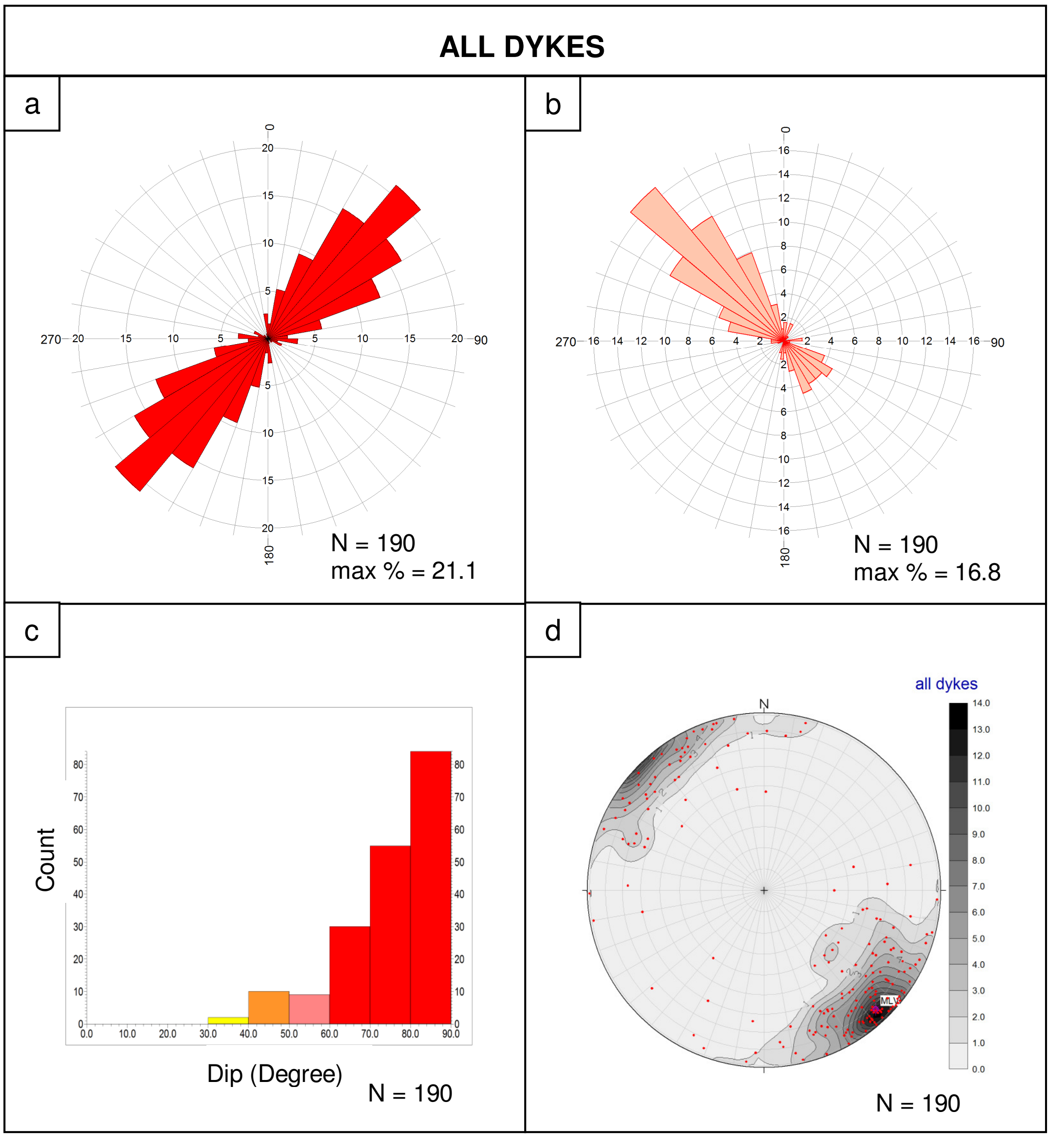

Figure 4.8: Diagrams for the dykes in all domains. (a) Rose diagram of strikes; (b) Rose diagram of dip directions; (c) Dip amount histogram; (d) Contour diagram.

b. Dip Direction and Dip Amount of All Dykes

The majority of the NE-SW-trending dykes are dipping towards NW (Figure 4.8b). The measured dip directions emerging in the NW quadrant of the rose diagram occupies the 63.7% of the whole data (121 out of 190) which is more than twice of the amount of dip direction measurements lying in the opposite SE quadrant (50 out of 190). Among the rest of the measurements, the dykes dipping towards NE is slightly greater than the ones dipping towards SW both of which constitute only the 10% of the total population.

The Kalecik dykes are generally sub-vertical, of which 84 out of 190 measured dykes have dips greater than 80° degrees (~44%) (Figure 4.8c). As it can be seen from the dip amount histogram, even if beginning with 33°, the dip amount increases abruptly towards vertical. The majority of the population is located between 60°-90° interval (89% of total). Thus, the arithmetic mean of dip amounts is significantly high as 75°.

The contour diagram of the poles of all the dykes in the study area also indicates a major trend in NE-SW with gathered data on the opposite NW-SE margins, a dominant dip direction towards NW with the point maximum and most of the data on the opposite SE quadrant, and sub-vertical to vertical dips with the poles gathered mostly along the margin of the diagram (Figure 4.8d).

4.2.4.2. Beds

a. Strike of All Beds

The total 141 bedding plane measurements from all over the study area can be grouped into five sets, trending roughly WNW-ESE, NNW-SSE, E-W, ENE-WSW and NNE-SSW, in decreasing order of population, respectively (Figure 4.9a). Considering the total data, the first set is the dominant trend for bedding planes in the study area. The bed trends peak in the class of 290°N-300°N with the maximum percentage (21.3%). The next crowded class is the neighboring 300°N-310°N interval with more than 10% of data. In fact, these two most crowded populations represent the dominant WNW-ESE trend with more than 30% of the total data, and grouped as a single dominant set of beds for the study area.

The second crowded set can be represented by the 320°N-360°N intervals, significant population of which, is bounded between the 320°N-340°N intervals. The other three minor trends (E-W, ENE-WSW and NNE SSW) are mostly represented by the 270°N-280°N, 060°N-070°N and 030°N-040°N class intervals, respectively.

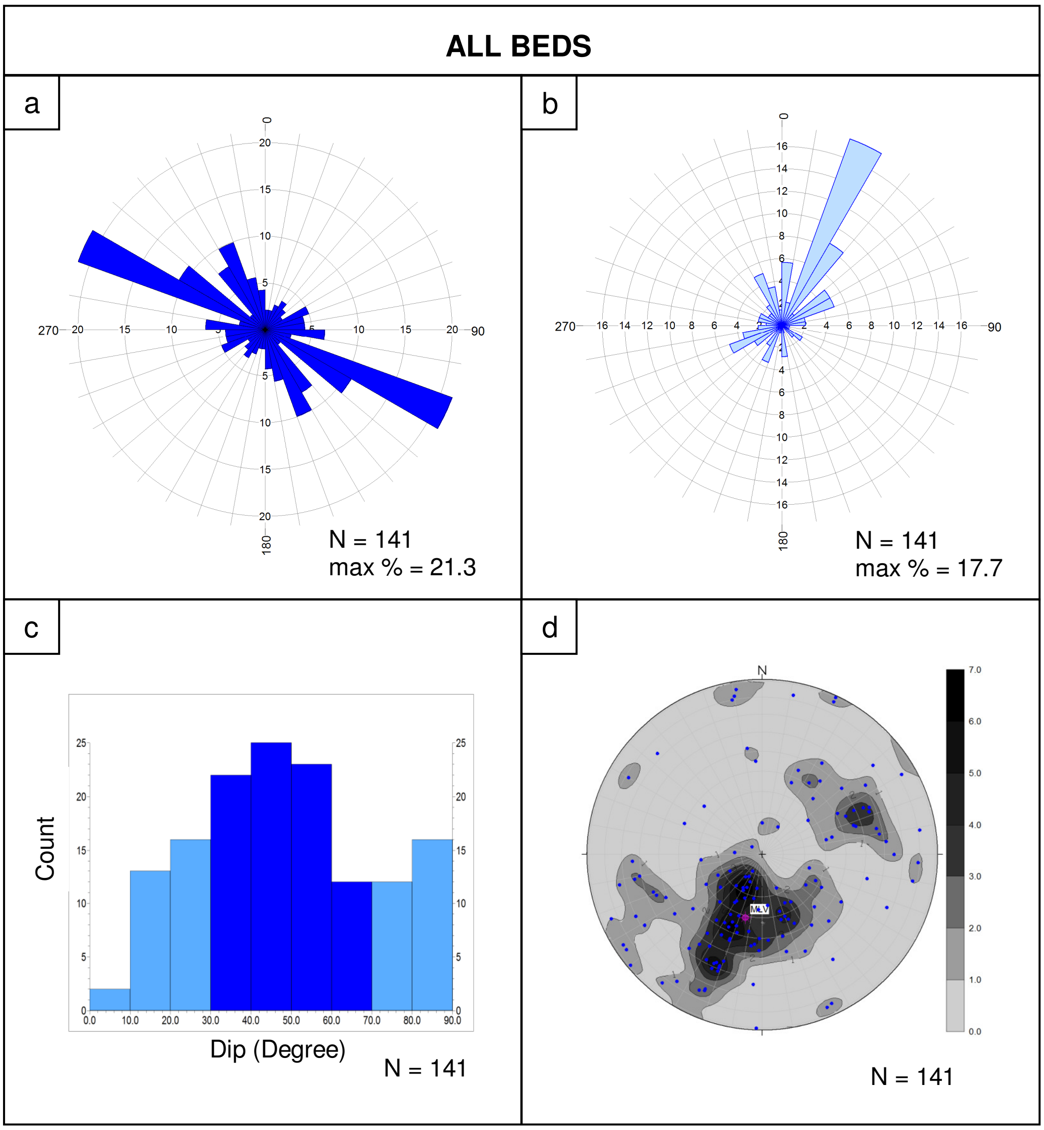

Figure 4.9: Diagrams for the bedding planes in all domains. (a) Rose diagram of strikes; (b) Rose diagram of dip directions; (c) Dip amount histogram; (d) Contour diagram.

b. Dip Direction and Dip Amount of All Beds

Almost all the beds belonging to the dominant WNW-ESE trend, are dipping towards NE (between 020°N-040°N with ~25% of the total data), which is enough to make most of the population gather in the NE quadrant of the dip direction rose diagram (Figure 4.9b). The peak is at the 020°N-030°N interval with 17.7% out of total. However, the beds belonging to the second major trend (NNW-SSE), are dipping in both NE and SW directions with similar sized populations. The other three minor sets are mostly dipping towards N. In general, majority of the dip direction data is gathered on the northern half of the diagram indicating the preferred N direction and the dominant dip direction is towards NE for the measured bedding planes in the study area.

The dip amount of beds measured in the study area ranges widely from 06° to 90°, but the histogram displays a more or less normal distribution with a mean of 48° (almost equal to the midpoint) (Figure 4.9c). The peaking class is again the middle 40°-50° interval having 25 data of the total 141 measurements. Half of the bedding plane population has dips between 30°-60° (70 out of 141). There are also gently dipping and steeply inclined beds in considerable amounts. The least populated class is the 00°-10° interval with only 2 measurements and the size of the 80°-90° interval unexpectedly increases (with 16 measurements) which contradicts to the general appearance of the distribution. In general, the study area mostly possesses beds with moderately to steeply inclined bedding planes.

From the contour diagram of bedding planes for the total data, 2 major and 3 minor bullseye populations attracts attention (Figure 4.9d). The major ones and one of the minors seem to be on the same great circle and the other minor population deviates from the common great circle. Thus, these populations may be the faulted derivatives of a common fold or a composite folding might be occurred in the study area. It represents the tectonic complexity of the region. However, a rough trend of WNW-ESE may reflect a region wide folding occurred in the region.

The results of the overall analyses of the dykes and beds were summarized in the table below (Table 4.2).

Table 4.2: The results of the overall evaluation of the dyke and bed orientation data for the whole study area.

Structure	Parameters	ALL DOMAINS
DYKES	Population	190
	Strike range (min-max)	002°N-359°N
	Peaking interval of strikes (max%)	040°N-050°N (21.1%)
	Vector mean of strikes	50.64°N
	Confidence interval of strikes (95%)	5.4°
	Major trend set/preferred dip direction	(1) NE-SW / NW
	Dip direction range (min-max)	003°N-354°N
	Peaking interval of dip directions (max%)	310°N-320°N (16.8%)
	Dip amount range (min-max)	33°-90°
	Peaking interval of dip amounts (max%)	80°-90° (44.2%)
	Arithmetic mean of dip amounts	74.97°
	Mean lineation azimuth / plunge	136.8°N / 7.5°
	Great circle azimuth / plunge	355.7°N / 11.8°
BEDS	Population	141
	Strike range (min-max)	004°N-357°N
	Peaking interval of strikes (max%)	290°N-300°N (21.3%)
	Vector mean of strikes	289.9°N
	Confidence interval of strikes (95%)	9.52°
	Major trend set/preferred dip direction Other trend sets/preferred dip directions	(1) WNW-ESE / NE (2) NNW-SSE / NE, SW (3) E-W / N (4) ENE-WSW / N (5) NNE-SSW / N
	Dip direction range (min-max)	002°N-356°N
	Peaking interval of dip directions (max%)	020°N-030°N (17.7%)
	Overall preferred dip direction	NE
	Dip amount range (min-max)	06°-90°
	Peaking interval of dip amounts (max%)	40°-50° (17.7%)
	Arithmetic mean of dip amounts	47.83°
	Mean lineation azimuth / plunge	195.0°N / 59.1°
	Great circle azimuth / plunge	048.6°N / 71.7°
	Fold axis azimuth / plunge	318.6°N / 18.3°

4.3. Faults

During the field studies, various fault plane data from different structural domains in the study area, also gathered and analyzed for structural and statistical purposes. Faults, which are cross-cutting the previously mentioned dykes and displacing them, were recognized and measured around the west of Bayamlı Hill in the northwest of the study area, and along the northern and southern sides of the Kızılırmak River in the central part, respectively. Some fault plane measurements were taken from a major fault, informally named in this study as the "Kızılırmak River Fault", which trends parallel to the Kızılırmak River course. Lastly, some fault measurements were taken from the Miocene volcanics unconformably overlying the Cretaceous melange units (Figure 4.2). No travertine formations were observed related to faulting in the study area.

In the field studies, totally 100 fault data were taken from 54 fault planes at 33 measurement stations. However, slip data could not be measured on some of the fault planes because of the difficulties in observing the sense indicators on highly eroded or altered fault plane surfaces. In the analyses, fault planes lack of slip data were only used in the lineament analyses (rose diagrams). The faults with slip data were utilized in the kinematic analyses for the identification of the principle stress directions.

4.3.1. The "Kızılırmak River Fault"

The fault plane data of the informally named "Kızılırmak River Fault" were measured in the south of Aktepe Hill from a station located in the north side of the river, very close to its NE-SW trending river course which is dissecting the whole study area from west to east (Figure 3.2 and 4.2). According to the measurements, the strikes of the fault plane data ranges in between 221°N-261°N, in other words, corresponding to an ENE-WSW trend on the rose diagram for strikes (Figure 4.10a) which is parallel to the river course. In fact, according to the field observations, the trend of the fault plane follows the river course throughout the study area. The measured length of the exposed fault is approximately 1,350 meters but it possibly reaches to a length of more than 7 kilometers to the NE and SW, within the margins of the study area. The fault plane is dipping towards NW with measured dip amounts ranging from 68° to 77° and rake values from 03° to 11° (Figure 4.11).

As it can be understood from the field measurements, observations and from the slip analysis carried out, it is a right lateral strike-slip fault extending in a roughly NE-SW trend parallel to the Kızılırmak river course with a north verging fault plane and a revealed reverse component (Figure 3.2, Figure 3.6 and 4.12). The Cretaceous ophiolitic melange units, the Upper Cretaceous radiolarites and the tectonic contact between them on each side of the river were displaced by this system. It is the structural controlling factor for the course of the Kızılırmak River in the study area accompanied by the alluvial fan deposition all along the both sides of the Kızılırmak River related with faulting. The "Kızılırmak River Fault" probably cuts also the faults displacing the dykes. Geologically, the Quaternary terraces are hanged about 30 meters above the today's river bottom, which is probably related with the activiy of this fault during Quaternary.

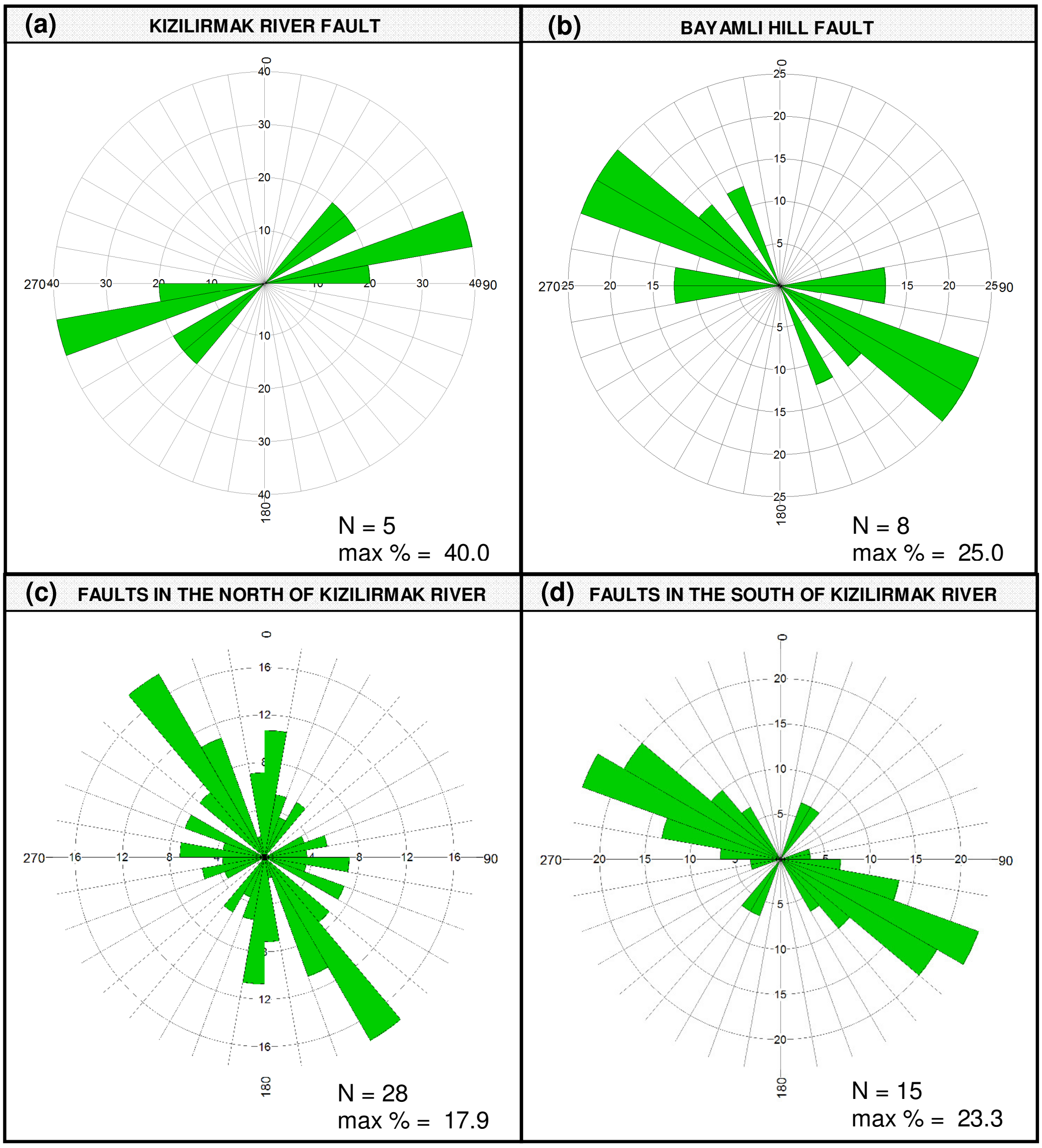

Figure 4.10: Length-weighted rose diagrams of the faults in different domains in the study area.

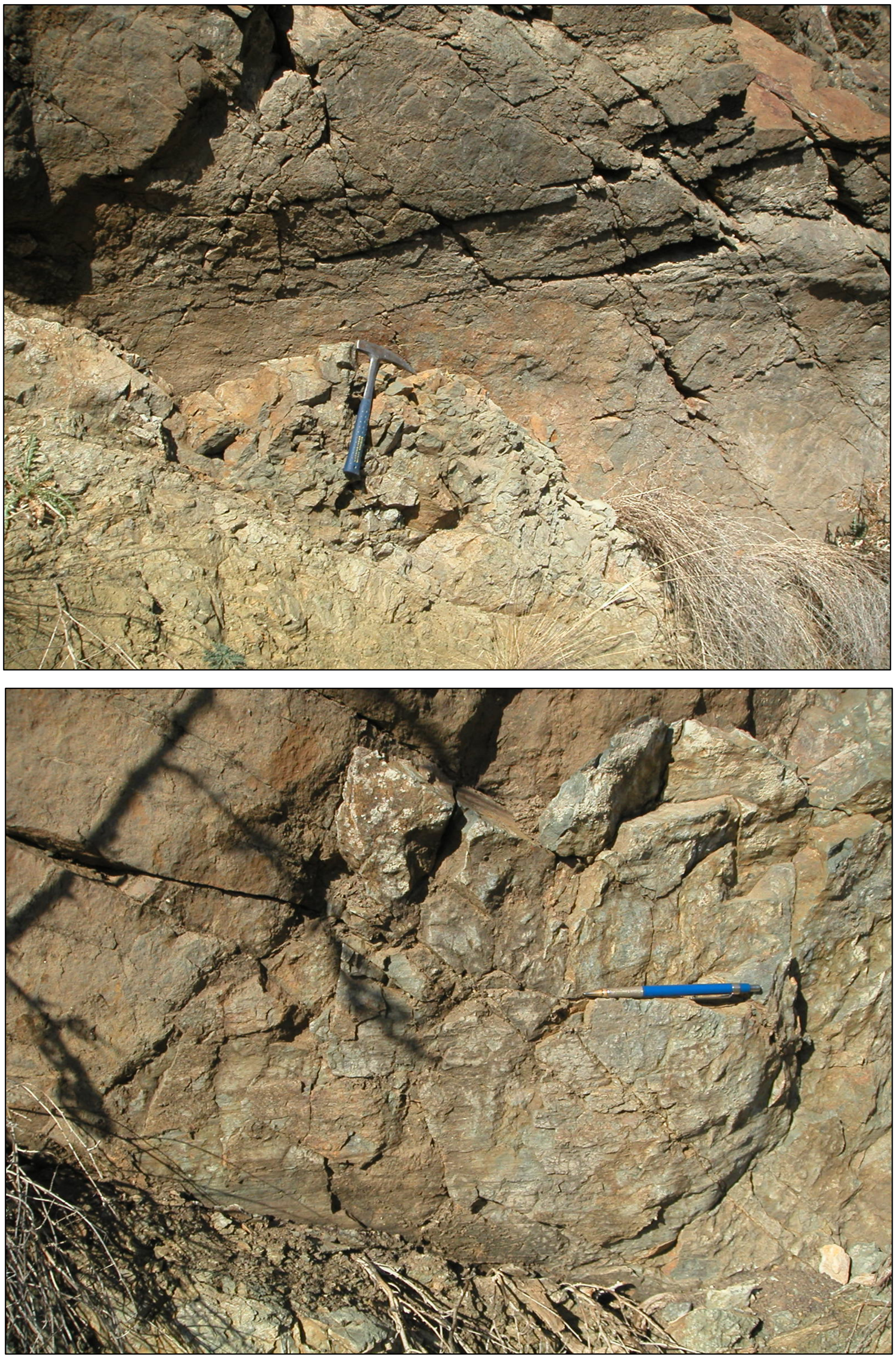

Figure 4.11: Kızılırmak River Fault Plane, along the north side of the Kızılırmak River.

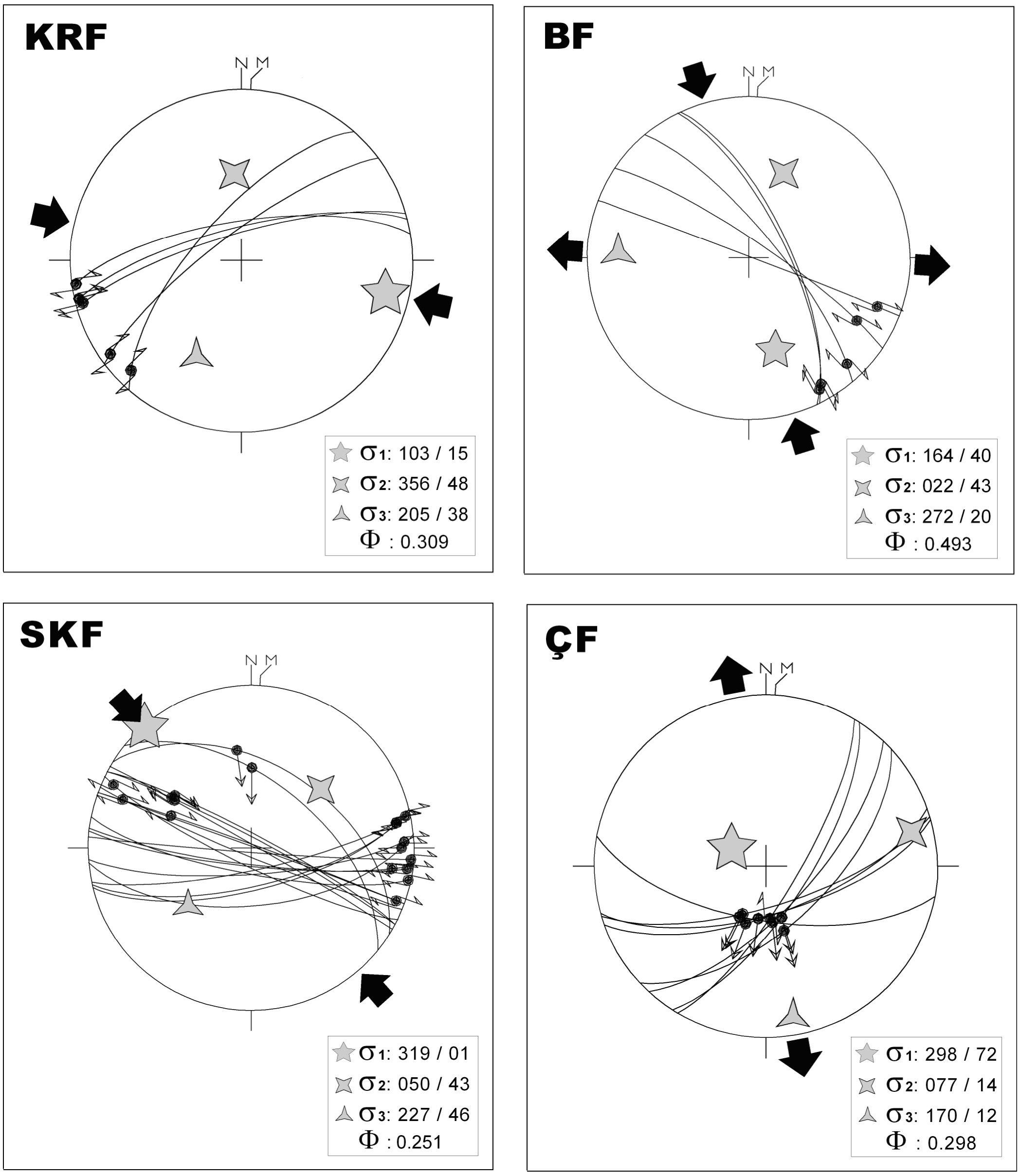

Figure 4.12: Paleostress tensors obtained by the fault slip data in kinematic analyses for the faults in different domains of the study area. KRF: Kızılırmak River Fault, BF: Bayamlı Hill Fault, SKF: South of Kızılırmak Faults, ÇF: Çamın Hill Fault.

4.3.2. Bayamlı Hill Faults

Faults mentioned here are exposed around the Bayamlı Hill, within a tectonic window of Upper Cretaceous radiolaria-bearing units (Figure 3.2 and 4.2).

According to the fault measurements taken from several fault planes in different stations around the Bayamlı Hill, the strikes of the faults trend mostly in NW-SE direction. more than half of the population lies in 290°-320° interval with the peaking interval of 290°N-310°N (Figure 4.10b). Faults planes trending in NNW-SSE and E-W directions are also present.

Except two SW dipping fault planes, the major dip direction is towards NE with dip amounts ranging between 41°-89°.

However due to inadequacy of the slip data belonging to reverse fault planes with strike-slip components, a certain decision cannot be achieved. According to the kinematic analysis carried out on the fault plane measurements with measured slip data which cut and displace dykes and related Upper Cretaceous radiolarian bearing units, the faults around the Bayamlı Hill display a right lateral strike-slip faulting with normal component (Figure 4.12b).

4.3.3. Faults in the northern side of the Kızılırmak River

Several faults that are cutting and displacing the previously mentioned dykes and related Upper Cretaceous radiolarian bearing units were recognized and measured at different stations belonging to different fault planes mainly within Upper Cretaceous radiolarian bearing units. The measured fault planes are exposed along the north of the Kızılırmak river valley, towards the south of Aktepe Hill, towards the southwest of Kabak Hill, between the south of Çamın Hill and north of Aktepe Hill (Figure 3.2 and 4.2). There are some measurements taken from a few stations towards the east of the study area where the Cretaceous ophiolitic melange units and the dykes cutting them were displaced.

The major trend of the faults is NW-SE represented mostly by the 310°N-340°N intervals with the peak of the rose diagram as 320°N-330°N interval (17.9% out of total) (Figure 4.10c). Another highly populated trend is in N-S direction represented by the 350°N-020°N intervals with most of its data in 360°N-010°N interval. Some E-W trending faults can also be observed.

The inclination of the fault planes ranges between 15°-90° and dips are both towards N and S. Some of the faults are dip-slip faults, but in some, the dominant motion is strike-slip. There are both left lateral and right lateral strike-slip faults with normal and reverse components and also some dip-slip normal and reverse faults (Figure 4.13). However, kinematic analysis could not be carried out due to inadequate slip data to be analyzed together.

They cut and displace the dykes together with the Upper Cretaceous radiolarian bearing units and the other Cretaceous mélange units.

4.3.4. Faults in the southern side of the Kızılırmak River

Fault plane measurements were taken from stations along the southern slope of Kızılırmak River valley from the Upper Cretaceous radiolaria-bearing units along the course of the Kızılırmak River which was partly covered by Plio-Quaternary units (Figure 3.2 and 4.2).

The major trend of the faults is WNW-ESE with the peaking 290°N-300°N interval followed by the 300°N-310°N interval as the secondmost crowded class of the rose diagram (Figure 4.10d). Few of the measurements lie in the 020°N-040°N intervals corresponding to a NNE-SSW trend. The 90° difference between these two trends probably indicates the conjugate faults.

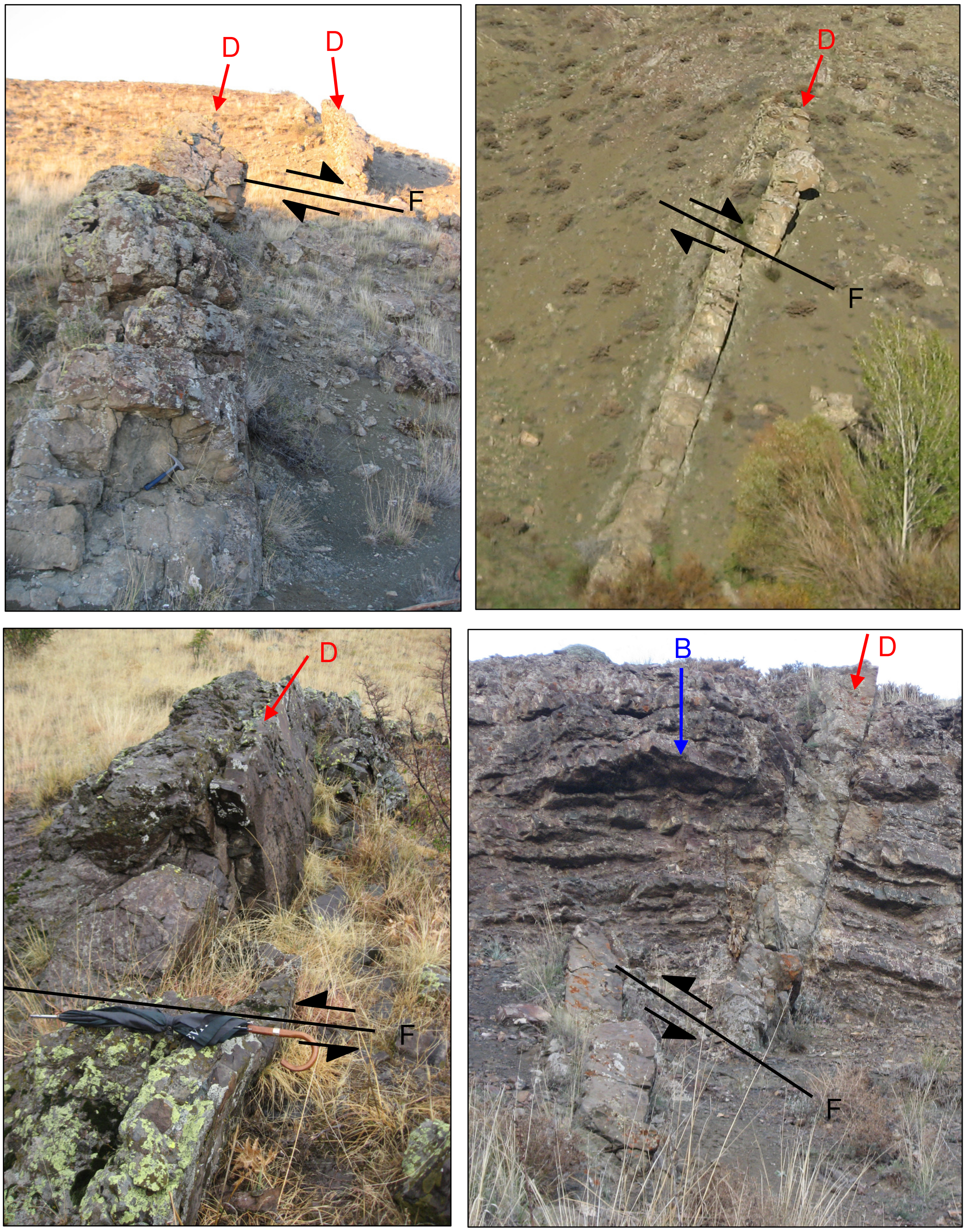

Figure 4.13: Faults in the north of Kızılırmak River (D: dyke, B: bed, F: fault, arrows indicate relative sense of motion along faults).

The measured faults displace the Upper Cretaceous radiolaria-bearing units, the Cretaceous ophiolitic melange units and the dykes.

According to the kinematic analysis carried out on the fault plane measurements with measured slip data which cut and displace dykes and related Upper Cretaceous radiolarian bearing units, the faults in the south of the Kızılırmak river display a right-lateral reverse motion (Figures 4.12 and 4.14).

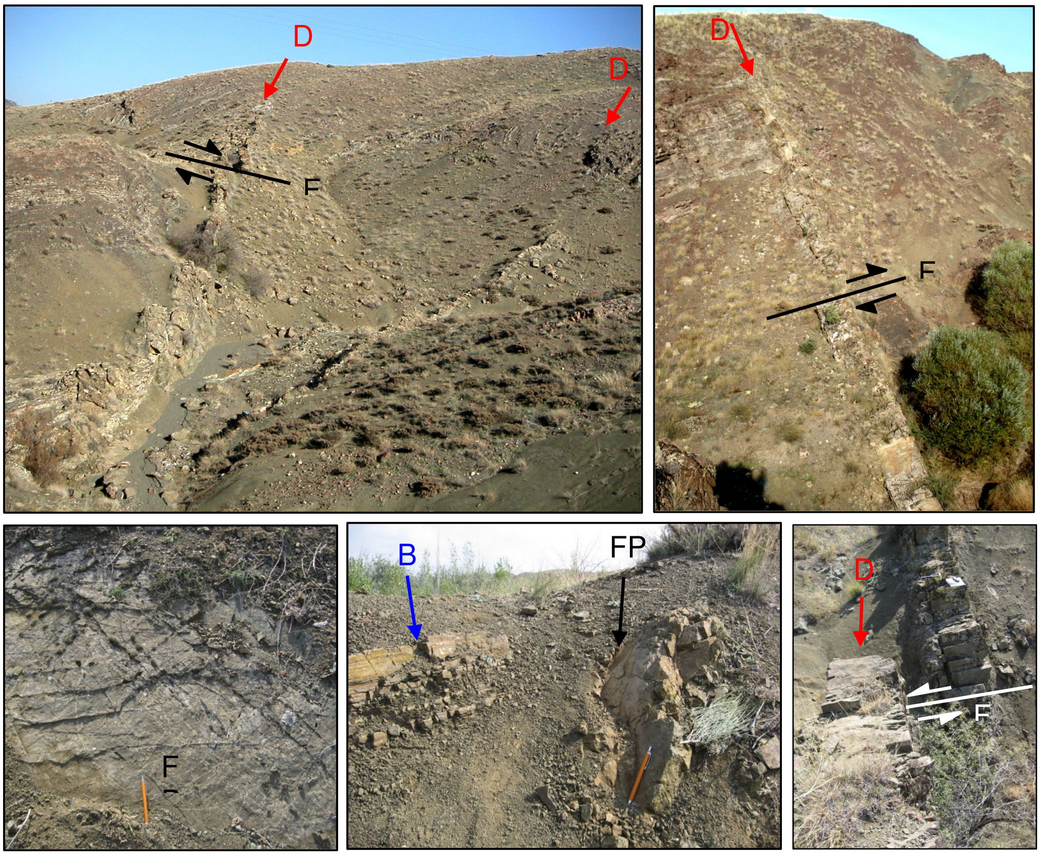

Figure 4.14: Faults in the south of Kızılırmak River (D: dyke, B: bed, F: fault, FP: Fault plane, arrows indicate relative sense of motion along faults).

4.3.5. Çamın Hill Faults

These are relatively small-scale faults exposed around the Çamın Hill in the northeast of the study area. Their extent is limited in the study area within the lithological boundaries of the Miocene cover composed mainly of volcaniclastics.

The fault data were taken from two stations in the northwest of Çamın Hill belonging to two different fault planes. The general trend of the relatively major one is in NE-SW direction, mostly between 030°N to 050°N and 070°N to 080°N. The fault plane is dipping towards south with dip amunts ranging from 61° to 76° degrees and rakes ranging from 43° to 82° SW displaying a normal motion on the fault plane (Figure 4.12 and 4.15).

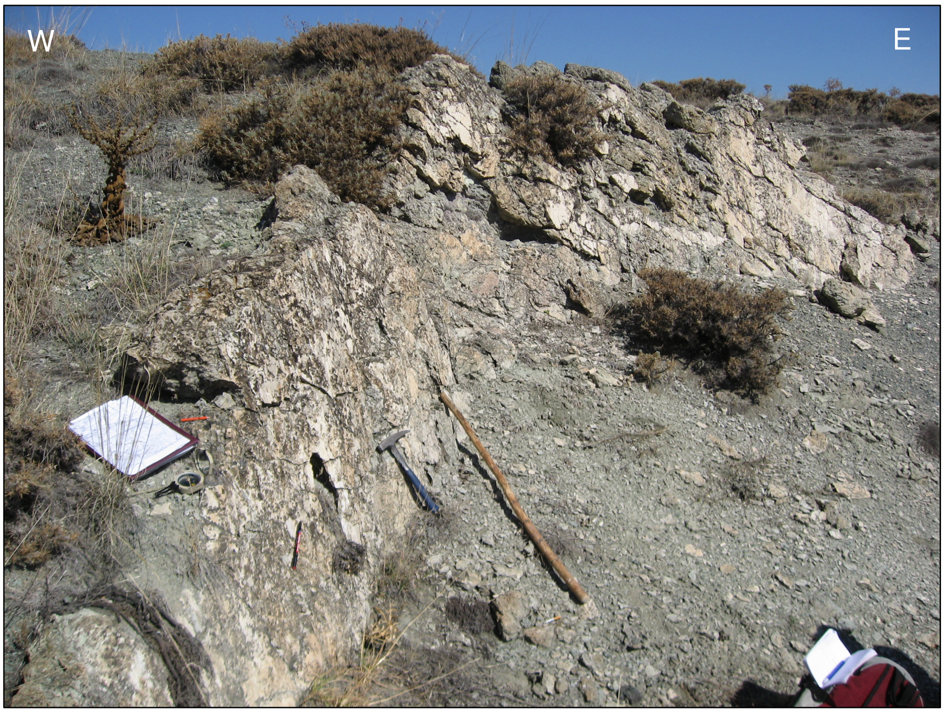

Figure 4.15: Fault plane displaying a normal motion, measured from the northwest of Çamın Hill, east of Kalecik.

The second minor fault plane trends in NW-SE direction. The fault plane is sub-vertical and slightly undulating with dip amounts ranging in between 080° to 89° and mostly dipping towards SW with rakes lower than 20° but displaying over printed two phases of strike-slip motion as an older right-lateral and a younger left-lateral motion on the same fault plane according to field observations. The slip data analysis for this fault plane can not be done due to insufficient data.

4.3.6. Kinematic Analyses of the Fault Planes (Fault-slip Analyses)

A computation of the paleostress tensor geometry was performed according to the method of Angelier (1984) by the “Angelier Direct Inversion Method (version 5.42)” software, using fault-slip data sets acquired from the measurement stations at the structural domains of the study area, in addition with the Kızılırmak River Fault and Çamın Hill faults. It is tried to obtain a best fit between the reconstructed tensor quality and the greatest number of used fault planes with slip data. the fault plane-slip data for a fault more than three, were analyzed and the results are summarized (Table 4.3). The fault-slip data constitutes the 83% (83 out of 100) of the total fault measurements and 43.4% of the available slip data were used in the slip analyses. 4 tensor sites were identified namely, (i) the Kızılırmak River Fault, (ii) Bayamlı Hill faults, (iii) the faults in the southern side of the Kızılırmak River, and (iv) the Çamın Hill Faults, respectively (Figure 4.12). The paleostress tensor analysis can not be done for the faults in the northern side of the Kızılırmak River and for the faults trending along the western margin of the study area due to lack of enough fault-plane-slip data.

(i) Kızılırmak River Fault (KRF)

The slip tensor analysis were carried out on 5 stations. The results show that KRF is a dextral strike-slip fault with a reverse component (Figure 4.12 and Table 4.3). The principal stress axis (σ_1) is on circle (horizontal), whereas the minimum stress axis (σ_3) is oblique. The confidence on phi-ratio (0.309) points out the more clearance for σ_1 indicating a transpressional faulting.

ii) Bayamlı Hill Faults (BF)

The slip tensor analysis were carried out on 3 stations. According to the prepared tensor for the Bayamlı faults (Figure 4.12), the maximum principal stress axis (σ_1) is between the circumference and centre of the tensor indicating an inclined axis operating in a roughly N-S trend. The minimum principle stress axis (σ_3) have a gentler plunge (close to the circumference) acting in E-W direction. It can be concluded from the phi-ratio of about average (0.493) that, the reliability of the positions of both axis is same but not very definite. Regarding the two principal axes (σ_1 and σ_3), the Bayamlı Hill faults were roughly N-S-trending dextral strike-slip faults with E-W-trending normal components as a result of a transtensional stress field effected on the region (Table 4.3).

iii) Faults in the south of Kızılırmak River (SKF)

The paleostress tensor is obtained by the combination of 18 slip data measured on 6 different fault planes from 2 measurement stations (Figure 4.12). According to the phi-ratio closer to zero value and less than 0.3 (0.251), the orientation of the maximum principle stress axis (σ_1) is much more reliable than the (σ_3) axis (Table 4.3). It is horizontal (on the circumference of the tensor field) and operating in a NW-SE trend on the roughly E-W-trending fault planes resulting in a dominant dextral strike slip motion with reverse component, with an inclined minimum principle stress axis (σ_3) acting in NE-SW direction. The confidence of the phi-ratio indicates a transpressional stress field.

iv) Çamın Hill Fault (ÇF)

The paleostress tensor (ÇF) was obtained for a fault plane measured at a station on the Çamın Hill which is covered by Miocene volcanics. The results show that ÇF is a normal fault (Figure 4.12, Table 4.3). The maximum principle stress axis (σ_1) is vertical (at the center of the tensor) and trending in WNW-ESE direction with higher reliability according to phi ratio (0.298). Whereas, the minimum principle stress axis (σ_3) is on the circumference (horizontal) trending in N-S direction. The relationship between the (σ_1) and (σ_3) indicates an extension in almost N-S direction (Figure 4.12). The confidence of the phi-value which is less than 0.3 (0.298) points out an extensional faulting.

Table 4-3: Palaeostress tensors computed from fault-slip data.

Domain	**Tensor**	**Average trend of faults**	**Orientation of palaeostress** (Trend / Plunge) in degrees			**Ratio PHI** $[(\sigma_2-\sigma_3)/(\sigma_1-\sigma_3)]$	**Population**	**Fault type**	**Regime**	**Relative age**
			σ_1	σ_2	σ_3	Φ	N			
Kızılırmak River Fault	KRF	ENE-WSW	103/15	356/48	205/38	0.309	5	Dextral reverse	Transpression	post-dyke emplacement -Quaternary
Bayamlı Hill Faults	BF	NW-SE	164/40	022/43	272/20	0.493	5	Dextral normal	Transtension	post-dyke emplacement
South of Kızılırmak Faults	SKF	NW-SE	319/ 01	050/43	227/46	0.251	18	Dextral reverse	Transpression	post-dyke emplacement
Çamın Hill Faults	ÇF	NE-SW	298/72	077/14	170/12	0.298	8	Normal	NNW-SSE Extension	post-dyke emplacement

CHAPTER 5

RESULTS AND DISCUSSIONS

According to the field observations, structural and statistical analyses that were carried out on the Kalecik basaltic dykes together with beds and faults, the results were evaluated and discussed in terms of the orientations of dykes, beds and faults, their age relationships with respect to each other and regional deformations indicated by these structures.

5.1. Age relationships of dykes

In relative age dating, the relationship of dykes with other successions including the ones that are commented or relatively dated is very important. The dykes of the Kalecik region are interpreted as a part of the ophiolites and accepted same age with the Cretaceous ophiolitic suite (e.g. Tankut and Sayın 1989). However, the basic dykes cross-cut the Melange and its blocks (Figure 3.18).

Kalecik dykes and cross-cutting contacts are unconformably overlain by the Miocene volcaniclastics, Pliocene clastics and Quaternary age river terraces (Rojay et al., 2007). These relationships show that the emplacement of the Kalecik dykes is pre-Miocene in the region. On the other hand, since the dykes cut the Upper Cretaceous ophiolitic melange which had been overthrust on the Paleocene sequences and the Upper Cretaceous radiolaria-bearing units, the emplacement age of the dykes should be post-Paleocene – pre-Miocene.

5.2. Trends of beds and the cross-cutting dykes

According to the results of the analyses of beds, it became obvious that the region have had a very complex tectonic deformation. The units are observed as intensely folded and faulted as a result of the compressional regime acted on Central Anatolia during Cretaceous which is also responsible from the mélange formation. However, in spite of this complex deformation, the contour diagram of the poles of beds excluding some deviations, revealed a rougly common great circle from which the trend of the fold axis could be determined as NW-SE (~319°N) (Figure 5.1). It might roughly be the indication of the compressional regime with the maximum principle stress axis (σ_1) oriented normal to the fold axis in the opposite NE-SW direction.

Basaltic dykes in the Kalecik region are sub-vertical and aligned in a nearly parallel fashion with respect to each other with a trend of NE-SW (045°N) (Figures 5.1 and 5.2). According to the results of the analyses carried out for three domains, it is revealed that the general orientation of the dykes did not considerably effected by other structural elements. It is obvious from both the field observations and the analyses that, they were not coeval with the beds they cut because they were not deformed in a similar way as the Cretaceous Mélange and the Upper Cretaceous-Paleocene units. They must had been intruded after the effects of compressional regime ended in the region. Thus, it can be concluded that the dykes and highly deformed, intruded beds were the results of different tectonic regimes.

No offset of beds were observed along the dyke cutting contacts of the beds. Besides, magma injection do not caused an additional considerable folding or deformation of the beds at the cross-cutting contacts. Therefore, these facts indicate that the forceful injection of the magma is not the case in Kalecik region. Instead, all the clues show that Kalecik dykes were formed as a result of the intrusion of magma into previously formed weakness zones. The alignment and sub-vertical dips of dykes without any offset can be concluded as that they are tensional fractures dilated by magma under the effect of a NW-SE trending minimum tensile stress (σ_3) acted normal to the trend of dykes.

TRENDS OF STRUCTURES FOR ALL DOMAINS		
DYKES	BEDS	DYKE-CUTTING FAULTS
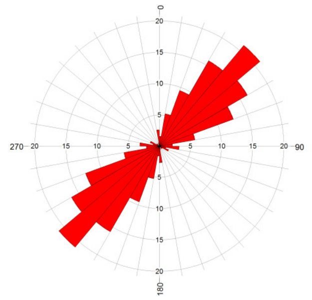	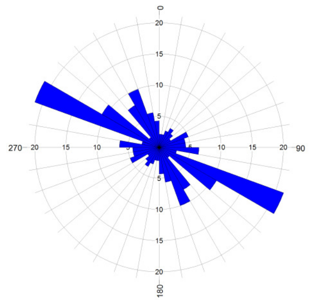	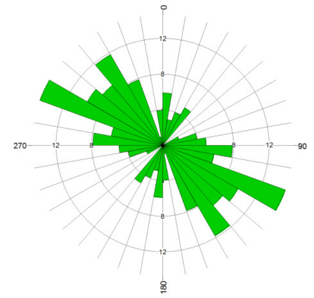
N = 190 max% = 21.1	N = 141 max% = 21.3	N = 51 max% = 14.7

Figure 5.1: Overall comprasion of the dyke, bed and dyke-cutting fault trends for all domains in the study area.

The reason for this extension might be either due to a local stress-relaxation such as in the case of folding and formation of tensional joints that cut the bedded units of a fold almost perpendicular or a local or regional regime change after Paleocene in the region. The major trend of dykes and the trend of the dominant bed set are ~045°N and ~297°N, respectively. If only the major classes of trends are taken into account, than the interval of the dykes strikes and bed strikes are 040°N-050°N and 290°N-300°N, respectively. The angular difference is ~108°. Even if the bedded units display a rough fold axis, it is difficult to accept it as the real case in the study area due to intense deformation of the Cretaceous units observed in the field.

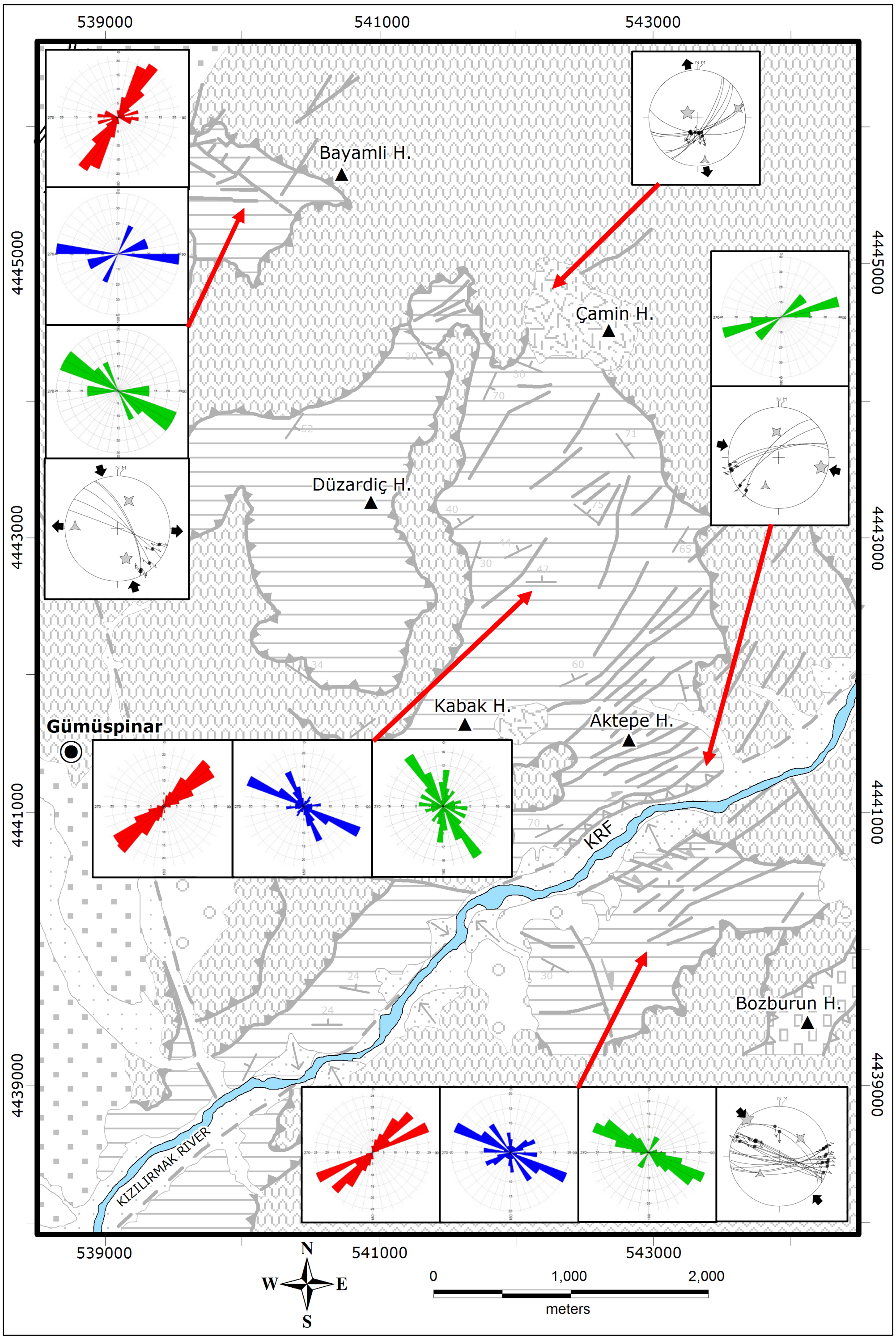

Figure 5.2: The cumulative results of the structural, statistical and kinematic analyses over the study area for different domains (Red: Dyke orientation. Blue: Bed orientation. Green: Fault orientation. Black: Paleostress orientations).

Establishing a direct relationship between the strikes of the bedding planes and the strikes of the dykes (even though they indicate a 108° angular relationship) will not be healthy in terms of structural correlation, based on the knowledge of the complex tectonic history of the region, concerning that the bedded units which are cut by these dykes are already involved in the Cretaceous ophiolitic melange in Kalecik region.

5.3. Trends of the dykes and cross-cutting faults

The dyke cutting faults (measured on both sides of the Kizilirmak River and also around the Bayamli Hill) also displace the beds. The major trends of dyke cutting faults are in WNW-ESE and NNW-SSE directions; the minor sets of faults trend in E-W, N-S and NE-SW directions, in decreasing order of populations, respectively. The dominant direction of dyke trends are not conformable with the major orientations of the fault sets indicating a different fracturing mechanism in the case of faulting. In fact, since the faults displace dykes, their relative ages can be determined as post-intrusion which also indicates the change in orientations of principle stresses after the dyke emplacement along the previously formed fractures.

The trend of the faults cross-cutting the dykes being in the same age are utilized in the interpretation of the possible rotations in the region. The faults on the northern block of the 080°N trending KRF trends 030°N and the ones on the southern block trends 075°N (Figures 5.2 and 5.3).

Therefore, there might be a rotation during the KRF activity which might be clockwise or counterclockwise. However, if there is rotation in the region, this rotation should be in concordance with the Kırşehir Block indentation which must be counterclockwise. The NW block must be relatively stable when compared with the SE block. If it is the case, then the age of transcurrent faulting should be Eocene in the region.

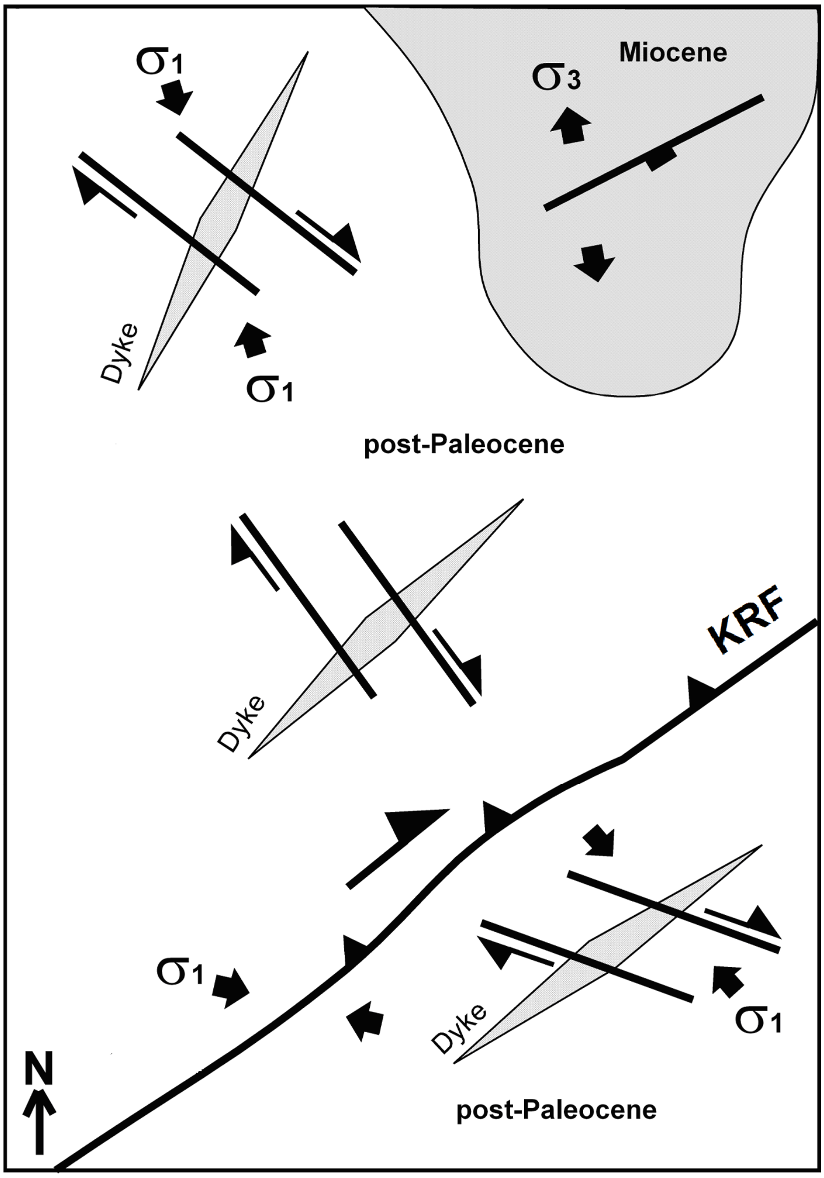

Figure 5.3: The different stages of tectonic deformations which took place in different time periods over the study area with related structures.

5.4. Regional Deformations

Since the region is deformed intensely during Cretaceous various types of small scaled faults cutting and offsetting the various units are abundant in the study area and it is difficult to determine the mechanism of these faults according to the tectonic complexity of the region. However, the faults that cuts and displaced the dykes were distinguished from the remaining faults in the study area in order to define palaeostress orientations of a certain time, in oher words, after the intrusion. By measuring and analyzing the dyke-cutting faults a sequential order of stress change was achieved for the study area. the dyke-cutting faults which are younger than the dykes, were measured in 3 domains, namely from both sides of the Kizilirmak River and from Bayamli Hill. The lineament analysis of dyke-cutting faults revealed 4 sets in WNW-ESE, NNW-SSE, E-W and N-S directions, respectively. The majot trend is the WNW-ESE trending set. However, slip data is crucial for palaeostress reconstructions. The faults measured in the northern side of Kizilirmak river are insuffienct due to slip data because of the insufficiency of the sense indicators on fault planes. However the slip data taken from the southern side of the Kizilirmak River and from the Bayamli hill revealed that a transtensional stress field effected on the region. however the a transpressional regime is indicated by the slip data from the faults in the south of Kizilirmak River for the same time interval. in addition to that some measurements were taken from the Micene volcanics which indicates an extensional regime and revealed a definite change in regime after Miocene over the region.

The influence of the rotational movements of the compressional regime caused by the beginning of the closure of Neo-Tethys in Late Cretaceous, lasted until Late Miocene-Pliocene and replaced by an extensional regime after the Late Miocene (Koçyiğit et al., 1995; Rojay and Karaca, 2008). In a general perspective, the north-south compression continued from Cretaceous to Late Miocene and in this intensely folded-thrusted- region, it caused E-W trending structures with various scale and nature and also caused thrusts and related rised areas.

Four different deformation phases have taken place in Çankırı Basin and its surroundings. These are; (1) the NW-SE thrusting period, (2) Paleocene – Oligocene period of combination of thrusting (at the north) and transpression (at the south), (3) extensional deformation due to post-orogenic collapse, (4) currently active transcurrent tectonics from Late Miocene until present (evolution of the NAFZ and escape of Anatolia to the west) (Kaymakçı 2000).

In the Kalecik and its surroundings, located in west of Çankırı basin, it is characterized by the presence of three different tectonic regimes; firstly old compressional tectonic regime (thrusting-folding), secondly extensional regime and finally new strike-slip tectonic regime (Koçyiğit et al., 1995). Compressional tectonic regime is generally represented by the N-S oriented folds of the successions found within the basins that evolved under the west-dipping thrust faults. The new tectonic regime, which becomes obvious by the N-S compressional, N-NE trending left lateral strike slip faulting system, began in Late Miocene-Pliocene time. Since the age controls of the successions are inadequate in the study area, there occur differences in deformation history compared to the other areas in the region. In previous studies, it was suggested that, the thrust system lasted from Eocene till Pliocene. Nevertheless, there is no relationship observed on the geological maps that proves it is a post-Pliocene thrusting. Previous field studies in Ankara region indicates that thrusting regime ended before Pliocene.

As a result of principal stress direction studies in the Kalecik area, a continuous compressional tectonic regime (thrusting-folding-transcurrent tectonics) oriented between NNW - SSE and WNW - ESE compression during post-Paleocene that is followed by WNW-ESE oriented transcurrent tectonic regime (Figure 5.2). With a considerably time gap, approximately NNW-SSE-oriented extensional regime acted in the region during post-Miocene. As it is clearly documented in the area, at the final stage, compressive tectonic regime is interrupted by normal faulting with a left lateral component. The informally named Kizilirmak River Fault was observed as displacing the Quatertary unit so it may still be active which revealed a transpressional motion.

The last tectonic phases possibly acting in the region are interpreted as transcurrent faulting under NNW-SSE compression by the correlation of the continuation of the western margin faults in north (Çankırı area, Kaymakçı, 2000) and as the replacement structure evolution, i.e. re-activation of KRF, during Quaternary with extensional components.

When the trajectories of the principal stresses are taken into account, there is a principal stress orientation rotation from 164/40 to 319/01, NNW to WNW (Figure 5.2). This might be in concordance with the counterclockwise rotation in the region, which is ended in Eocene (Kaymakçı 2000).

CHAPTER 6

CONCLUSIONS

The conclusions on the post-Paleocene deformational history of the Kalecik region by use of the orientation of dykes, beds and faults and kinematic analysis of faults are as follows;

- on dykes; the emplacement ages of the Kalecik dykes are found as post-Paleocene – pre-Miocene based on the stratigraphic relationships. They were emplaced along fractures evolved under NW-SE oriented tensile stresses.

- on bedding planes; the general trend of the strikes of the bedding planes was found as 297°N (WNW-ESE tendency) in the Kalecik region. However, the general trend of the fold axis is observed as ~318°N (NW-SE tendency).

- on the fault analysis; the general trend of the strikes of the same age dyke-cutting faults are found as ~300°N (NE-SW tendency) in the Kalecik region. Depending on the results of the analyses, the orientation of the principal stress direction (σ_1) is moved from NW-SE to WNW-ESE (Figure 5.3). The relationship between the normal faulting and the strike-slip faulting is not clear. However, the slip data measured on a fault plane shows that normal faulting with a left-lateral component was developed at the final stage.

- Dyke, bed and fault attitudes indicate different orientations of palaeostresses which reveals different mechanisms of deformation for different time intervals revealed by cross-cutting relationships.

Therefore, these results seem to be conformable with the previously defined, continuous oriented stress between NNW - SSE and WNW - ESE compression during post-Paleocene that is followed by WNW-ESE-oriented transcurrent tectonic regime. Lately, approximately NNW-SSE-oriented extensional regime acted in the region during post-Miocene. As it is clearly documented in the area, at the final stage, compressive tectonic regime is interrupted by normal faulting with a left lateral component.

To conclude, post-Paleocene – pre-Miocene Kalecik basaltic dykes are evolved under a nearly NE-SW-oriented stress regime and deformed under a continuous NW-SE-oriented post-Paleocene compressional to strike-slip tectonic regime which is followed by a NNW-SSE-oriented post-Miocene extensional-transtensional regime.

REFERENCES

Akıman, O., Erler, A., Göncüoğlu, M.C., Güleç, N., Geven, A., Türeli, T.K. and Kadıoğlu, Y.K., 1993. Geochemical characteristics of granitoids along the western margin of the Central Anatolian Complex and their tectonic implications. Geol. Journal 28, 371-382.

Akyürek, B., 1981. Basic geological characteristics of the northern portion of the Ankara Melange (Ankara Melanjı'nın kuzey bölümünün temel jeoloji özellikleri). Proceedings of the Symposium on the Geology of Central Anatolia, Ankara, March 1981, Geological Society of Turkey 35th Annual Meeting, 41-45.

Akyürek, B., Bilginer, E., Çatal, E., Dağer, Z., Soysal, Y. and Sunu, O., 1979. Eldivan-Şabanözü (Çankırı) dolayında ofiyolit yerleşimine ilişkin bulgular. Chamber of Geological Engineers of Turkey Bulletin, 9, 5-11.

Akyürek, B., Bilginer, E., Çatal, E., Dağer, Z., Soysal, Y. and Sunu, O., 1980. Eldivan-Şabanözü (Çankırı) Hasayaz-Çandır (Kalecik-Ankara) dolayının jeolojisi. MTA report no. 6741 (unpublished).

Akyürek, B., Bilginer, E., Akbaş, B., Hepşen, N., Pehlivan, Ş., Sunu, O., Soysal, Y., Dağer, Z., Çatal, E., Sözeri, B., Yıldırım, H. and Hakyemez, Y., 1984. The geology of the Ankara-Elmadağ-Kalecik region (Ankara-Elmadağ-Kalecik dolayının temel jeoloji özellikleri). Chamber of Geological Engineers of Turkey Bulletin, 20, 31-46 [in Turkish with English abstract].

Anderson, E. M., 1942. The Dynamics of Faulting (1st edn). Oliver and Boyd, Edinburg.

Anderson, E. M., 1951. The Dynamics of Faulting and Dyke Formation with Applications to Britain (2nd edn). Oliver and Boyd, Edinburg, 206p.

Angelier, J., 1979. Determination of the mean principal directions of stresses for a given fault population. Tectonophysics 56, T17-T26.

Angelier, J., 1984. Tectonic analysis of fault slip data sets. Journal of Geophysical Research 80, 5835–5848.

Angelier, J., 1989. From orientation to magnitudes in palaeostress determinations using fault slip data. J. Struct. Geol. 11, 37-50.

Angelier, J., 1990. Inversion of field data in fault tectonics to obtain regional stress. III: A new rapid direct inversion method by analytical means. Geophysical Journal International 103, 363–376.

Angelier, J., 1994. Fault slip analysis and paleostress reconstruction. In: (ed. Hancock, P.L.) Continental deformation. Pergamon Press, Oxford. 53-100.

Armijo, R., Carey, E. and Cisternas, A., 1982. The inverse problem in microtectonics and the separation of tectonic phases. Tectonophysic. 82, 145-169.

Arthaud, F., 1969. Méthode de determination graphique des directions de raccourcissement, d'allongement et intermédiaire d'une population de failles. Bull. Soc. Geol. Fr. 7, 729-737.

Ataman, G., 1972. Ankara'nın güneydoğusundaki granit-granodiyoritik kütlelerden Cefalık Dağ'ın radyometrik yaşı hakkında ön çalışma. Hacettepe Fen ve Müh. Bil. Derg., 2 (1): 44-49.

Ayan, M., 1963. Contribution a l'étude petrographique et géologique de la region située au Nord-Est de Kaman. MTA publication, 115: 1-332.

Bailey, E. B. and Mc.Callien, W. J., 1950. Ankara Melanjı ve Anadolu Şariyajı. MTA, Derg. 40, 12-22.

Bailey, E. B. and Mc.Callien, W. J., 1953. Serpentine lavas, the Ankara Mélange and the Anatolian Thrust. Trans. Royal Soc. Edinburgh, 62/2, 403-442.

Batman, B., 1978. Geological Evolution of northern part of Haymana region and the study of mélange in the area (Haymana kuzeyinin jeolojik evrimi ve yöredeki melanjın incelenmesi). Bulletin of Earth Science Application and Research Centre of Hacettepe University, 4/1-2, 95-134.

Batman, B., 1981. Study of the ophiolitic melange (Dereköy Formation) in the northern area of Haymana (SW Ankara) (Ofiyolitli Melanjın (Dereköy Formasyonu) Haymana kuzeyindeki yörede (GB Ankara) incelenmesi) [in Turkish with English abstract]. Yerbilimleri, 8, 61-70.

Bilgütay, Ü., 1960. Hasanoğlan-Ankara civarının jeolojisi. MTA, Derg., 54, 46-53.

Billings, M.P., 1972. Structural Geology (3rd edn.), Prentice Hall, Englewood Cliffs, N. J., 606p.

Bingöl, E., Akyürek, B. and Korkmazer, B., 1973. Biga Yarımadasının Jeolojisi ve Karakaya Formasyonu'nun Bazı Özellikleri. Cumhuriyetin 50. yılı Yerbilimleri Kongresi Tebliğleri, MTA Enst. Yayınları, 70-76.

Birgili, Ş., Yoldaş, R. and Ünalan, G., 1975. Çankırı-Çorum Havzası'nın Petrol Olanakları. MTA Report no. 5621.

Blumenthal, M., 1941a. Eskipazar Transversal Dağları Jeolojisi ve Maden Suyu Menbaları (Çankırı Villayeti). (Geologie des montagnes de la transversale d'Eskipazar et al., leurs sources minerales) MTA Bull., 3/24, 320-352.

Blumenthal, M., 1941b. Eskipazar Transversal Dağları Jeolojisi ve Maden Suyu Menbaları II.Part (Geologie des montagnes de la transversale d'Eskipazar et al., leurs sources minerales) . MTA Bull., 4/25, 550-593.

Blumenthal, M., 1948. Bolu Civarı ile Aşağı Kızılırmak Mecrası Arasındaki Kuzey Anadolu Silsilelerinin Jeolojisi (Un apperçu de la geologie des chaines nordanatoliennes entre l'Ova de Bolu et le Kizilirmak inferieur). MTA Publ., Seri B/13.

Boccaletti, M., Bortolotti, V. and Sagri, M., 1966. Richerche sulle ofioliti della catena Alpina. 1 – Osservazioni sull Ankara Mélange nella zona di Ankara. Geological Society of Italy Bulletin, 85, 485-508.

Bott, W.H.P., 1959. The mechanics of oblique slip faulting. Geol. Mag. 96, 109-117.

Buket, E., 1969. Geology of the Aktepe-Buğra region (Kalecik, Ankara, Turkey). (M. Sc. Thesis) METU, Geol. Eng. Dept., Ankara, 92p.

Caputo, M. and Caputo, R., 1988. Estimate of the regional stress field using joint systems. Bull. Geol. Soc. Greece 23, 101-118.

Chaput, E., 1931. Ankara mıntakasının 1/135000 mikyasında jeoloji haritasına dair izahat. İstanbul Darülfununu Geologie Enstitüsü Neşriyatı 7, 3.

Chaput, E., 1936. Voyages d'etudes geologiques et geomorphogeniques en Turquie: Mem. de I' Inst. Fr. d' Archeol, de Satmboul. II, VIII. Paris.

Çalgın, R., Pehlivanoğlu, H., Ercan, T. and Şengün, M., 1973. Ankara civarının jeolojisi, MTA report no. 6487 (unpublished), 55p.

Çapan, U. Z., 1972. Geology of Gökdere region and its ophiolite suite, Kalecik, Ankara, Turkey. (M. Sc. Thesis) METU, Geol. Eng. Dept., Ankara, 122p.

Çapan, U.Z., 1981. Ankara Melanjı hakkındaki görüşler ve Melanjın Gökdere-Aktepe yöresindeki özelliklerine ait gözlemler. Proceedings of the Symposium on the Geology of Central Anatolia, March 1981, Geological Society Turkey 35th Annual Meeting, 27-31.

Çapan, U.Z. and Buket, E., 1975. Geology of Aktepe-Gökdere Region and Ophiolitic Melange (Aktepe-Gökdere Bölgesinin Jeolojisi ve Ofiyolitli Melanj). TJK Bulletin, 18/1, 11-16.

Çapan, U. Z. and Floyd, P. A., 1985. Geochemical and petrographic features of metabasalts within units of the Ankara Mélange, Turkey. Ofioliti, 10/1, 3-18.

Davis, G. H., 1984, Structural Geology of Rocks and Regions, John Wiley and Sons, Inc., New York, 492p.

Dellaloğlu, A.A., Tüysüz, O., Kaya, O.H. and Harput, B., 1992. Kalecik (Ankara)-Eldivan-Yapraklı (Çankırı)- İskilip (Çorum) ve Devrez Çayı arasindaki alanın jeolojisi ve petrol olanakları. TPAO report no. 3194.

Demirer A., Özçelik Y. and Özkan, R., 1992. Çankırı-Çorum Havzasındaki Eosen Volkaniklerinin Petrografisi TPAO report no. 1810.

Dilek, Y. and Thy, P., 2006. Age and petrogenesis of plagiogranite intrusions in the Ankara Melange, central Turkey. Islan Arc, 15, 44-57.

Dunne, W. M. and P. L. Hancock, 1994. Palaeostress analysis of small-scale brittle structures. In: (ed. Hancock, P.L.) Continental deformation. Pergamon Press, Oxford. 101-120.

Engelder, T. and Geiser, P., 1980. On the use of regional joint sets as trajectories of paleostress fields during the development of the Appalachian Plateau, U.S.A J. Geophys. Res. 85, 6319-6341.

Erk, A.S., 1981. Ankara Melanjının tortul kayaçlarının stratigrafisi. Proceedings of the Symposium on the Geology of Central Anatolia, Ankara, March 1981, Geological Society of Turkey 35th Annual Meeting, 34-40.

Erler, A., Akıman, O., Unan, C., Dalkılıç F., Dalkılıç, B., Geven, A. and Önen, P., 1991. Petrology and geochemistry of the magmatic rocks of the Kırşehir Masif in the Kaman (Kırşehir) and Yozgat regions (Kaman (Kırşehir) ve Yozgat yörelerinde Kırşehir masifi magmatik kayaçlarının petrolojisi ve jeokimyası). Doğa Tr. J. Eng. Environm. Sci., 15: 76-100.

Erol, O., 1956. Ankara güneydoğusundaki Elma Dağı ve çevresinin jeolojisi ve jeomorfolojisi üzerinde bir araştırma. MTA Publications, Seri D, 9, 99p.

Erol, O., 1958. Ankara, Çorum, Amasya, Yozgat civarı jeolojisi, pafta no. 41-42, 1,2,3,4. MTA report no. 2647 (unpublished).

Erol, O, 1961. Ankara bölgesinin tektonik gelişmesi. Bull. Geol. Soc. Turkey, VII/1, 57-85.

Etchecopar, A., Vasseur, G. and Daignieres, M., 1981. An inverse problem in microtectonics for the determination of stress tensors from fault striation analysis. J. Struct. Geol. 3, 51-65.

Eyal, Y. and Reches, Z., 1983. Tectonic analysis of the Dead Sea Rift regions since the late-Cretaceous based on meso-structures. Tectonics 2, 167-185.

Floyd, P. A., 1993. Geochemical discrimination and petrogenesis of alkalic basalt sequences in part of the Ankara mélange, central Turkey. J. Geol. Soc., London, 150, 541-550.

Gannser, A., 1974. The ophiolitic melange, a world-wide problem on Tethyan Examples. Eclog. Geol. Helv., 67/3, 479-507.

Gephart, J.W., 1990. Stress and direction of slip on fault planes. Tectonophysics 8, 845-858.

Gephart, J.W. and Forsyth, D.W., 1984. An improved method for determining regional stress tensor using earthquake focal mechanism data: an application to the San Fernando earthquake sequence. J. geophys. Res., B 89, 9305-9320.

Gökten, E. and Floyd, P. A., 2007. Stratigraphy and geochemistry of pillow basalts within the ophiolitic melange of İzmir-Ankara-Erzincan suture zone: implications for the geotectonic character of the northern branch of Neotethys. Int. J. Earth Sci. 96, 725-741.

Gökten, E., Kazancı, N. and Acar, Ş., 1988. Ankara kuzeybatısında (Bağlum-Kazan arası) Geç Kretase-Pliyosen serilerinin stratigrafisi ve tektoniği [Stratigraphy and tectonics of Late Cretaceous−Pliocene sequences in the northwest of Ankara (the area between Bağlum and Kazan)]. MTA Dergisi 108, 69-81 [in Turkish with English abstract].

Göncüoğlu, M. C. and Türeli, T. K., 1994. Alpine collisional-type granitoids from western Central Anatolian Crystalline Complex, Turkey. Journal of Kocaeli University, Earth science section, 1/ 39-46.

Göncüoğlu, M. C., Erler, A., Toprak, V., Yalınız, K., Olgun, E. and Rojay, B., 1992. Orta Anadolu Masifinin batı bölümünün jeolojisi, Bölüm II: Orta kesim. TPAO Rap. No: 3155, 76p.

Göncüoğlu, M.C., Erler, A., Toprak, V., Olgun, E., Yalınız, K., Kuşçu, İ., Köksal, S. and Dirik, K., 1993. Orta Anadolu masifinin orta bölümünün jeolojisi, Bölüm 3; Orta Kızılırmak Tersiyer Baseninin jeolojik evrimi. ODTU-AGUDOS Rap. (unpublished).

Gudmundsson, A., 1987. Tectonics of the Thingvellir fissure swarm, SW Iceland. J. Struct. Geol. 9, 61-69.

Gürsoy, H., Piper, J. D. A. and Tatar, O., 1999. Paleomagnetic study of the Galatean Volcanic Province north-central Turkey: Neogene deformation at the northern border of the Anatolian Block. Geological Journal 34, 7-23.

Hancock, P.L., 1985. Brittle microtectonics: principles and practice. J. Struct. Geol. 7, 437-457.

Hardcastle, K.C., 1989. Possible palaeostress tensor configurations derived from fault-slip data in eastern Vermont and eastern New Hampshire. Tectonics 8(2), 265-284.

Karadenizli, L., Seyitoğlu, G., Saraç, G., Kazancı, N., Şen, Ş., Hakyemez, H.Y. and Savaşçı, D., 2003. Early-Middle Miocene palaeogeographic evolution of the western margin of the Çankırı-Çorum Basin. MTA Derg., 126, 69-86.

Kaymakçı, N., 2000. Tectono-stratigraphical Evolution of the Çankırı Basin (Central Anatolia, Turkey). PhD Thesis, Universiteit Utrecht, Utrecht, 248p.

Kaymakçı, N., White, S. H. and VanDijk, P. M., 2000. Paleostress inversion in a multiphase deformed area: Kinematic and structural evolutionof the Çankırı Basin (Central Turkey), part 1 – northern area. In: Bozkurt, E., Winchester, J.A. and Piper, J.D.A. (eds), Tectonics and Magmatism in Turkey and the Surrounding Area. Geological Society, London, Special Publications 173, 295-323.

Kaymakçı, N., White, S.H. and VanDijk, P.M., 2003a. Kinematic and structural development of the Çankırı Basin (Central Anatolia, Turkey): a paleostress inversion study. Tectonophysics 364, 85-113.

Kaymakçı, N., Özçelik, Y., White, H.S. and Van Dijk, P.M., 2001. Neogene tectonic development of the Çankırı basin (Central Anatolia, Turkiye). TAPG Bulletin, 13/1, 27-56.

Kaymakçı, N., Duermeijer, C.E., Langereis, C., White, S.H., and van Dijk, P.M., 2003b. Oroclinal bending due to indentation: a paleomagnetic study for the early Tertiary evolution of the Çankiri Basin (central Anatolia, Turkey) Geological Mag. 140/3, 343-355.

Ketin, İ., 1961. Türkiye'de magmatik faaliyet, TJK Bulletin, 7/2, 1-15.

Ketin, İ., 1962. 1/500.000 ölçekli Türkiye Jeoloji Haritası ve izahatnamesi, Sinop paftası. MTA Publications, 111p.

Ketin, İ., 1963. 1/500.000 ölçekli Türkiye Jeoloji Haritası ve izahatnamesi, Kayseri paftası. MTA Publications, 82p.

Ketin, İ., 1966. Tectonic units of Anatolia. MTA Bulletin, 66, 20-34.

Kissel, C., Laj, C., Poisson, A., and Görür, N., 2003. Paleomagnetic reconstruction of the Cenozoic evolution of the Eastern Mediterranean. Tectonophysics, 362, 199-217.

Kleinsorge, H., 1940. Ankara Vilayeti, Karapürçek ve Bayramlıtepe Havalisinde Yapılan Jeolojik Tetkikata Dair Rapor. MTA report no. 1079.

Koçyiğit, A., 1987. Tectono-stratigraphy of the Hasanoğlan (Ankara) region: Evolution of the Karakaya orogen. Bulletin of Earth Sciences Application and Research Centre of Hacettepe University, 14, 269-293.

Koçyiğit, A., 1991. An example of an accretionary forearc basin from northern Central Anatolia and its implications for the history of subduction of Neo-Tethys in Turkey. Geological Society of America Bulletin, 103, 22-36.

Koçyiğit, A. and Lünel, A. T., 1987. Geology and tectonic setting of Alçı region, Ankara. METU Journal of Pure and Applied Sciences, 20/1, 35-59.

Koçyiğit, A., Özkan, S. and Rojay, B.F., 1988. Examples from the forearc basin remnants at the active margin of northern Neo-Tethys; development and emplacement ages of the Anatolian Nappe, Turkey. METU Journal of Pure and Applied Science, 21/1-3, 183-210.

Koçyiğit, A., Türkmenoğlu, A., Beyhan, A., Kaymakçı, N. and Akyol, E. 1995. Post-collisional tectonics of Eskişehir-Ankara-Çankırı segment of İzmir-Ankara-Erzincan Suture Zone (İAESZ): Ankara Orogenic Phase. Türkiye Petrol Jeologları Derneği Bülteni 6, 69-86.

Lacombe, O., Angelier, J. and Laurent, P., 1992. Determining paleostress orientations from faults and calcite twins: a case study near the Sainte-Victoire Range (southern France). Tectonophysics 201, 141-156.

Marinoni, L. B. and Gudmundsson, A., 2000. Dykes, faults and palaeostresses in the Teno and Anaga massifs of Tenerife (Canary Islands). Journal of Volcanology and Geothermal Research 103, 83-103.

Marshak, S. and Mitra, G. 1988. Basic Methods of Structural Geology. Prentice Hall, New Jersey.

Michael, A., 1984. Determination of stress from slip data: fault and folds. J. geophys. Res., B 89, 11517-11526.

Norman, T. N., 1972. Stratigraphy of Upper Cretaceous-Lower Tertiary strata of Yahşıhan area, east of Ankara. Geological Society of Turkey Bulletin, XV-2, 180-276.

Norman, T. N., 1973. On the structure of Ankara Mélange. Cumhuriyetin 50. Yılı Yerbilimleri Kongresi Tebliğleri, MTA Publications, 78-94.

Norman, T., 1975. Flow features of Ankara Melange. 9th Inter. Sediment. Congr. Proceedings, 4, 261-267.

Norman, T. N., 1984. The role of the Ankara Mélange in the development of Anatolia, Turkey. In: (ed. Dixon, J. E. and Robertson, A.H.F) The geological evolution of the eastern Mediterranean. Geol. Soc. London Spec. Publ. 17, 441-447.

Okay, A. İ. and Göncüoğlu, M. C., 2004. The Karakaya Complex: A Review of Data and Concepts. Turkish Journal of Earth Sciences, 13, 77-95.

Okay, A.I. and Tüysüz, O., 1999. Tethyan sutures of northern Turkey. In: Durand, B., Jouvet, L., Horvath, E. and Seranne, M. (eds.), The Mediterranean Basins: Tertiary Extension within the Alpine Orogen. Geological Society, London, Special Publications, 156, 475-515.

Özçelik, Y., 1994. Laçin (Çorum – Türkiye) alanının tektonostratigrafisi. M.Sc. Thesis, METU Geol. Eng. Dept., Ankara, 133p.

Özçelik, Y. and Savun, C., 1993. İskilip-Osmancık–Çorum–Sungurlu arasındaki alanın jeolojisi ve petrol olanakları TPAO report no. 3290.

Özkaya, I., 1982. Origin and tectonic setting of some mélange units in Turkey. J. Geol., 90, 269-278.

Piper, J. D. A., Tatar, O. and Gürsoy, H., 1997. Deformational Behaviour Of Continental Lithosphere Deduced From Block Rotations Across The North Anatolian Fault Zone In Turkey. Earth and Planetary Sci. Letters 150, 191-203.

Pollard, D.D., Saltzer, S.D., and Rubin, A.M. 1993. Stress inversion methods: are they based on faulty assumptions? J. Struct. Geol. 15/8, 145– 154.

Price, N. and Cosgrove, J.W., 1990. Analysis of Geological Structures. Cambridge University Press, Cambridge.

Ragan, D. M., 1985, Structural Geology an introduction to geometrical techniques, John Wiley and Sons, Inc., New York, 166p.

Ramsay, J. G., 1980. Shear zone geometry; a review. J. Struct. Geol. 2, 83-99.

Reches, Z., 1987. Determination of the tectonic stress tensor from slip along faults that obey the Coulomb yield criterion. Tectonics 6, 849-861.

Robertson, A.H.F. and Dixon, J.E., 1984. Introduction: aspects of the geological evolution of the Eastern Mediterranean, 1-74. In: J.E. Dixon and A.H.F. Robertson (eds.), The Geological Evolution of the Eastern Mediterranean, Blackwell Sci. Publ., Oxford, London, 824p.

Rojay, B., 1995. Post-Triassic evolution of Central Pontides: Evidence from Amasya region, Northern Anatolia. Geologica Romana, 31, 329-350.

Rojay, B. and Süzen, M. L., 1997. Tectonostratigraphic evolution of the Cretaceous dynamic basins on accretionary ophiolitic melange prism, SW of Ankara region. TAPG Bulletin, 9/1, 1-12.

Rojay, B. and Karaca A., 2008. Post-Miocene deformation in south of the Galatian volcanic province, NW of Central Anatolia (Turkey). T. Jour. of Earth Sci. 17, 4, 653-672.

Rojay, B., Yalınız, K. M. and Altıner, D., 2001. Tectonic Implications of Some Cretaceous Pillow Basalts from the North Anatolian Ophiolitic Melange (Central Anatolia-Turkey) to the Evolution of Neotethys. Turkish Journal of Earth Sciences, 10/3, 93-102.

Rojay, B., Kasımoğlu, P. and Seyrek, E., 2007. The orientation of principle stress direction during post-Cretaceous and post-Eocene periods in northern Central Anatolia (Kuzey Orta Anadolu`da Kretase sonrasi ile Eosen sonrasi dönemlerde ana stres yöneliminin değişimi). TUBITAK project report no. ÇAYDAG-106Y122, 56p.

Rojay, B., Altıner, D., Altıner, S. Ö., Önen, A. P., James, S. and Thirlwall, M. F., 2004. Geodynamic significance of the Cretaceous pillow basalts from North Anatolian Ophiolitic melange Belt (Central Anatolia, Turkey): geochemical and paleontological constraints. Geodinamica Acta, 17/5, 349-361.

Stewart, I.S. and Hancock, 1994. Neotectonics. In: (ed. Hancock, P.L.) Continental deformation. Pergamon Press, Oxford. 370-409.

Salomon, C.W., 1940. Geologische wander ungen bei Ankara (Ankara civarında jeolojik geziler). MTA Derg., 20, 380-400 and 21, 601-619.

Seymen, İ., 1985. Kırşehir masifi metamorfitlerinin jeoloji evrimi. Türk. Jeol. Kur., Ketin Symp., 133-148.

Şengör, A. M. C. and Yılmaz, Y., 1981. Tethyan Evolution of Turkey: A Plate Tectonic Approach. Tectonophysics 75, 181-241.

Şengör, A. M. C., Yılmaz, Y. and Sungurlu, O., 1984. Tectonics of the Mediterranean Cimmerides: Nature and evolution of the western termination of Paleo-Tethys. In: (ed. Dixon, J. E. and Robertson, A.H.F) The geological evolution of the eastern Mediterranean. J. Geol. Soc. London, Spec. Publ., 17, 77-112.

Tankut, A., 1984. Basic and ultrabasic rocks from the Ankara Melange, Turkey. In: (eds. Dixon, J.E. and Robertson, A.H.F.) The geological evolution of eastern Mediterranean. J. Geol. Soc. London Spec. Publ. 17, 441-447.

Tankut, A., 1985a. Geochemistry of the Neogene volcanics around Ankara (Ankara dolaylarındaki Neojen yaşlı volkaniklerinin jeokimyası). Geological Society of Turkey Bulletin, 28, 55-66 [in Turkish with English abstract].

Tankut, A., 1985b. Basic and ultrabasic rocks from the Ankara melange, Turkey. In: (eds. Dixon, J. E. and Robertson, A.H.F) The geological evolution of the eastern Mediterranean. J. Geol. Soc. London, Spec. Publ., 17, 449-454.

Tankut, A., 1990. Geochemical implications for tectonic setting of the ophiolitic rocks from the ophiolite melange belt of the Ankara Melange, MTA Bulletin, 110, 17-28.

Tankut, A. and Sayın, M.N., 1989. Edige ultramafic body, Doğa Türk Müh. ve Çevre Bilim. Dergisi, 13-2, 229-224.

Tankut, A. and Gorton M.P., 1990. Geochemistry of a mafic-ultramafic body in the Ankara Melange, Anatolia, Turkey: Evidences for a fragment of oceanic lithosphere, Ophiolites-Crustal Analogues, 339-349.

Tankut, A., Dilek, Y. and Önen, P., 1998. Petrology and geochemistry of Neo-Tethyan volcanism as revealed in Ankara Mélange, Turkey. J. Volcanology and Geochem. Res. Spec. Publ., 85, 265-284.

Tekeli, O., 1981. Subduction complex of pre-Jurassic age, northern Anatolia, Turkey. Geology, 9, 68-72.

Tokay, M., Lünel, A.T. and Koçyiğit, A., 1988. Geology and petrology of the Gökdere stock of the Orhaniye syenite. METU Jour. of Pure and Applied Sci. 21/1-3, 183-210.

Turner, J.P. and Hancock, P.L., 1990. Relationships between thrusting and joint systems in the Jaca thrust-top basin, Spanish Pyrenees. J. Struct. Geol. 12, 217-226.

Tüysüz, O. and Dellaloğlu, A. A., 1992. Geologic evolution of Çankırı Basin and its tectonic units. 9th Petroleum Congress of Turkey, 333-349.

Tüysüz, O., Dellaloğlu, A. A. and Terzioğlu, N., 1995. A magmatic belt within the Neo-Tethyan suture zone and its role in the tectonic evolution of northern Turkey. Tectonophysics, 243, 173-191.

Twiss, R. J. and Moores, E. M., 1992. Structural Geology, W. H. Freeman and Company, New York, 532p.

Twiss, R.J. and Unruh, J.R. 1998. Analysis of fault slip inversion; do they constrain stress or strain rate? J. Geophys. Res. 103 (B6), 12205– 12222.

Ünalan, G., 1981. Stratigraphy of Ankara mélange (SW Ankara) (Ankara Güneyindeki Ankara Melanjının stratigrafisi). Proceedings of the Symposium on the Geology of Central Anatolia, March 1981. Geol. Soc. Turkey 35th Annual Meeting, 46-52.

Ünalan, G., 1982. Kalecik-Tüney-Sulakyurt (Ankara) arasındaki bölgenin petrol olanaklarının araştırılması. TPAO report no. 2083.

Wallace, R.E., 1951. Geometry of shearing stress and relation to faulting. J. Geol. 59, 118-130.

Yamaji, A. 2000. The multiple inverse method: a new technique to separate stresses from heterogeneous fault-slip data. Journal of Structural Geology 22, 441-452.

Yeats, R.S., 1986. Active faults related to folding. In: (ed. Wallace, R.E.) Active tectonics. National Academic Press, Washington, 63-79.

Yıldırım, M., 1974. Geology of Kızıldağ – Edige Region. Elmadağ-east of Ankara. M.Sc. Thesis, METU Geol. Eng. Dept., Ankara, 80p.

Yılmazer, İ., 1994. Ankara'nın doğusunda yer alan Yayla olistostromunun jeolojisi. Bull. Geol. Soc. of Turkey, 37/1, 47-52.

Yoldaş, R., 1982. Tosya (Kastamonu) ile Bayat (Çorum) arasındaki bölgenin jeolojisi. Ph.D. Thesis, İst. Üniv., 311 pp.

APPENDIX A

DYKE MEASUREMENTS

Table A.1: Dyke measurements of Domain I.

DOMAIN I DYKES				
Data no	**Easting**	**Northing**	**Strike(°N)**	**Dip (°)**
d1	544881	4440356	359	90
d2	544940	4440628	198	87
d3	544647	4440469	242	67
d4	543110	4440509	227	89
d5	543187	4440354	245	65
d6	543233	4440357	063	87
d7	543321	4440283	228	81
d8	543306	4440385	227	83
d9	543285	4440426	204	75
d10	543222	4440515	225	75
d11	543078	4440571	230	71
d12	543052	4440614	233	83
d13	545119	4440861	183	89
d14	545296	4440722	060	80
d15	545449	4440850	226	86
d16	543686	4440084	206	41
d17	543686	4440084	216	36
d18	543518	4440431	216	76
d19	543505	4440514	051	70
d20	543588	4440572	033	81
d21	543588	4440572	241	71
d22	542626	4440486	216	80
d23	542782	4440463	038	50
d24	542782	4440463	021	88
d25	543171	4440642	049	58
d26	543334	4440731	241	84
d27	543339	4440727	060	83
d28	543340	4440726	035	70
d29	543344	4440722	069	64

Table A.1: Continued.

DOMAIN I DYKES				
Data no	**Easting**	**Northing**	**Strike(°N)**	**Dip (°)**
d30	543342	4440724	242	77
d31	542329	4439988	072	86
d32	542197	4439928	194	89
d33	543573	4440480	223	89
d34	543361	4440915	042	73

Table A.2: Dyke measurements of Domain II.

DOMAIN II DYKES				
Data no	**Easting**	**Northing**	**Strike(°N)**	**Dip (°)**
d35	543987	4443671	225	85
d36	543987	4443671	350	60
d37	544525	4442424	208	84
d38	544235	4442260	263	79
d39	544086	4442231	250	75
d40	544086	4442231	242	66
d41	544199	4442211	180	33
d42	544157	4443181	227	42
d43	542608	4440984	230	83
d44	542749	4441331	053	87
d45	542715	4441460	050	88
d46	542665	4441498	203	64
d47	542665	4441498	220	65
d48	542665	4441498	068	79
d49	542599	4441543	020	75
d50	542594	4441637	276	88
d51	542622	4441676	195	86
d52	542610	4441808	350	89
d53	542574	4441810	039	76
d54	542556	4441775	075	50
d55	542564	4441812	273	82
d56	542630	4441890	225	78
d57	542630	4441890	240	67
d58	542630	4441890	234	65
d59	542616	4441982	226	86
d60	542686	4441941	247	79
d61	542722	4441868	244	67
d62	542917	4441838	228	46
d63	542942	4441798	190	50
d64	543014	4441720	240	83
d65	542531	4445018	073	89
d66	542148	4444144	275	64
d67	542137	4444056	230	90
d68	542137	4444056	218	88
d69	542137	4444056	233	84
d70	542137	4444056	230	88
d71	542137	4444056	227	85

Table A.2: Continued.

DOMAIN II DYKES				
Data no	**Easting**	**Northing**	**Strike(°N)**	**Dip (°)**
d72	542477	4443871	030	81
d73	542490	4443864	043	88
d74	542326	4443597	222	75
d75	542354	4443582	238	85
d76	542366	4443583	231	83
d77	542366	4443583	222	89
d78	542563	4443490	230	76
d79	542625	4443435	227	80
d80	542680	4443381	210	71
d81	542680	4443381	210	82
d82	542680	4443381	221	90
d83	542705	4443361	194	58
d84	542705	4443361	201	64
d85	542792	4443343	080	89
d86	542792	4443343	207	78
d87	542887	4443275	053	70
d88	542933	4443243	228	65
d89	542942	4443279	177	60
d90	542981	4443267	165	44
d91	543128	4443218	191	48
d92	543128	4443218	215	43
d93	543520	4443163	234	74
d94	543498	4443167	233	63
d95	543491	4443171	232	74
d96	543474	4443204	222	72
d97	542776	4442568	223	76
d98	542776	4442568	221	43
d99	542976	4442383	221	83
d100	543805	4441714	216	75
d101	543805	4441714	190	74
d102	543953	4441896	226	54
d103	543876	4441959	227	80
d104	543678	4442054	219	57
d105	543574	4442103	210	61
d106	543574	4442103	225	71
d107	543574	4442103	228	83
d108	543400	4442493	210	63

Table A.2: Continued.

DOMAIN II DYKES				
Data no	**Easting**	**Northing**	**Strike(°N)**	**Dip (°)**
d109	543365	4442522	230	85
d110	543270	4442482	319	74
d111	542961	4442382	220	90
d112	543032	4442375	205	69
d113	543063	4442353	230	65
d114	543079	4442340	297	60
d115	543115	4442325	231	86
d116	543095	4442257	219	90
d117	543095	4442254	245	75
d118	543055	4442083	307	40
d119	543126	4441579	249	90
d120	543148	4441540	239	87
d121	543084	4441465	247	61
d122	543227	4441271	230	86
d123	543234	4441248	220	70
d124	541588	4444651	236	75
d125	541556	4444679	223	71
d126	541556	4444707	207	57
d127	541499	4444663	217	67
d128	541094	4441072	219	88
d129	541332	4441142	046	79
d130	541330	4441204	058	84
d131	541380	4441200	084	79
d132	541404	4441176	058	79
d133	541429	4441191	046	79
d134	541464	4441204	062	82
d135	541510	4441180	061	76
d136	542316	4440776	074	89
d137	542635	4441009	038	74
d138	542796	4441050	247	73
d139	542828	4441060	236	43
d140	542982	4441069	211	79
d141	543070	4441074	257	89
d142	542950	4441684	234	89
d143	542950	4441684	239	82
d144	543000	4441680	251	76
d145	542927	4441603	066	89

Table A.2: Continued.

DOMAIN II DYKES				
Data no	**Easting**	**Northing**	**Strike(°N)**	**Dip (°)**
d146	542934	4441443	241	90
d147	542978	4441431	252	73
d148	543296	4441386	053	79
d149	543311	4441363	224	89

Table A.3: Dyke measurements of Domain III.

DOMAIN III DYKES				
Data no	**Easting**	**Northing**	**Strike(°N)**	**Dip (°)**
d150	540908	4446523	020	68
d151	540843	4446359	204	70
d152	540843	4446359	259	68
d153	540748	4446262	194	56
d154	540782	4446275	234	82
d155	540737	4446327	076	74
d156	540737	4446327	040	83
d157	540755	4446477	216	89
d158	540505	4445810	215	70
d159	540505	4445810	196	66
d160	540534	4445824	215	64
d161	540534	4445824	030	81
d162	539877	4445509	091	80
d163	539877	4445509	206	86
d164	539897	4445509	026	84
d165	539918	4445552	264	76
d166	539919	4445647	259	84
d167	539908	4445731	226	85
d168	539875	4445807	212	88
d169	539843	4445896	057	77
d170	539798	4445911	043	88
d171	539798	4445911	170	74
d172	539768	4445971	020	62
d173	539728	4445957	104	88
d174	539709	4445914	043	78
d175	539710	4445896	002	67
d176	539800	4445800	098	78
d177	539660	4445845	024	62
d178	539696	4445822	091	47
d179	539576	4445717	024	69
d180	539544	4445696	019	71
d181	539495	4445729	204	87
d182	539469	4445736	216	77
d183	539395	4445752	103	82
d184	539415	4445732	069	88
d185	539449	4445685	216	87
d186	539423	4445638	223	76

Table A.3: Continued.

DOMAIN III DYKES				
Data no	**Easting**	**Northing**	**Strike(°N)**	**Dip (°)**
d187	539425	4445633	291	86
d188	539412	4445622	296	81
d189	539411	4445611	033	86
d190	539470	4445567	033	81

APPENDIX B

BED MEASUREMENTS

Table B.1: Bed measurements of Domain I.

DOMAIN I BEDS				
Data no	**Easting**	**Northing**	**Strike(°N)**	**Dip (°)**
b1	544647	4440469	183	79
b2	544647	4440469	190	77
b3	544647	4440469	171	81
b4	543110	4440509	308	83
b5	543110	4440509	304	77
b6	543187	4440354	348	73
b7	543187	4440354	329	68
b8	543233	4440357	305	53
b9	543233	4440357	350	61
b10	543321	4440283	336	51
b11	543321	4440283	322	42
b12	543306	4440385	115	87
b13	543306	4440385	115	90
b14	543285	4440426	308	58
b15	543222	4440515	325	85
b16	543222	4440515	320	89
b17	543686	4440084	180	65
b18	543505	4440514	209	32
b19	543505	4440514	215	25
b20	543588	4440572	239	26
b21	543588	4440572	225	35
b22	543588	4440572	274	26
b23	543588	4440572	256	48
b24	542626	4440486	236	62
b25	542626	4440486	250	31
b26	542626	4440486	248	33
b27	542626	4440486	235	41
b28	542782	4440463	294	58
b29	542822	4440490	245	84
b30	542846	4440500	291	43

Table B.1: Continued.

DOMAIN I BEDS				
Data no	**Easting**	**Northing**	**Strike(°N)**	**Dip (°)**
b31	543334	4440731	275	43
b32	543334	4440731	300	51
b33	543339	4440727	280	37
b34	543340	4440726	298	32
b35	543340	4440726	279	16
b36	543344	4440722	299	25
b37	543344	4440722	277	44
b38	543342	4440724	247	17
b39	543342	4440724	245	36
b40	542329	4439988	112	37
b41	542154	4439921	357	64
b42	543573	4440480	294	14
b43	543573	4440480	298	19
b44	543361	4440915	146	61

Table B.2: Bed measurements of Domain II.

DOMAIN II BEDS				
Data no	**Easting**	**Northing**	**Strike(°N)**	**Dip (°)**
b45	544086	4442231	150	82
b46	544086	4442231	327	85
b47	542608	4440984	299	37
b48	542608	4440984	288	39
b49	542749	4441331	293	74
b50	542749	4441331	295	75
b51	542715	4441460	305	38
b52	542715	4441460	119	15
b53	542665	4441498	037	06
b54	542665	4441498	004	13
b55	542599	4441543	349	64
b56	542610	4441808	307	13
b57	542610	4441808	312	30
b58	542574	4441810	294	35
b59	542564	4441812	295	38
b60	542630	4441890	154	49
b61	542630	4441890	162	46
b62	542630	4441890	123	53
b63	542686	4441941	113	44
b64	542686	4441941	298	58
b65	542917	4441838	196	23
b66	542917	4441838	167	31
b67	542942	4441798	158	56
b68	543014	4441720	155	54
b69	543132	4441710	128	45
b70	542137	4444056	030	78
b71	542477	4443871	291	61
b72	542477	4443871	294	61
b73	542490	4443864	291	59
b74	542490	4443864	290	55
b75	542326	4443597	291	44
b76	542326	4443597	297	43
b77	542354	4443582	293	57
b78	542354	4443582	305	46
b79	542366	4443583	291	58
b80	542366	4443583	293	73
b81	542563	4443490	301	12

Table B.2: Continued.

DOMAIN II BEDS				
Data no	**Easting**	**Northing**	**Strike(°N)**	**Dip (°)**
b82	542563	4443490	300	18
b83	542619	4443457	335	23
b84	542619	4443457	254	32
b85	542625	4443435	300	26
b86	542792	4443343	256	40
b87	542792	4443343	290	36
b88	542942	4443279	225	45
b89	542942	4443279	272	40
b90	543520	4443163	090	15
b91	542709	4442950	245	25
b92	542730	4442812	295	17
b93	542730	4442812	310	19
b94	542730	4442812	333	17
b95	542689	4442696	322	25
b96	542689	4442696	300	09
b97	543900	4441873	101	83
b98	543876	4441959	334	70
b99	543678	4442054	080	82
b100	543678	4442054	079	80
b101	543574	4442103	044	73
b102	543574	4442103	030	78
b103	543400	4442493	211	44
b104	543365	4442522	339	55
b105	543365	4442522	040	36
b106	542961	4442382	292	22
b107	543095	4442257	022	40
b108	543095	4442254	355	29
b109	543095	4442254	332	30
b110	543148	4441540	170	58
b111	543084	4441465	140	50
b112	541588	4444651	337	84
b113	541588	4444651	341	56
b114	541556	4444679	326	51
b115	542316	4440776	203	67
b116	542316	4440776	167	57
b117	542635	4441009	291	31
b118	542635	4441009	281	21

Table B.2: Continued.

DOMAIN II BEDS				
Data no	**Easting**	**Northing**	**Strike(°N)**	**Dip (°)**
b119	542982	4441069	266	41
b120	543070	4441074	264	24
b121	543070	4441074	246	51
b122	542950	4441684	166	34
b123	542950	4441684	163	47
b124	542950	4441684	143	27
b125	543004	4441707	156	57
b126	543000	4441680	141	71
b127	542927	4441603	132	36
b128	542827	4441554	151	41
b129	542880	4441503	272	46
b130	542907	4441487	123	41
b131	542934	4441443	082	52
b132	542978	4441431	081	86
b133	542978	4441431	086	45
b134	543296	4441386	155	44
b135	543311	4441363	174	61
b136	543311	4441363	193	52

Table B.3: Bed measurements of Domain III.

DOMAIN III BEDS				
Data no	**Easting**	**Northing**	**Strike(°N)**	**Dip (°)**
b137	540852	4446232	272	90
b138	540852	4446232	274	64
b139	540852	4446232	247	85
b140	540833	4446181	253	28
b141	540755	4446477	206	28

APPENDIX C

FAULT MEASUREMENTS

Table C.1: Fault measurements around the Bayamlı Hill.

BAYAMLI HILL FAULTS							
Data no	**Easting**	**Northing**	**Strike (°N)**	**Dip (°)**	**Dip Dir.**	**Rake (°)**	**R. Dir.**
f1	540534	4445824	119	78	SW		
f2	539843	4445896	120	41	SW		
f3	539798	4445911	304	81	NE	24	S
f4	539800	4445800	099				
f5	539660	4445845	089				
f6	539544	4445696	291	89	NE	16	SE
f7	539469	4445736	335	69	NE	09	SE
f8	539469	4445736	334	71	NE	12	SE
f9	539469	4445736	320	76	E	12	S
f10	539439	4445668	139				

Table C.2: Fault measurements in the northern side of the Kızılırmak River.

FAULTS IN THE NORTH OF KIZILIRMAK RIVER							
Data no	**Easting**	**Northing**	**Strike (°N)**	**Dip (°)**	**Dip Dir.**	**Rake (°)**	**R. Dir.**
f11	544525	4442424	015	35	SE	20	N
f12	544525	4442424	090	79	S	10	E
f13	544525	4442424	090	81	S	15	E
f14	544525	4442424	282	85	NE	42	W
f15	544525	4442424	288	43	NE	03	E
f16	544525	4442424	067	81	SE	01	W
f17	544525	4442424	074	80	SE	25	W
f18	544270	4442245	038	46	SE	45	S
f19	544270	4442245	064	30	SE	75	W
f20	544235	4442260	088	64	SE	86	W
f21	542981	4443267	296	26	NE	46	SE
f22	542981	4443267	294	22	NE	41	SE
f23	542981	4443267	329	25	NE	85	SE
f24	542981	4443267	325	19	NE	82	SE
f25	543128	4443218	009	90		77	S
f26	543128	4443218	016	86	SE	72	S
f27	543128	4443218	358	81	NE	83	N
f28	543128	4443218	005	75	SE	87	N
f29	543893	4441940	317	40	NE	30	NW
f30	542961	4442382	113	15	SW	90	
f31	543079	4442340	215	74	NW	10	N
f32	543079	4442340	093	88	SW	25	E
f33	541332	4441142	339	47	NE		
f34	541330	4441204	170	88	SW		
f35	541380	4441200	320	69	NE		
f36	541404	4441176	149	76	SW	86	SW
f37	541404	4441176	152	76	SW	87	SW
f38	541404	4441176	150	76	SW	88	SW
f39	541404	4441176	354	61	NE	83	SE
f40	541404	4441176	349	57	NE	81	SE
f41	541404	4441176	339	51	NE	77	SE
f42	541404	4441176	006	64	SE	81	SE
f43	541464	4441204	131	87	SW	59	SW
f44	541464	4441204	004	56	SE	71	SE
f45	541510	4441180	146	51	SW		
f46	541510	4441180	144	71	SW	74	SW
f47	542316	4440776	333				

Table C.2: Continued.

FAULTS IN THE NORTH OF KIZILIRMAK RIVER							
Data no	**Easting**	**Northing**	**Strike (°N)**	**Dip (°)**	**Dip Dir.**	**Rake (°)**	**R. Dir.**
f48	542316	4440776	021				
f49	542316	4440776	006				
f50	542316	4440776	351	83	NE	27	NE
f51	542336	4440774	322	56	NE		
f52	542336	4440774	324	46	NE		
f53	542982	4441069	255	42	NW		

Table C.3: Fault measurements in the southern side of the Kızılırmak River.

FAULTS IN THE SOUTH OF KIZILIRMAK RIVER							
Data no	**Easting**	**Northing**	**Strike (°N)**	**Dip (°)**	**Dip Dir.**	**Rake (°)**	**R. Dir.**
f54	542626	4440486	321	56	NE		
f55	542626	4440486	298	85	NW	42	W
f56	542626	4440486	290	88	NW	46	W
f57	542626	4440486	298	83	NW	43	W
f58	542626	4440486	300	88	NW	44	W
f59	542626	4440486	302	47	NW	60	W
f60	542626	4440486	309	56	NW	66	W
f61	542626	4440486	305	55	NW	88	W
f62	542626	4440486	313	63	NW	64	W
f63	542626	4440486	215	67	NW	83	E
f64	543334	4440731	207	84	NW	34	NE
f65	543344	4440722	307	58	NW	60	SW
f66	543573	4440480	112	86	SW	17	W
f67	543573	4440480	116	81	SW	08	W
f68	543573	4440480	097	82	SW	04	E
f69	543573	4440480	094	88	SW	02	E
f70	543573	4440480	101	77	SW	02	E
f71	543573	4440480	101	77	SW	46	SE
f72	543573	4440480	100	71	SW	60	SE
f73	543573	4440480	077	71	SE	04	E
f74	543573	4440480	078	79	SE	11	E
f75	543573	4440480	086	77	SE	07	E
f76	543573	4440480	076	69	SE	11	E
f77	543573	4440480	085	61	SE	10	E
f78	543573	4440480	096	81	SW	14	E
f79	543573	4440480	291	89	NE	16	E
f80	543573	4440480	290	89	NE	06	E
f81	543588	4440572	311	66	NE	06	N
f82	543588	4440572	104	79	SW		

Table C.4: Fault plane measurements of the Kızılırmak River Fault.

KIZILIRMAK RIVER FAULT							
Data no	**Easting**	**Northing**	**Strike (°N)**	**Dip (°)**	**Dip Dir**	**Rake(°)**	**R. Dir**
f83	542796	4441050	254	77	NW	05	W
f84	542791	4441045	261	71	NW	03	W
f85	542787	4441038	256	74	NW	03	W
f86	542780	4441030	221	68	NW	11	W
f87	542778	4441026	233	77	NW	07	W

Table C.5: Fault Measurements around the Çamın Hill.

ÇAMIN HILL FAULTS							
Data no	**Easting**	**Northing**	**Strike (°N)**	**Dip (°)**	**Dip Dir.**	**Rake (°)**	**R. Dir.**
f88	542085	4444825	043	69	SE	73	SW
f89	542085	4444825	033	70	SE	74	SW
f90	542085	4444825	074	67	SE	80	W
f91	542085	4444825	070	67	SE	72	W
f92	542085	4444825	073	71	SE	73	W
f93	542085	4444825	100	64	SW	82	W
f94	542085	4444825	031	75	SE	70	SW
f95	542085	4444825	047	61	SE	76	SW
f96	542085	4444825	063	76	SE	43	SW
f97	542192	4445017	148	82	SW	19	N
f98	542192	4445017	148	80	SW	05	S
f99	542192	4445017	324	89	NE	12	N
f100	542192	4445017	146	83	SW	03	N